AD-A114 057 MITRE CORP BEDFORD MA F/G 9/6
MULTIPATH ANALYSIS OF TELEMETRY SUPPORT POSITIONS FOR APATS.(U)
APR 82 G A ROBERTSHAW F19628-82-C-0001
UNCLASSIFIED MTR-8277 ESD-TR-81-395 NL

1 OF 2
AD A
114057

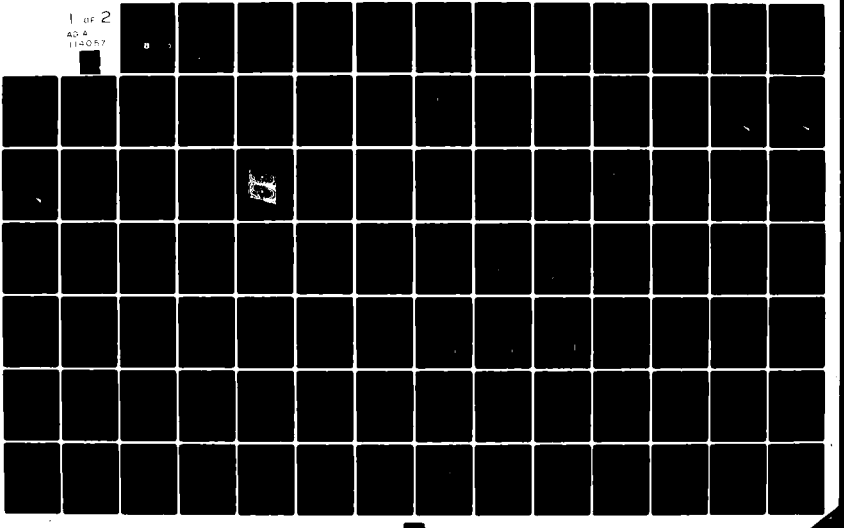

ESD-TR-81-395

MTR-8277

MULTIPATH ANALYSIS OF TELEMETRY SUPPORT POSITIONS FOR APATS

By

G. A. ROBERTSHAW

APRIL 1982

Prepared for

Deputy/Mission Support Systems
ELECTRONIC SYSTEMS DIVISION
AIR FORCE SYSTEMS COMMAND
UNITED STATES AIR FORCE
Hanscom Air Force Base, Massachusetts

Project No. 4290

Prepared by

THE MITRE CORPORATION
Bedford, Massachusetts

Contract No. F19628-82-C-0001

REVIEW AND APPROVAL

This technical report has been reviewed and is approved for publication.

MICHAEL ZYMARIS
Project Engineer

FOR THE COMMANDER

EDWIN C. DOBKOWSKI, Lt Col, USAF
Systems Program Director, APATS

UNCLASSIFIED
SECURITY CLASSIFICATION OF THIS PAGE (When Data Entered)

REPORT DOCUMENTATION PAGE	READ INSTRUCTIONS BEFORE COMPLETING FORM
1. REPORT NUMBER: ESD-TR-81-395	2. GOVT ACCESSION NO.: AD-A117057
	3. RECIPIENT'S CATALOG NUMBER:
4. TITLE (and Subtitle): MULTIPATH ANALYSIS OF TELEMETRY SUPPORT POSITIONS FOR APATS	5. TYPE OF REPORT & PERIOD COVERED:
	6. PERFORMING ORG. REPORT NUMBER: MTR-8277
7. AUTHOR(s): G. A. ROBERTSHAW	8. CONTRACT OR GRANT NUMBER(s): F19628-82-C-0001
9. PERFORMING ORGANIZATION NAME AND ADDRESS: The MITRE Corporation, P. O. Box 208, Bedford, MA 01730	10. PROGRAM ELEMENT, PROJECT, TASK AREA & WORK UNIT NUMBERS: Project No. 4290
11. CONTROLLING OFFICE NAME AND ADDRESS: Deputy/Mission Support Systems, Electronic Systems Division, AFSC, Hanscom Air Force Base, MA 01731	12. REPORT DATE: APRIL 1982
	13. NUMBER OF PAGES: 112
14. MONITORING AGENCY NAME & ADDRESS(if different from Controlling Office)	15. SECURITY CLASS. (of this report): UNCLASSIFIED
	15a. DECLASSIFICATION DOWNGRADING SCHEDULE

16. DISTRIBUTION STATEMENT (of this Report)

Approved for public release; distribution unlimited

17. DISTRIBUTION STATEMENT (of the abstract entered in Block 20, if different from Report)

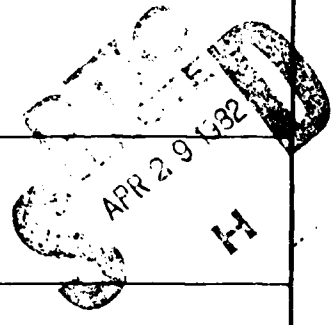

18. SUPPLEMENTARY NOTES

19. KEY WORDS (Continue on reverse side if necessary and identify by block number)

APATS
ARIA
MULTIPATH

20. ABSTRACT (Continue on reverse side if necessary and identify by block number)

It is anticipated that multipath propagation interference due to reflection from the sea will degrade APATS (ARIA Phased Array Telemetry System) reentry vehicle (RV) telemetry links. However, it is often feasible to reduce such interference by proper tailoring of the receiver position to the RV reentry parameters and telemetry characteristics. Theoretical analyses are presented which advocate specific ARIA flight constraints for several examples of P-band and S-band links in the context of nominal RV-aircraft (APATS) configurations. Issues such as APATs antenna gain, intersymbol interference, coherent (over)

DD FORM 1 JAN 73 1473

UNCLASSIFIED
SECURITY CLASSIFICATION OF THIS PAGE (When Data Entered)

20. (concluded)

and incoherent reflection from the sea, RV antenna gain, differential Doppler, RV-APATS geometry and RV trajectory are addressed in sufficient generality to permit application of basic multipath mitigation principles to a wide range of mission scenarios.

ACKNOWLEDGMENTS

This report has been prepared by The MITRE Corporation under Project No. 4290. The contract is sponsored by the Electronic Systems Division, Air Force Systems Command, Hanscom Air Force Base, Massachusetts.

TABLE OF CONTENTS

LIST OF ILLUSTRATIONS

LIST OF ILLUSTRATIONS (CONTINUED)

LIST OF ILLUSTRATIONS (CONTINUED)

LIST OF ILLUSTRATIONS (CONCLUDED)

LIST OF TABLES

SECTION I

INTRODUCTION AND SYNOPSIS

Occasionally telemetry links between missiles or reentry vehicles (RVs) and airborne receiving platforms such as the ARIA (Advanced Range Instrumentation Aircraft) exhibit "anomalous" degradation. If the link performance is seriously impaired, an investigation is undertaken to identify the source of the difficulty and determine what remedial actions, if any, are appropriate. Anomalous degradation of RV-ARIA links at both P-band and S-band[1] has been reported, and in the former case a detailed analysis [2] indicates that the data quality suffered as a result of multipath interference due to reflection from the sea. Furthermore, this study recommends that the ARIA telemetry support position (TSP) altitude be constrained in order to limit relative multipath channel delays to 10% or less of the telemetry bit period for the lower segment of the RV trajectory. In practice these constraints have led to typical TSP altitudes of 2.4 km (8,000 ft.) or less.

Since the APATS will operate at S-band and all terminal test area reentry missions supported by the ARIA are now at S-band (2.2 - 2.3 GHz), it is legitimate to question the applicability of flight constraints predicated upon multipath degradation experienced at P-band. The effectiveness and justifiability of these altitude recommendations must be scrutinized since low TSP altitudes adversely impact fuel consumption and aircraft environment control, and therefore reduce the ARIA's time on station.

This report presents a detailed theoretical investigation of multipath propagation for RV-ARIA telemetry links at both S- and P-band, with emphasis on the TSP altitude dependence of the

interference. The factors upon which multipath interference severity depends, in the context of the overall terminal area geometry, include,

1) RV antenna gain pattern,

2) Receiving antenna directivity,

3) Relative path delay (line-of-sight vs. reflected),

4) Relative path Doppler shifts, and

5) Coherent and incoherent forward sea scatter for various sea states, for the appropriate transmitted carrier frequency.

This work also places great emphasis on the impact which RV antenna pattern nulls can have on multipath, and investigates the relationship between receiver altitude, RV trajectory and RV antenna gains in the line-of-sight and reflected (specular) path directions.

It has been determined that selection of a near-optimum TSP altitude is feasible if most of the following mission parameters are known:

1) RF carrier frequency (e.g. S-band),

2) Serial bit rate employed for the telemetry modulation format,

3) RV penetration angle,

4) Approximate RV-ARIA baseline separation near splashdown, and

5) Sea surface roughness as characterized by, for example, sea state number.

This investigation also concludes that TSP altitude constraints recommended for P-band telemetry acquisition are not, in general, appropriate for S-band telemetry reception since,

1) The beamwidth of the receiving antenna is much smaller at S-band than at P-band,

2) Attenuation of the coherent power in the sea-reflected channel caused by sea surface roughness is much greater at S-band than at P-band for non-smooth sea states and typical grazing angles of incidence, and, to a lesser extent,

3) The Fresnel reflection coefficients for sea water at S-band are significantly different from those at P-band for vertical polarization.

When consideration 1) above is combined with a stipulation of 10% or less intersymbol interference in the multipath environment, maximum ARIA TSP altitudes, as a function of bit rate, can be calculated, and appear in tables 1 and 2 for P-band and S-band telemetry respectively. These findings, which are discussed in detail in the next section, provide a rough guide only, since several other factors must be considered when choosing an ARIA TSP, as illustrated by the examples which appear in section IV of this report. For example, lower TSP altitudes will reduce RV antenna gain imbalances of the line-of-sight and specular channel and therefore alleviate fades associated with nulls in the RV antenna pattern. For a given ARIA TSP, the fades associated with these nulls will be worst for RVs with trajectories having low penetration angles.

TABLE 1 (P-BAND, 226 MHz)

MAXIMUM TSP ALTITUDE FOR 10% INTERSYMBOL INTERFERENCE

MAXIMUM SERIAL BIT RATE (kBs^{-1})	MAXIMUM ARIA TSP ALTITUDE km (kft.)		
	Reentry Vehicle - ARIA BASELINE km (n mi)		
	20 (10.8)	40 (21.6)	60 (32.4)
10	10.9* (36.0)	11.4* (37.6)	11.6* (38.3)
15	6.2 (21)	6.8 (21)	7.0 (23)
20	4.6 (15)	5.1 (17)	5.2 (17)
30	3.0 (9.9)	3.4 (11)	3.5 (12)
40	2.2 (7.4)	2.5 (8.4)	2.6 (8.6)
60	1.5 (4.9)	1.7 (5.6)	1.7 (5.7)
80	1.1 (3.7)	1.3 (4.2)	1.3 (4.3)
100	0.9 (3.0)	1.0 (3.3)	1.0 (3.4)
120	0.7 (2.5)	0.8 (2.8)	0.9 (2.9)
160	0.6 (1.8)	0.6 (2.1)	0.6 (2.1)
200	0.5 (1.7)	0.5 (1.7)	0.5 (1.7)

*Under most circumstances the ARIA is not capable of altitudes greater than 9.4 km (31 kft.)

TABLE 2 (S-BAND, 2.26 GHz)

MAXIMUM TSP ALTITUDE FOR 10% INTERSYMBOL INTERFERENCE

MAXIMUM SERIAL BIT RATE (kBs^{-1})	MAXIMUM ARIA TSP ALTITUDE km (kft.)		
	Reentry Vehicle - ARIA BASELINE km (n mi)		
	20 (10.8)	40 (21.6)	60 (32.4)
100	10.8* (35.6)	11.3* (37.3)	11.5* (37.9)
120	7.9 (26)	8.5 (28)	8.7 (29)
140	6.6 (22)	7.3 (24)	7.5 (25)
160	5.8 (21)	6.3 (21)	6.5 (22)
200	4.5 (15)	5.0 (17)	5.2 (17)
240	3.7 (12)	4.2 (14)	4.3 (14)
300	3.0 (9.8)	3.4 (11)	3.5 (11)
400	2.2 (7.3)	2.5 (8.3)	2.6 (8.5)
500	1.8 (5.9)	2.0 (6.6)	2.1 (6.8)
750	1.2 (3.9)	1.3 (4.4)	1.4 (4.6)
1000	0.9 (3.0)	1.0 (3.3)	1.0 (3.3)
1500	0.6 (2.0)	0.7 (2.3)	0.7 (2.3)

*Under most circumstances the ARIA is not capable of altitudes greater than 9.4 km (31 kft.)

The remainder of this report is organized into three sections: Section II covers the multipath environment in three subsections devoted to the receiving antenna gain, RV antenna gain, and reflection from the sea. Section III addresses RF power fading in two subsections concerned with fade depth and fade frequency, respectively. In section IV ARIA TSP altitude recommendations are discussed in the context of the preceding analysis for both P- and S-band mission support under a variety of circumstances.

SECTION II

THE MULTIPATH ENVIRONMENT AT S-AND P-BAND

Low altitude (less that 8,000 ft.) TSPs extensively used for ARIA missions are intended to minimize intersymbol interference, which is believed to be responsible for periods of link degradation experienced during some high altitude (30,000 ft.) ARIA missions at P-band[2]. Intersymbol interference, in this context, refers to the amount of overlap of the line-of-sight channel bit stream and its delayed replica(s) from the multipath channel(s), expressed as a percentage of the bit period. The bit error rate (BER) caused by intersymbol interference is a function of bit stream redundancy, the relative level of the delayed stream, and the length of the delay. Low altitude TSPs reduce relative channel delay, as will be shown in this report, and thus reduce intersymbol interference.

Since, as indicated by the analysis referred to earlier[2], the geometrical relationship between the telemetry transmitter and receiver is crucial and central to an understanding of multipath interference, the comparison of S-and P-band multipath is performed in the context of a basic two path propagation model which has been elaborated upon elsewhere[3]. This model incorporates the RV trajectory, RV antenna gain, RV roll, receiving antenna gain and receiver position. In addition to these considerations, the reflection from the sea surface is characterized by the Fresnel reflection coefficients and a sea state dependent coherent power attenuation factor.

1. Receiving Antenna Gain

A. Defining the Severe Multipath Environment

The ARIA receiving antenna directivity or gain can provide considerable discrimination against the reflected channel power, which arrives at a different angle than the direct (line-of-sight) channel power. If the ARIA antenna tracks the RV, the antenna main beam direction is coincident with the direct path ray, and the specular path signal is received with less gain as illustrated in figure 1. When the RV is at an altitude A_1, the angular separation of the two paths is large compared to the antenna mainbeamwidth and the specular signal is suppressed in the sidelobes, however, if the antenna sidelobe levels are high, the discrimination provided may not be sufficient to compensate for the gain pattern of the RV antenna - a topic discussed in detail later. When the RV is at altitude A_2, as illustrated in figure 1, the specular beam power is reduced by only 3 dB relative to the direct beam power if it is assumed that the sea surface is a perfect reflector. The following criterion will be used to define the "severe multipath environment": The severe multipath interference environment obtains when the angular separation of the direct and specular rays at the ARIA antenna is less than one half of the 3 dB mainbeamwidth. It should be emphasized that this criterion is primarily used for comparision of the S- and P-band multipath environments, and does not imply that serious multipath degradation of the link will not occur when the criterion is not satisfied.

If the criterion discussed above is adopted, the severe multipath environment exists for an RV-ARIA geometry characterized by baseline B_2 and ARIA height H_A when the RV altitude A is less than A_2, which is determined by,

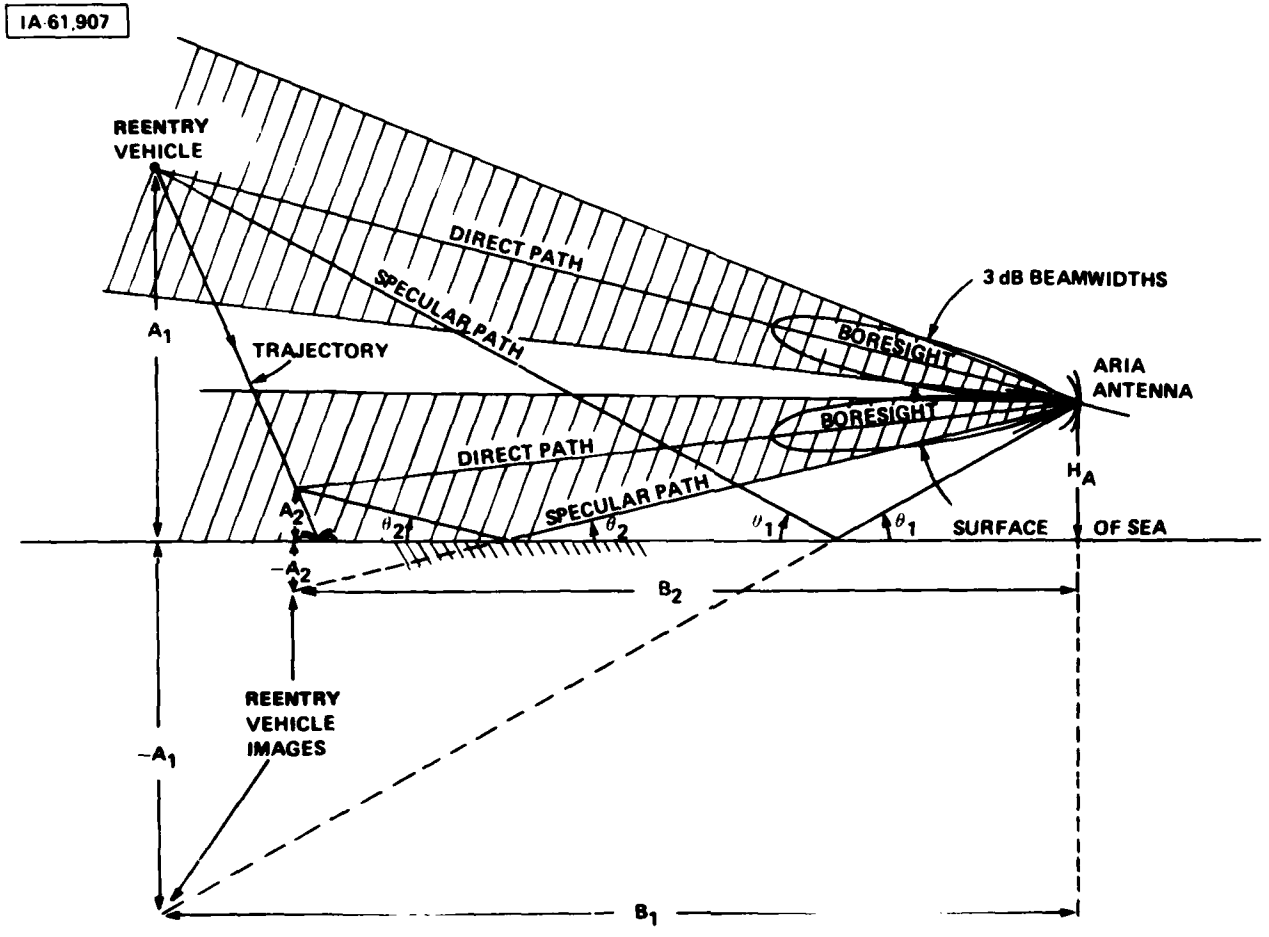

Figure 1. MULTIPATH ENVIRONMENT AS DEFINED BY RECEIVING ANTENNA

$$\tan^{-1}\left(\frac{B_2}{H_A - A_2}\right) - \tan^{-1}\left(\frac{B_2}{H_A + A_2}\right) = \frac{W}{2} \qquad (1)$$

or, solving for A_2,

$$A_2 = \left[B_2^2 \left(1 + \frac{1}{\tan^2\left(\frac{W}{2}\right)} \right) + H_A^2 \right]^{\frac{1}{2}} - \frac{B_2}{\tan\left(\frac{W}{2}\right)} \qquad (2)$$

in which W is the 3-dB beamwidth of the receiving antenna.

Using the 3-dB beamwidth formula for parabolic dish antennas[5],

$$W = 51\left(\frac{\lambda}{a}\right) \qquad (3)$$

in which λ is the RF wavelength and a is the diameter (2.1 m) of the ARIA dish antenna (or phased array antenna vertical dimension) values of 3.2^{o} and 32.3^{o} are obtained for the S-band (2.26 GHz) and P-band (226 MHz) 3 dB beamwidths, respectively. These values are consistant with the S-band (29 dBi) and P-band (12 dBi)[5] antenna gains.

Figure 2 illustrates the dependence of A_2, the altitude at which the RV enters the severe multipath environment, upon the RV-ARIA baseline, B_2, and the ARIA altitude, H_A, for S-band, while figure 3 illustrates the relationship among the same variables at P-band. Note that for each case A_2 is not very dependent upon the ARIA altitude unless the baseline is less than about 20 km - a situation which in practice should not occur because of range safety restrictions. For baselines greater than about 15 km, A_2 increases nearly linearly with baseline. Note also that for P-band reception the severe multipath environment is approximately 10 times larger than for S-band reception for a given baseline.

Assuming that the reflected, interfering signal has a strength comparable to the direct signal, the most important parameter used to

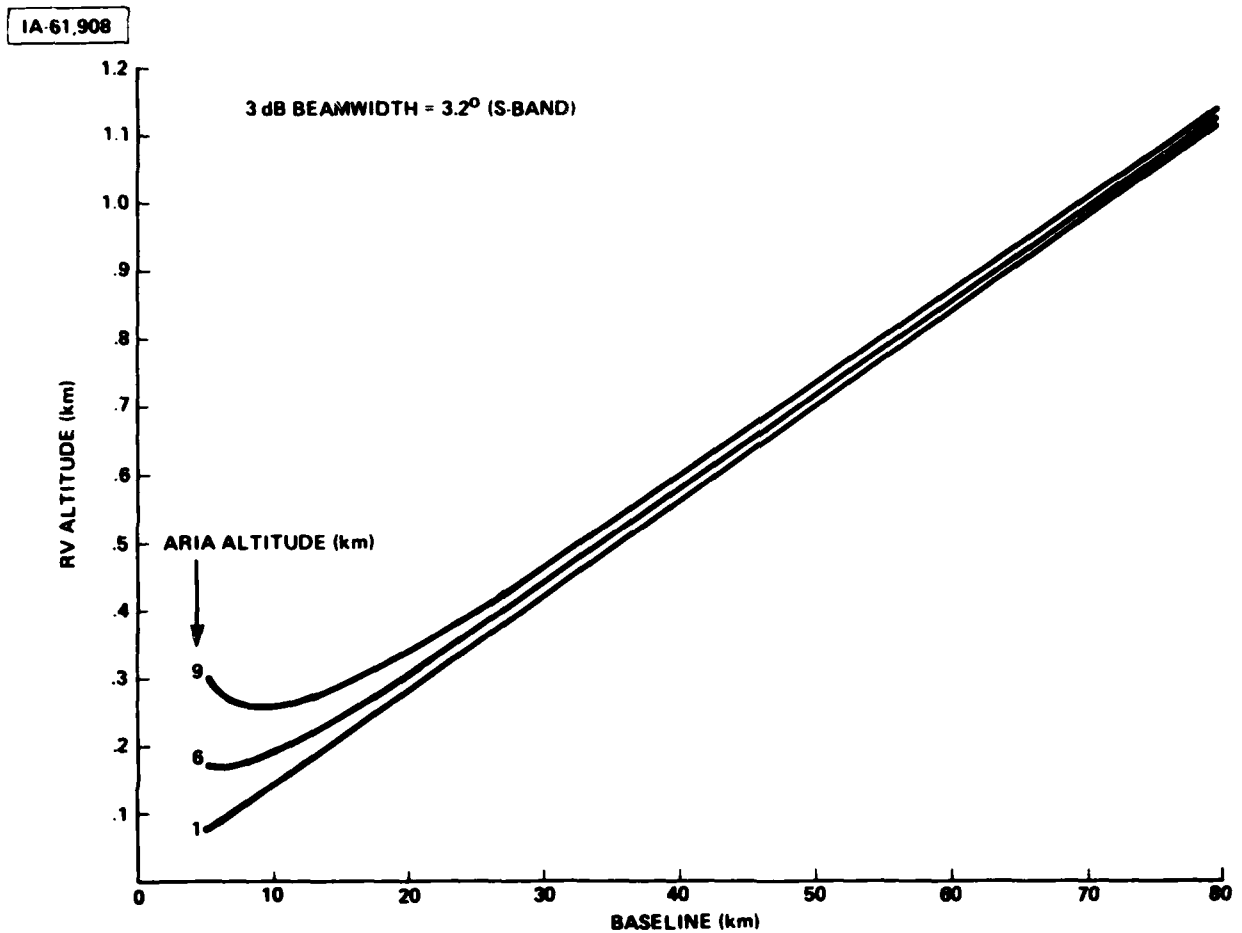

Figure 2. S-BAND SEVERE MULTIPATH ENVIRONMENT THRESHOLD VERSUS BASELINE SEPARATION

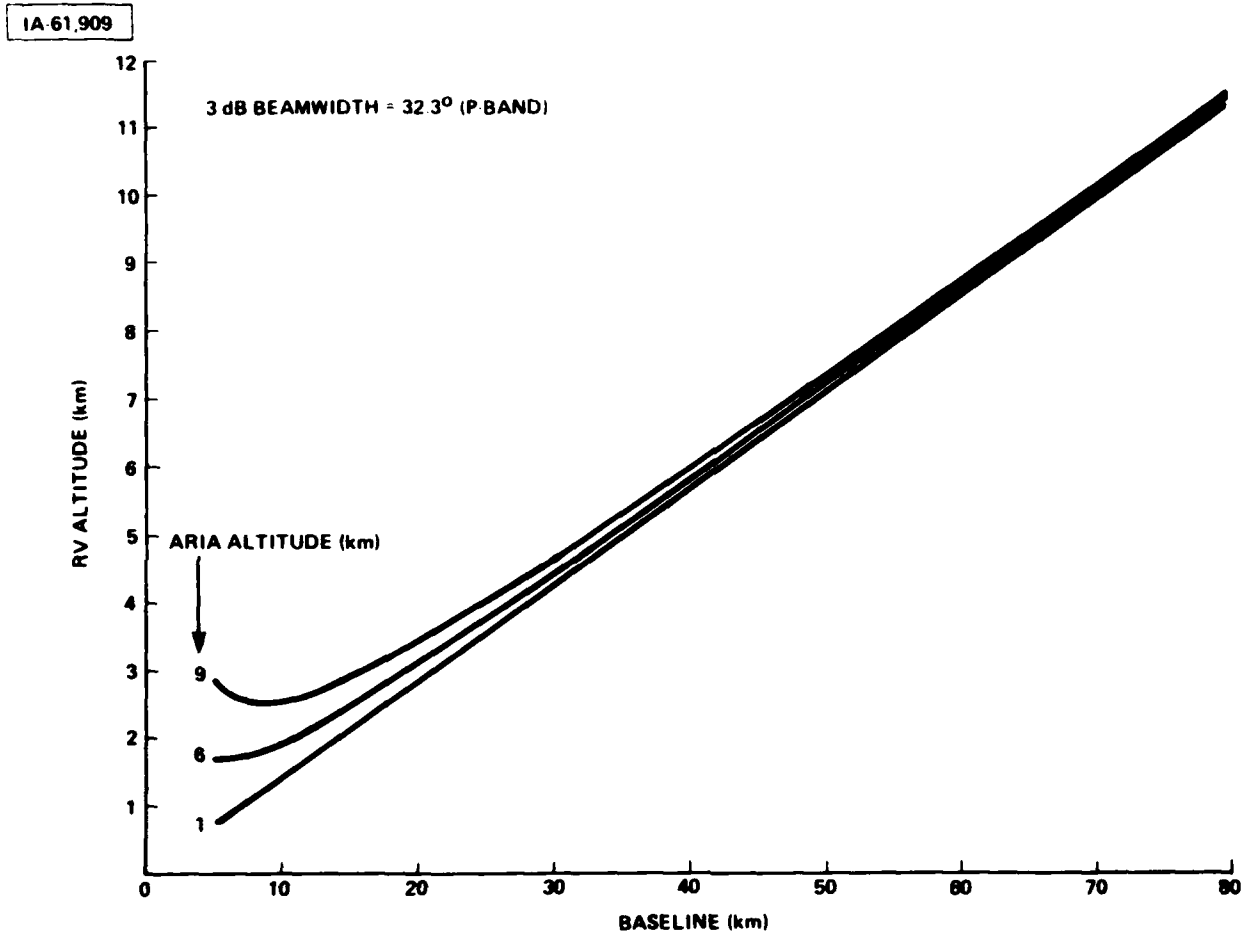

Figure 3. P-BAND SEVERE MULTIPATH ENVIRONMENT THRESHOLD VERSUS BASELINE SEPARATION

gauge the severity of the link degradation is the ratio of the relative channel delay to the bit period. The relative channel delay, in the context of the flat earth model geometry , is a purely geometrical quantity given by,

$$\tau = \frac{1}{c}\left[\left(B^2-(H_A+A)^2\right)^{\frac{1}{2}} - \left(B^2-(H_A-A)^2\right)^{\frac{1}{2}}\right] \qquad (4)$$

in which c is the velocity of light. In figures 4, 5 and 6 the relative delay versus ARIA altitude is plotted for a series of RV altitudes, for RV-ARIA baselines of 20 km, 40 km and 60 km respectively. Note in Eq. (4) that τ is symmetrical in H_A and A, so that figures 4, 5 and 6 are also valid with the RV altitude and ARIA altitude labels interchanged. The relative delay increases nearly linearly with RV or ARIA altitude for a given baseline, and decreases with increasing baseline for given RV and ARIA altitudes.

B. Preliminary ARIA Altitude Recommendations

Telemetry data analysis indicates that 10% intersymbol interference is tolerable and may be used as an upper limit in the multipath environment[6]. For a given RV-ARIA baseline and bit rate it is therefore possible to determine a maximum ARIA altitude at which intersymbol interference is 10% when the RV is on the threshold of the multipath environment defined by the receiving antenna beamwidth. Consider this example: if a bit rate of 200 kb/s is assumed, the maximum relative channel delay is 0.5 μs. If the RV-ARIA baseline is 60 km, the severe multipath region begins at an RV altitude of about 9 km at P-band and 0.9 km at S-band. Examination of figure 6 reveals that the 0.5 μs relative channel delay will not be exceeded while the RV is in the multipath environment if the ARIA altitude is less than 0.5 km (1700 ft.) for P-band and 5 km (16,600 ft.) for S-band. Other examples of ARIA altitude constraints applicable for P- and S-band

IA-61,910

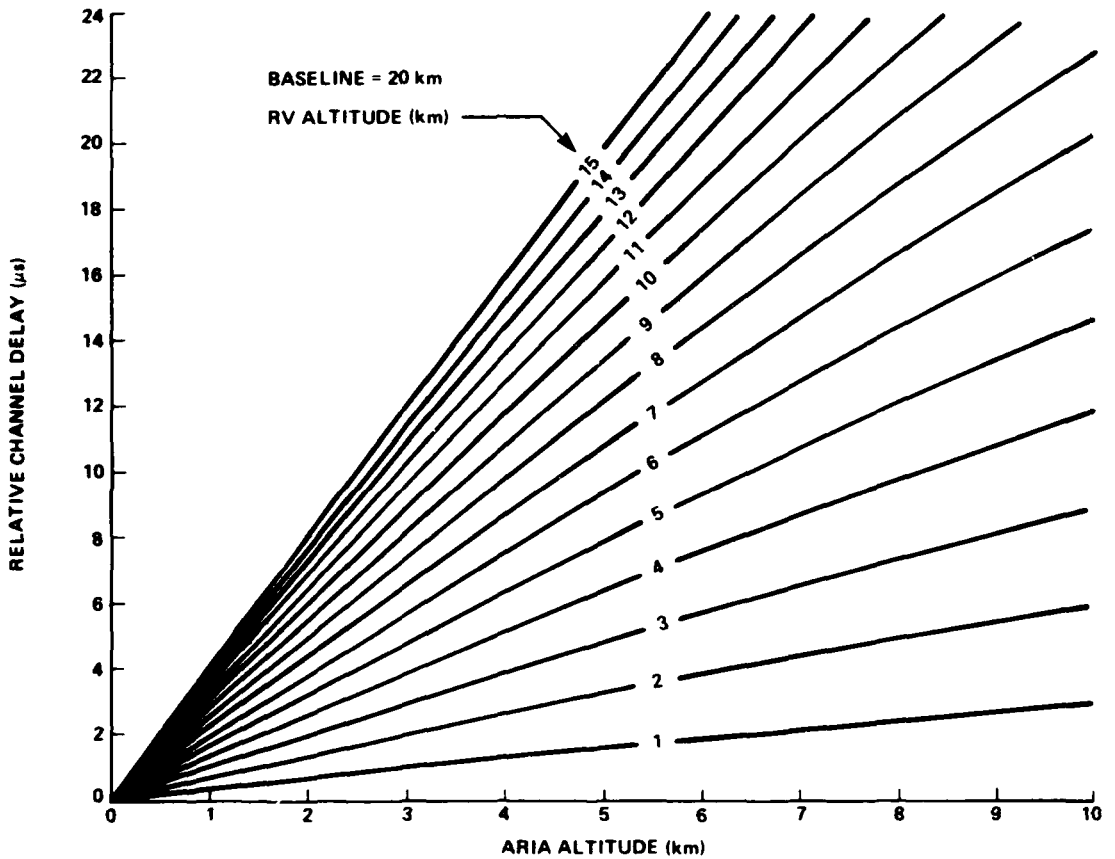

Figure 4. RELATIVE CHANNEL DELAYS FOR 20 km BASELINE

IA-61,912

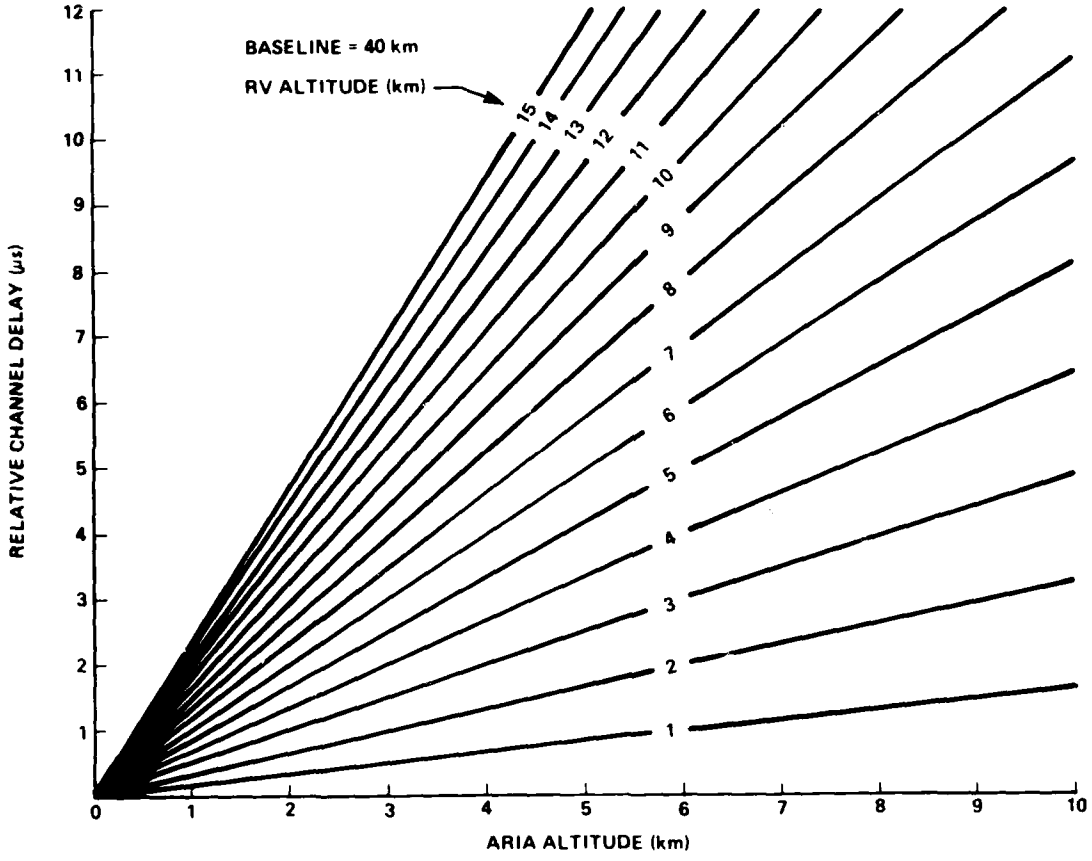

Figure 5. RELATIVE CHANNEL DELAYS FOR 40 km BASELINE

IA-61,913

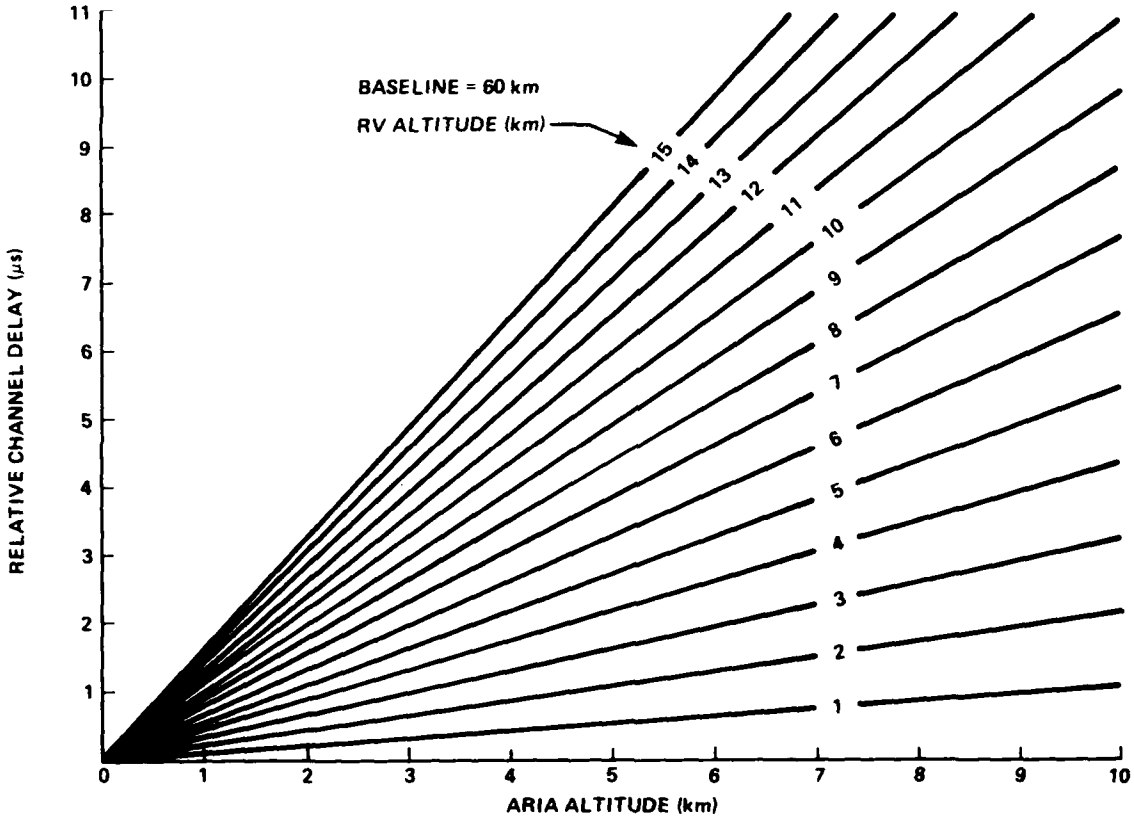

Figure 6. RELATIVE CHANNEL DELAYS FOR 60 km BASELINE

telemetry are given in tables 1 and 2 respectively. Note that the maximum ARIA altitudes for a particular bit rate are nearly independent of the RV-ARIA baseline, because the larger multipath region corresponding to a longer baseline is compensated for by the shorter relative path delays associated with the longer baseline. Note also that for those values of the bit rate for which the P and S-band constraints may be compared, the S-band telemetry may be supported at an altitude about 10 times greater than the maximum altitude recommended at P-band.

These results are useful for P- and S-band comparison, but the numerical values are based on assumptions that ignore important factors such as the RV antenna pattern, receiving antenna sidelobes, and sea state.

2. Transmitting Antenna Gain

A. The RV Antenna Pattern

Although the ARIA receiving antenna (APATS) gain is used to define the severe multipath environment, and the next section will show that the coherent power scattered from the sea surface increases as the RV descends, serious multipath losses can still occur for relatively high RV altitudes as a result of different RV antenna gains in the direct path and specular path directions.

Analysis is expedited by reference to the RV consolidated coordinate system (RVCCS) which is centered on and fixed to the RV antenna. The RVCCS polar axis is coincident with the RV longitudinal axis with its north pole in the direction of the RV nose as shown in figure 7. It is assumed that the RV rolls about its longitudinal axis with negligible wobble and that the RV velocity vector is parallel to the RVCCS polar axis.

An RV antenna pattern is typically characterized by six gain values per direction sampled in the RVCCS. The gain values, three of which are redundant for a polarized source, correspond to the powers associated with the linear polarization fields E_θ, E_ϕ, E_{45}, E_{135} and the circular polarization fields, E_{RH} and E_{LH}. Actual S-band antenna pattern data for a MK 12A RV reveals that nulls as deep as -30dBi and peaks as high as 10.7 dBi occur. The nulls tend to be arranged in groups which occupy narrow ranges of azimuth in the RVCCS. This is especially evident for the contour plot of the E_ϕ gains of figure 8.

RV antenna pattern measurements are typically performed at 2° increments in RVCCS azimuth and elevation. Thus if a minimum of three quantities (e.g. E_ϕ, E_θ, E_{RH}) are necessary to specify the field in a

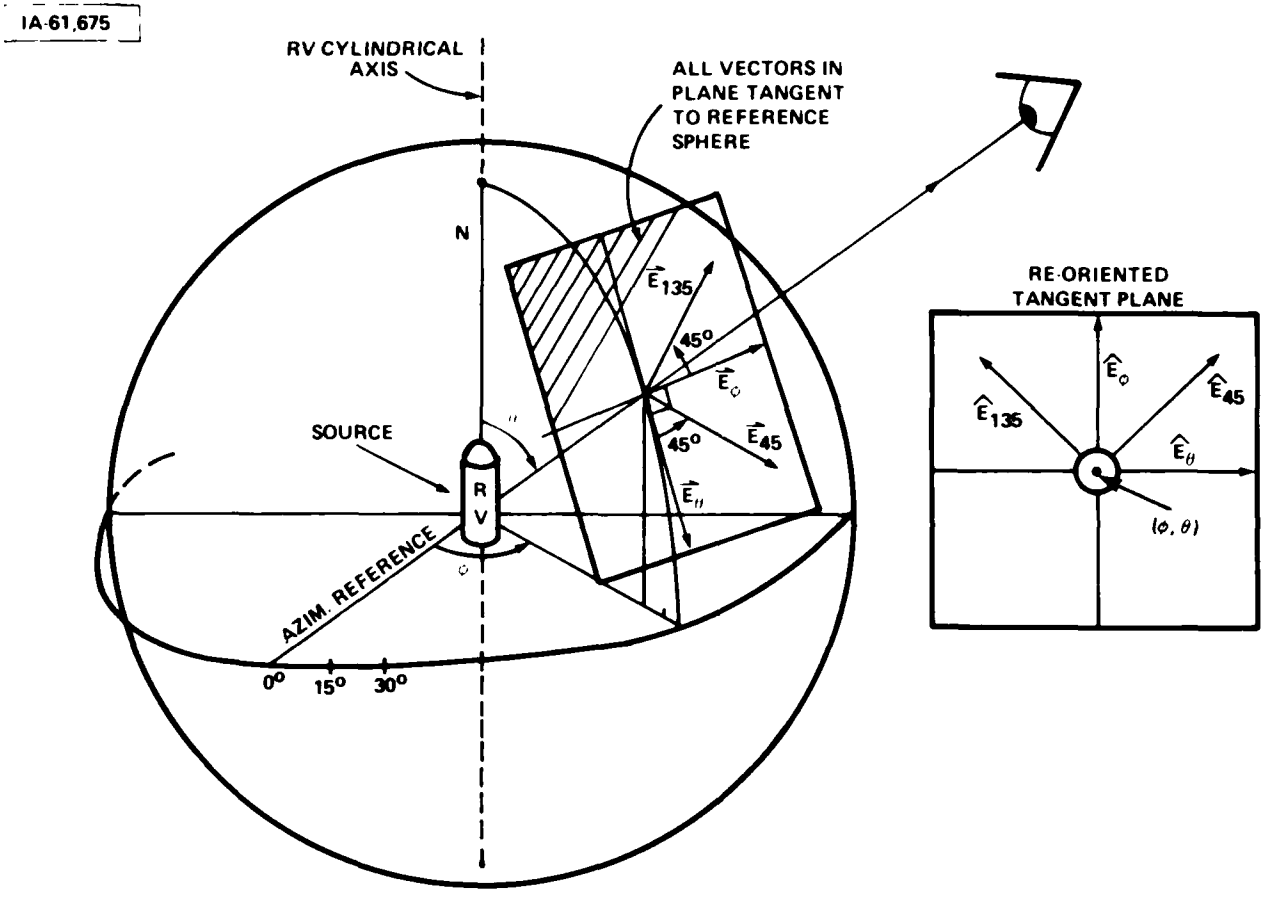

Figure 7. RV-ANTENNA CONSOLIDATED COORDINATE SYSTEM

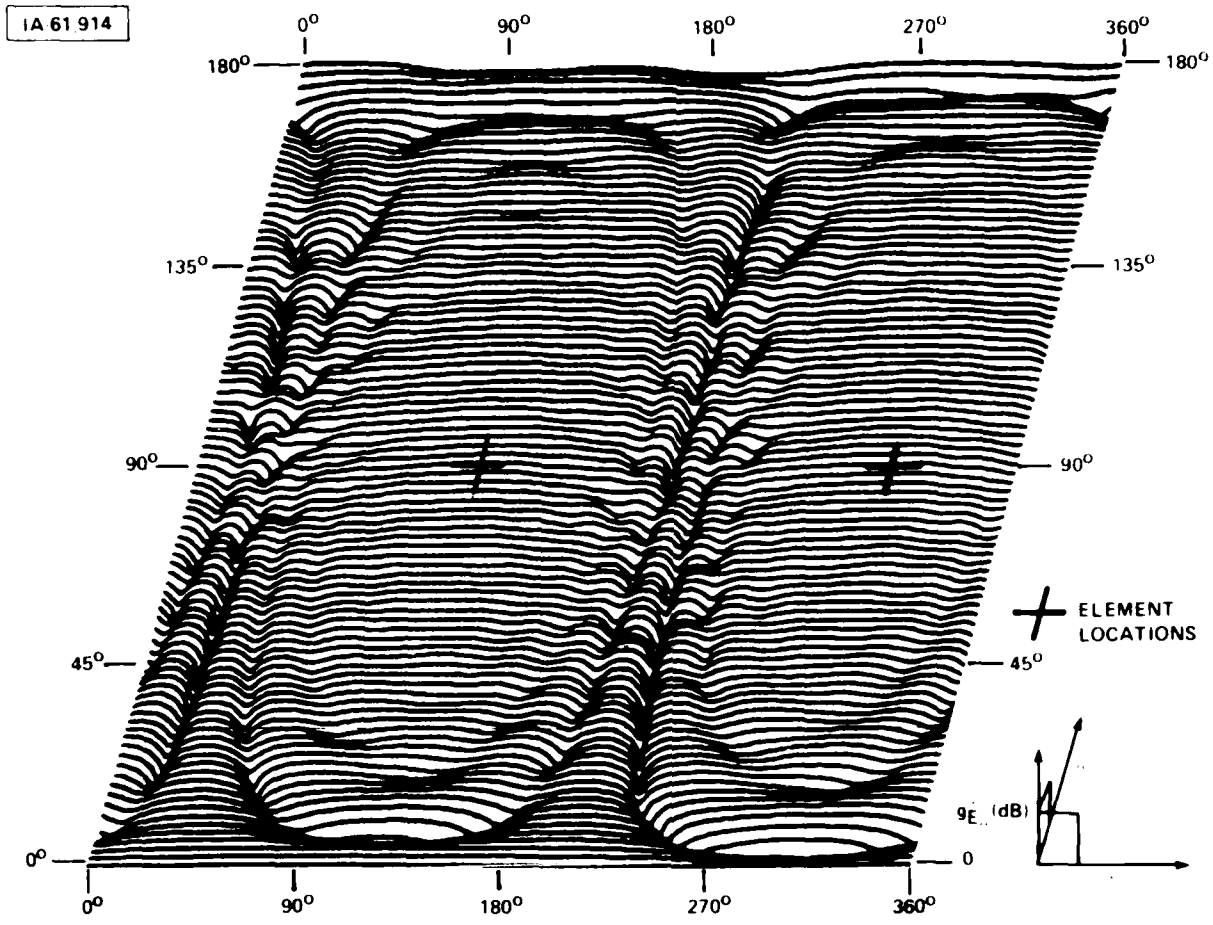

Figure 8. CONTOUR PLOT OF RV ANTENNA GAIN FOR $\hat{E}_\theta$ POLARIZATION DIRECTION

given direction, 180 x 91 x 3 = 49,140 numbers are required to characterize the entire RV antenna pattern. Ideally, these data would be stored in computer memory and retrieved when needed for multipath model calculations.

B. The RV Trajectory

The two-path multipath model geometry indicates that the line-of-sight path ray and reflected specular path ray originate from different directions in the RVCCS as illustrated in figure 9. If D, S and V are unit vectors in the direct, specular, and RV velocity directions respectively, then the direct and specular ray aspect angles in the RVCCS are,

$$\theta_D = \cos^{-1}[\hat{V} \cdot \hat{D}] \tag{5}$$

$$\theta_S = \cos^{-1}[\hat{V} \cdot \hat{S}] \tag{6}$$

and the magnitude of the separation of the rays in azimuth, Δ, is given by[12],

$$|\Delta| = \cos^{-1}\left[\frac{\hat{V} \times \hat{D} \cdot \hat{V} \times \hat{S}}{\sin\theta_D \sin\theta_S}\right] \tag{7}$$

From figure 8 it is evident that a Δ of as little as 12^o is sufficient to place the direct path ray in an antenna null while the specular path ray enjoys relatively high gain for short intervals in the course of RV rotation. Interference from the reflected field will obviously be most serious during these intervals. Although polarization diversity reception will greatly alleviate the direct signal drop-outs caused by RV antenna nulls, it is not unusual for nulls to overlap or occur simultaneously for both polarizations.

IA 61,896

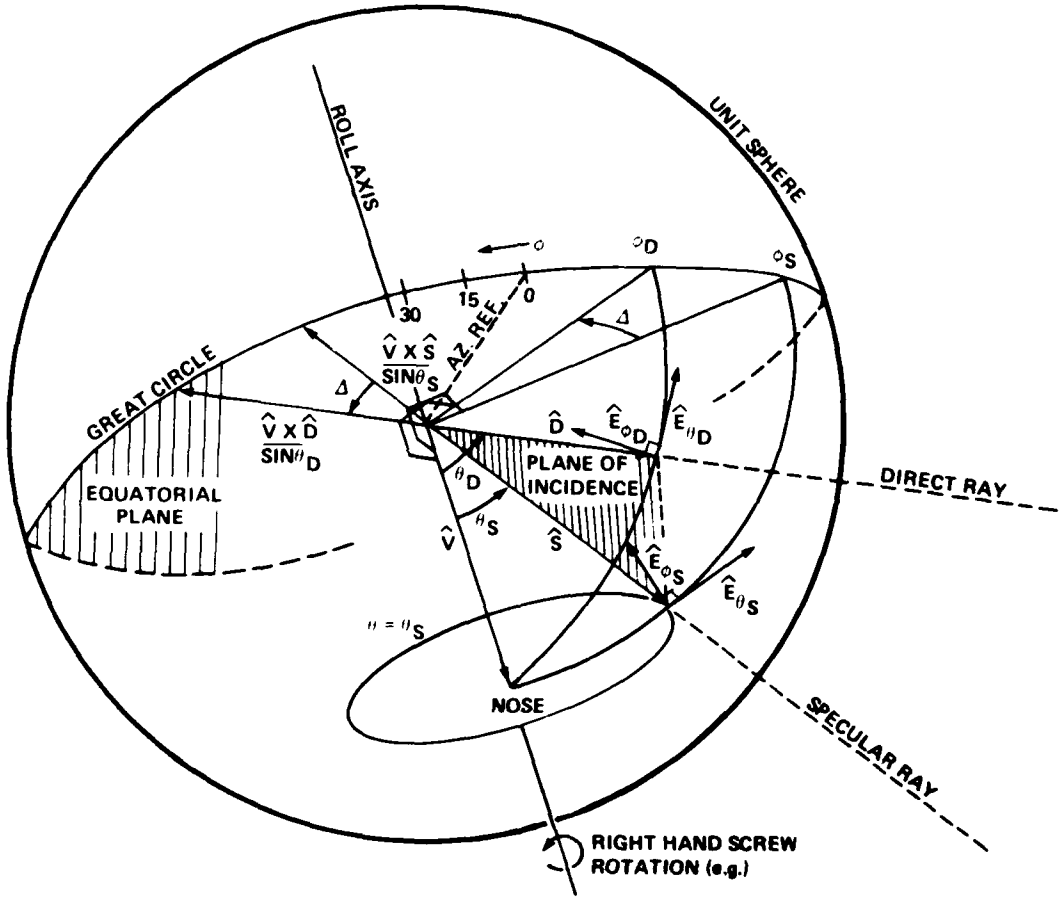

Figure 9. DIRECT AND SPECULAR RAYS REFERENCED TO RVCCS

Figure 10 illustrates the simplified local coordinate system geometry used for calculations whose results are presented here and in section III. It is instructive to calculate the azimuth angle and elevation angle differences between the direct and specular rays in the RVCCS as a function of ARIA altitude for a fixed RV position and orientation. RV position is denoted by specifying the baseline, B, and altitude, A, in the context of figure 10. The RV orientation is characterized by the velocity unit vector, which is taken as indicative of the RV trajectory in the multipath environment. A trajectory is denoted as "trans" if the RV motion is predominantly perpendicular to the line-of-sight and is denoted as "para" if the RV motion is predominantly parallel to the line-of-sight. A trajectory which conforms to neither of these descriptions is designated as "nom" (nominal). Another useful descriptor for the RV trajectory is the penetration angle, γ, which is the angle between the RV unit velocity vector and the local horizontal. In this work, the penetration angle is characterized as low ($\gamma < 35^{o}$), "mid" ($35 \leq \gamma \leq 65^{o}$) or high ($\gamma > 65^{o}$).

In figure 11 the magnitude of the azimuthal difference angle, Δ is plotted as a function of ARIA altitude for several RV trajectories. The RV is fixed at an altitude of 1 km at a baseline separation of 60 km. In most cases Δ increases linearly with ARIA altitude and the rate of increase is, evidently, inversely proportional to γ. The aspect (elevation) angle difference between the direct and specular rays also increases linearly with ARIA altitude as indicated by the plots of figure 12. It bears repeating that these difference angles are referenced to the RVCCS and should not be confused with the azimuth and elevation of the RV with respect to the ARIA or receiving antenna coordinate system.

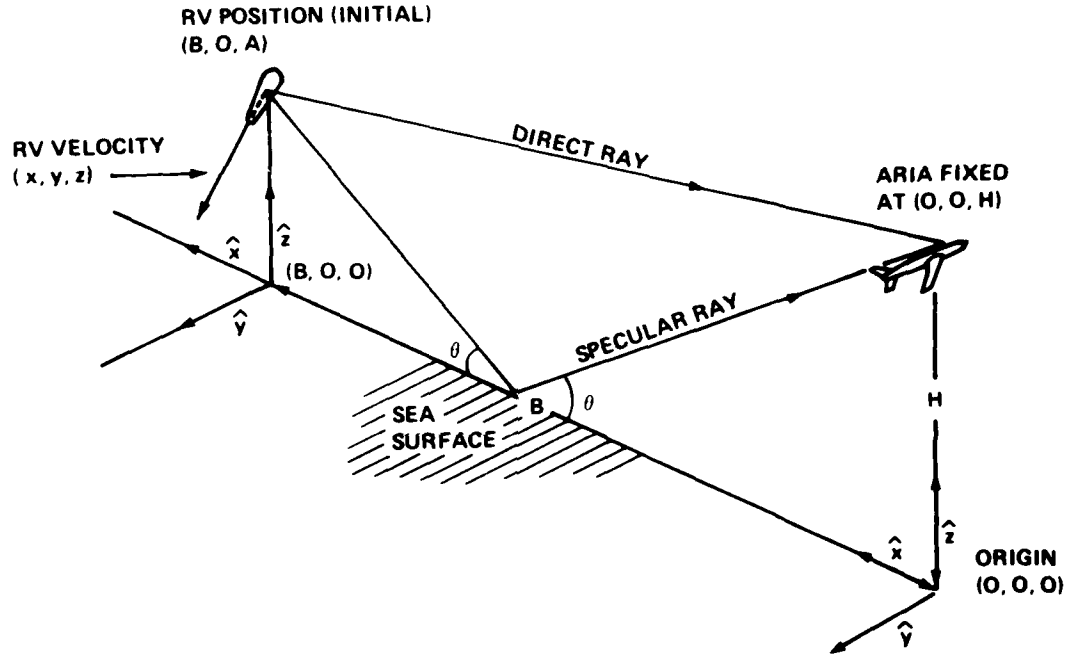

Figure 10. LOCAL COORD. SYSTEM FOR GEOMETRICAL CALCULATIONS

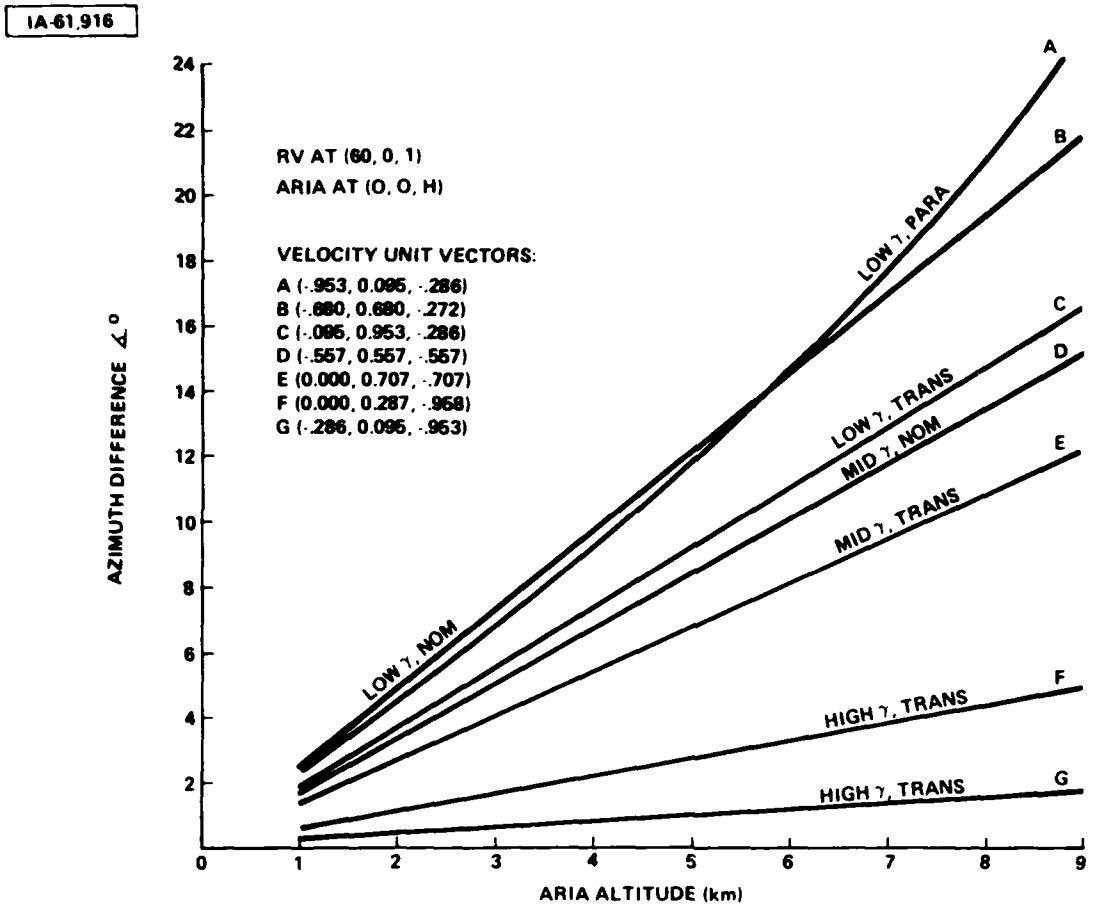

Figure 11. AZIMUTH DIFFERENCE ANGLE VERSUS ARIA ALTITUDE FOR SEVERAL RV TRAJECTORIES, A 60 km BASELINE AND RV ALTITUDE OF 1 km

IA-61,917

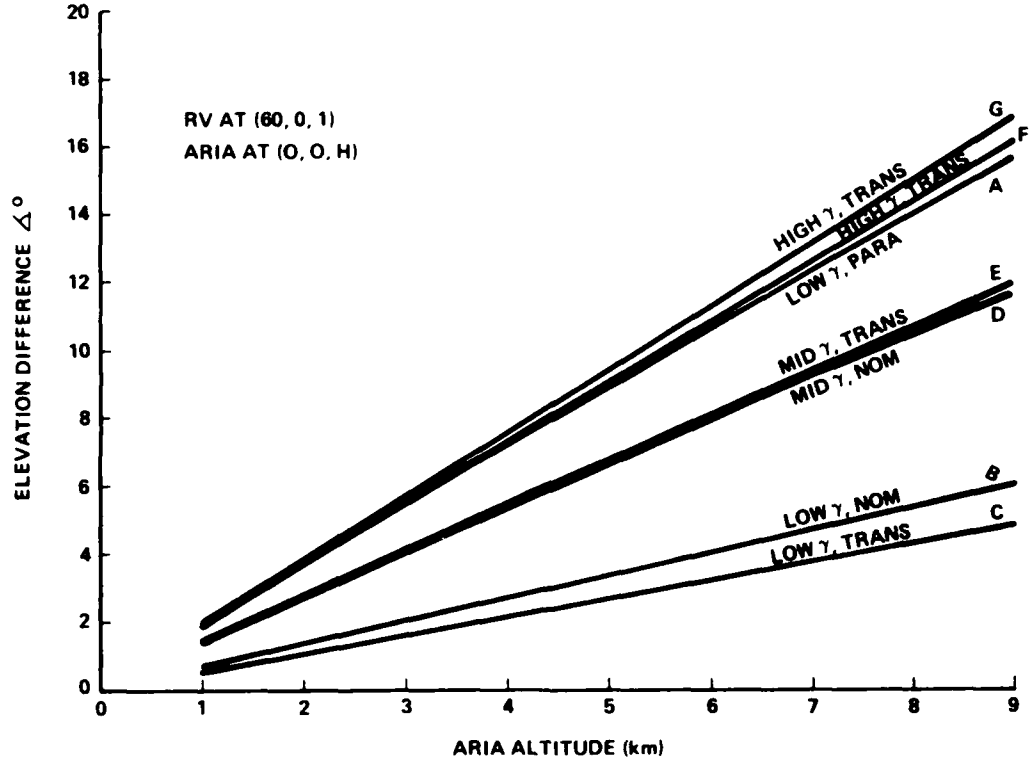

Figure 12. ELEVATION DIFFERENCE ANGLE VERSUS ARIA ALTITUDE FOR SEVERAL RV TRAJECTORIES, A 60 km BASELINE AND RV ALTITUDE OF 1 km

Since RV antenna pattern nulls, which are typically -20dBi to -30dBi for P[8] or S-band, tend to share relatively narrow ranges of RVCCS azimuth values, the azimuthal separation, Δ, will usually produce a much larger RV gain difference between the two paths than the aspect angle separation. From figure 8 it is evident that there will be two periods of large relative signal strength fluctuation per RV rotation if Δ is greater than approximately 5 degrees. The same conclusion would appear to be applicable for a P-band antenna pattern data published elsewhere[8].

The Δ results of figure 11 obtain for a 60-km baseline. If the baseline is shortened to 40 km the Δ values increase as displayed in figure 13. With the exception of case A, the Δ's vary inversely with RV-ARIA baseline (to a very good approximation).

In figure 14, Δ is plotted as a function of ARIA altitude for an RV at an altitude of 9 km and baseline of 60 km. Comparison with figure 11 indicates that, with the exception of trajectory A, the Δ's do not change significantly with RV altitude - at least within the range of the P-band severe multipath environment for a 60-km baseline.

The aberrant results obtained for case A devolve from the fact that it is only for this trajectory that the direct and specular path rays lie near the RVCCS polar axis. Small variations in the ray directions can cause large and non-linear changes in Δ. Figure 15 illustrates in more detail the relatively unusual variation of Δ as a function of ARIA altitude for several RV altitudes and a 40-km baseline for case A - a low γ trajectory close to the line-of-sight.

It is instructive to examine the case of an RV trajectory in the plane of incidence, as illustrated in figure 16. As long as the

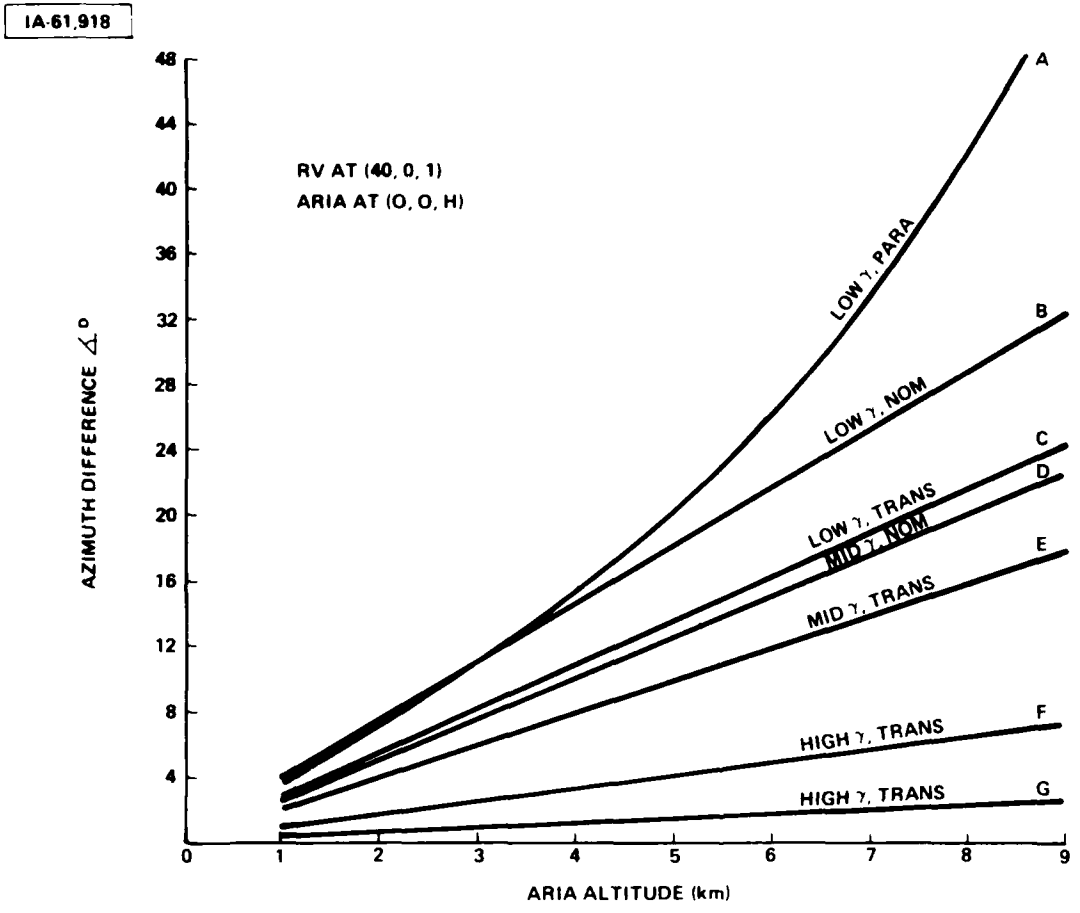

Figure 13. AZIMUTH DIFFERENCE ANGLE VERSUS ARIA ALTITUDE FOR SEVERAL RV TRAJECTORIES, A 40 km BASELINE AND RV ALTITUDE OF 1 km

IA-61,919

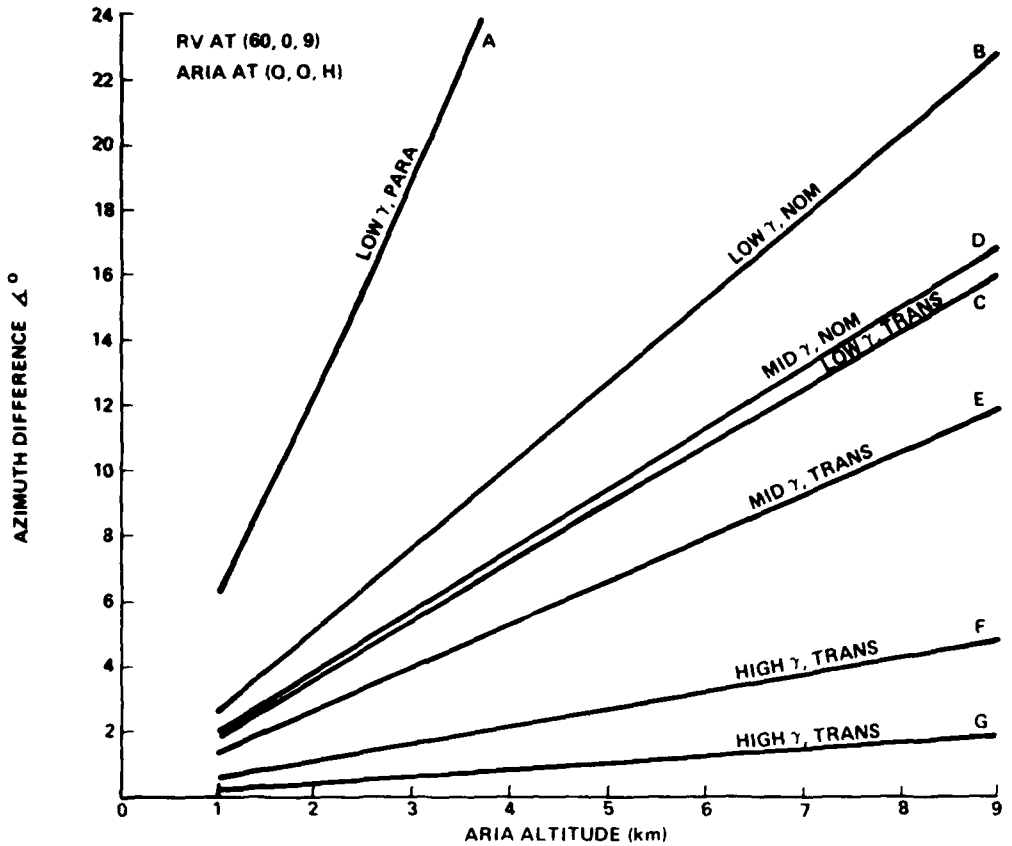

Figure 14. AZIMUTH DIFFERENCE ANGLE VERSUS ARIA ALTITUDE FOR SEVERAL RV TRAJECTORIES, A 60 km BASELINE AND RV ALTITUDE OF 9 km

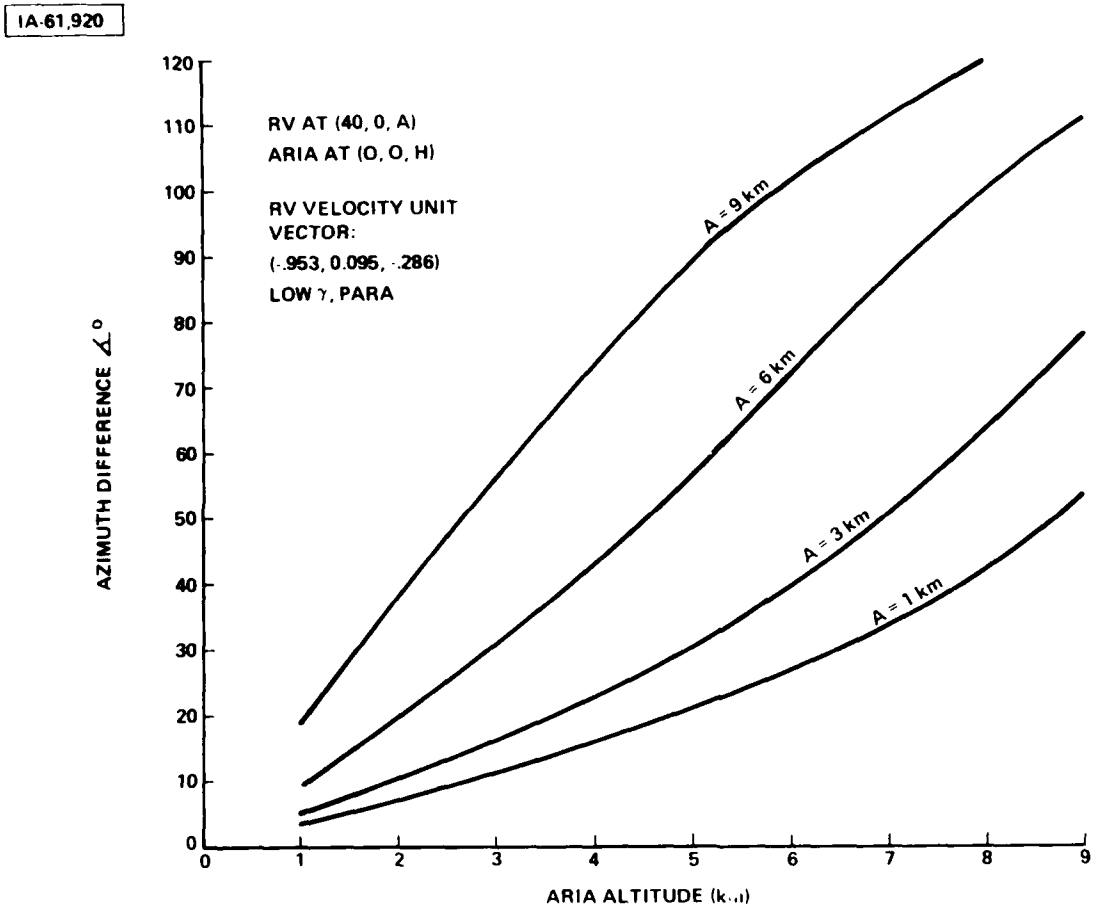

Figure 15 AZIMUTH DIFFERENCE ANGLE VERSUS ARIA ALTITUDE FOR SEVERAL RV ALTITUDES AND AN RV TRAJECTORY NEAR THE LINE OF SIGHT

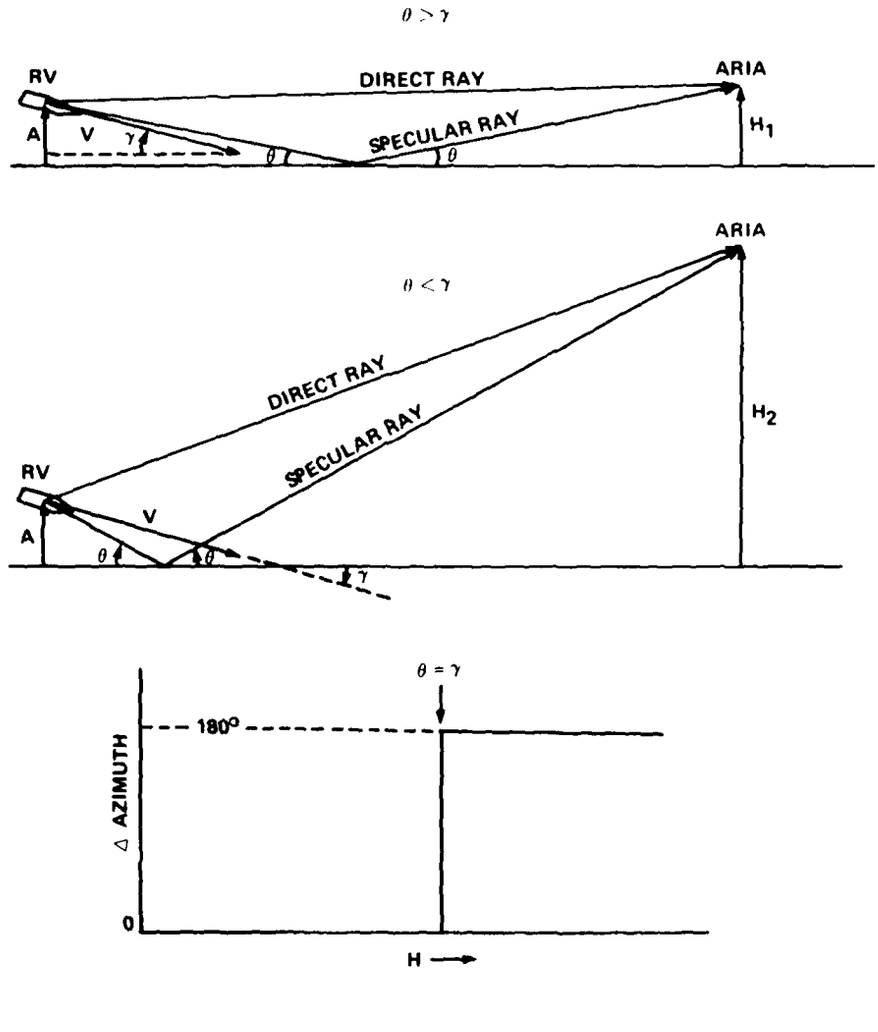

Figure 16. AZIMUTH DIFFERENCE ANGLE DEPENDENCE ON ARIA ALTITUDE FOR AN RV TRAJECTORY IN THE PLANE OF INCIDENCE OF THE SPECULAR RAY

grazing angle, θ, is less than γ, the azimuthal difference angle is zero. However, for θ greater than γ, which may occur for higher ARIA altitudes, as illustrated, Δ is 180^{o}. The transition at $\gamma = \theta$ is, in fact, a step function, as is also shown in figure 16.

The influence which the RV antenna pattern has on fading of the RF signal, in the context of the two path multipath model, is explored further in the next section.

3. Reflection From the Sea

A. The Fresnel Reflection Coefficients

If the sea surface were perfectly smooth and flat, reflection of electromagnetic waves would occur only in the specular direction and could be completely characterized by the Fresnel reflection *coefficients.* These coefficients, which are derived by applying Maxwell's equations at an interface, can be found in elementary textbooks on electricity and magnetism and are discussed at length with many examples in some books on propagation[9]. Since the reflected wave has undergone both a phase shift and amplitude reduction with respect to the incident wave, it is convenient to express the Fresnel coefficients as complex numbers which depend upon the polarization, wavelength, and grazing angle of the incident field, and the conductivity and relative dielectric constant of the reflecting medium. The horizontal polarization component is parallel to the plane of the surface, while the vertical polarization component lies in the plane of incidence.

In figure 17 the Fresnel coefficient amplitudes for representative wavelengths at P-and S-band are plotted for comparison over the range of grazing angles permitted by the RV-ARIA geometry with baselines as

IA-61,922

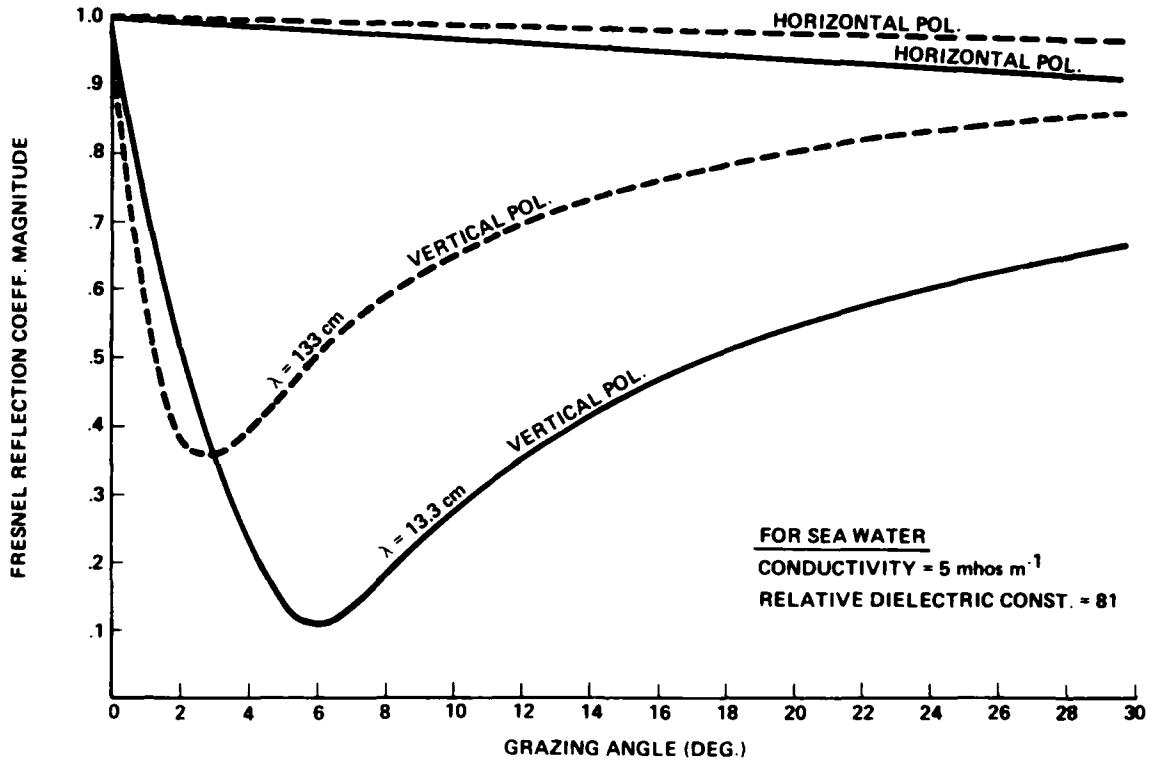

Figure 17. FRESNEL REFLECTION COEFFICIENT AMPLITUDES FOR TYPICAL WAVELENGTHS AT P AND S-BAND

short as 20 km when the RV is in the multipath environment. Although the conductivity of seawater can be as low as 3 mhos/m, the curves of figure 7 are not strongly altered by a variation of this size. For horizontal polarization, reflection is nearly complete for both P-and S-band, however, for vertical polarization, significant differences are evident. For grazing angles less ~ 3^{o} the P-band reflection has less strength, but for larger grazing angles the S-band reflection can be much weaker than that at P-band. Note that the vertical polarization coefficient magnitudes exhibit minima of 0.36 for 2.9^{o} at P-band and 0.114 for 6^{o} at S-band. This intrinsic suppression of the reflected power for vertical polarizaton (Brewster angle effect) may be exploited by the ARIA under certain circumstances to reduce multipath interference. Table 3 lists the appropriate ARIA altitude ranges for vertical polarization power reduction in the multipath environment for several baseline separations at P-and S-band.

B. The Coherent Reflected Power

Since the sea surface is not perfectly smooth or flat, the coherent power (defined below) reflected in the specular direction is reduced by surface roughness and divergence. For the short baselines which obtain for the multipath environment, the divergence, caused by the earth curvature of the mean sea surface, can be neglected; however, surface roughness will have a significant effect on the statistical distribution of the reflected power.

The coherent power is a statistical function of the normalized (complex) reflection coefficient which is defined on the set of surfaces whose profiles are characterized by a surface height random variable, h, and a surface autocorrelation coefficient function. The normalized reflection coefficient for the specular reflection direction is defined,

TABLE 3

ARIA ALTITUDES WHICH MINIMIZE VERTICAL POLARIZATION
SPECULAR POWER FOR SMOOTH* SEA STATES

RV-ARIA BASELINE	P-BAND (226 MHz) km (kft.)			S-BAND (2.26 GHz) km (kft.)		
	-6.0db (1.34°)	-9.0db (minimum)	-6.0db (6.02°)	-15.9db (4.78°)	-18.9db (minimum)	-15.9db (7.56°)
20	0.47 (1.5)	1.0 (3.3)	2.1 (7.0)	1.7 (5.5)	2.1 (7.0)	2.6 (8.8)
30	0.70 (2.3)	1.5 (5.0)	3.2 (10)	2.5 (8.3)	3.2 (10)	4.0 (13)
40	0.94 (3.1)	2.0 (6.6)	4.2 (14)	3.3 (11)	4.2 (14)	5.3 (17)
50	1.2 (3.9)	2.5 (8.3)	5.3 (17)	4.2 (14)	5.3 (17)	6.6 (22)
60	1.4 (4.6)	3.0 (9.9)	6.3 (21)	5.0 (17)	6.3 (21)	8.0 (26)
70	1.6 (5.4)	3.5 (12)	7.4 (24)	5.8 (19)	7.4 (24)	9.3 (31)
80	1.9 (6.2)	4.0 (13)	8.4 (28)	6.7 (22)	8.4 (28)	11 (35)

$$\rho \equiv \frac{E_h}{E_o} \tag{8}$$

in which E_0 is the field reflected by a perfectly smooth surface (h = 0), and the coherent power factor (CPF) is given by[10],

$$|\langle\rho\rangle|^2 = \langle\rho\rho^*\rangle - \langle|\rho - \langle\rho\rangle|^2\rangle \tag{9}$$

in which brackets denote ensemble averages, i.e., averages over the set of surfaces which are used to model the sea. The first term on the right is the average power reflected in the specular direction, and the second term represents the average incoherent power. For a perfectly smooth surface the incoherent term vanishes and the total power is coherent, and non-zero only in the specular direction (strictly true only if reflecting plane is infinite). For an ensemble of rough surfaces the coherent power represents the power associated with the average field amplitude, while the incoherent power is the power associated with amplitude fluctuations about the mean amplitude, i.e., the ensemble variance of the reflection coefficient.

Rough surface scattering models usually assume that the surface height random variable has a Gaussian probability density. This assumption leads to the following expression for the coherent power factor or "roughness factor"[11]:

$$|\langle\rho\rangle|^2 = \mathrm{EXP}(-g) \tag{10}$$

$$g^{1/2} = \frac{4\pi\sigma_h \sin\theta}{\lambda} \tag{11}$$

In the above, σ_h is the surface height standard deviation, θ is the grazing angle of incidence, λ is the electromagnetic wavelength, and $g^{1/2}$ is referred to as the Rayleigh parameter, which is a measure of apparent surface roughness.

Recent work[12] indicates that better agreement with experimental microwave sea-scatter data is obtained, especially for moderately rough surfaces, if a symmetrical, exponential surface height probability density is assumed. For the exponential density the roughness factor is given by[13]:

$$|\langle\rho\rangle|^2 = \left[1 + \frac{g}{2}\right]^{-2} \tag{12}$$

Note that for small values of the Rayleigh parameter, i.e., relatively smooth surfaces, both equations (10) and (12) yield,

$$|\langle\rho\rangle|^2 \cong 1 - g \tag{13}$$

However for rough surfaces, i.e., surfaces for which the Rayleigh parameter does not satisfy the Rayleigh criterion for smoothness[14],

$$g^{1/2} < \frac{\pi}{2} \tag{14}$$

Equation (10) seriously underestimates the coherent power.

The coherent power reflected by the sea, normalized to the incident power, is given by the product of the Fresnel coefficient magnitude and the CPF for each polarization;

Vertical Polarization: $$p_c^V = |F^V||\langle\rho\rangle|^2 \tag{15a}$$

Horizontal Polarization: $$p_c^H = |F^H||\langle\rho\rangle|^2 \tag{15b}$$

In the above, F represents the Fresnel coefficient. Note that the CPF is polarization independent. In figures 18 and 19 the vertical polarization CPF, P^V, is plotted as a function of grazing angle for

IA 61,923

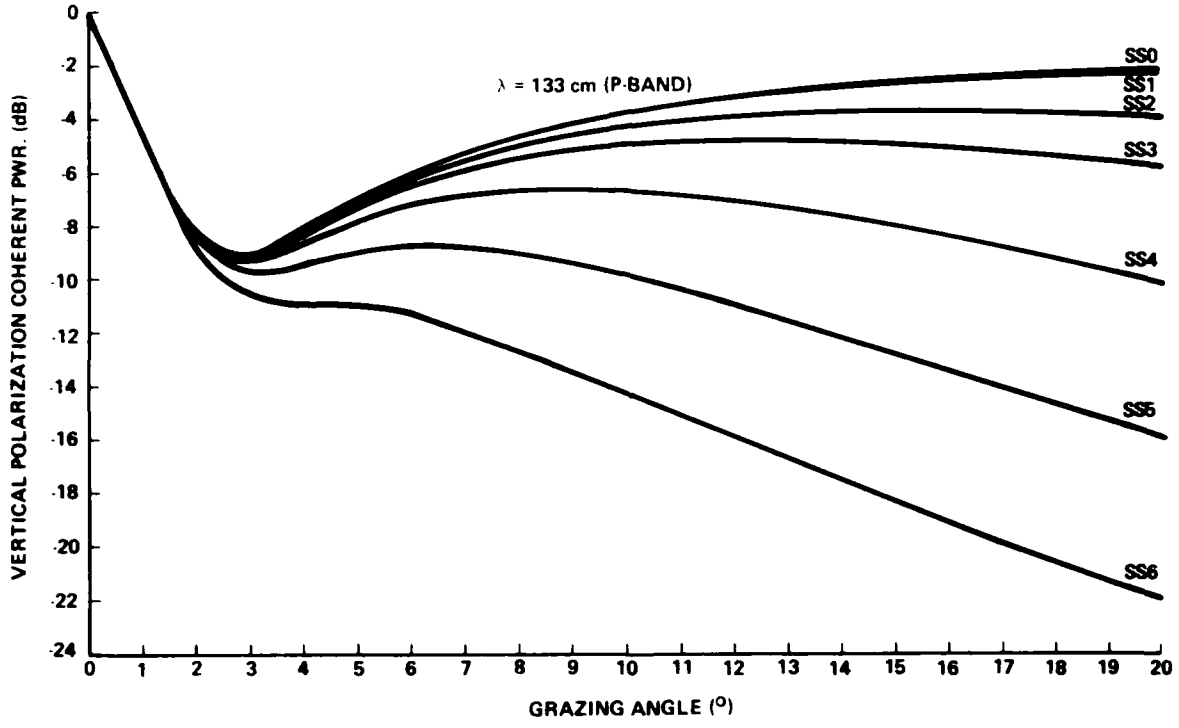

Figure 18. COHERENT POWER FACTOR AT P-BAND (226 MHz)

IA-61,924

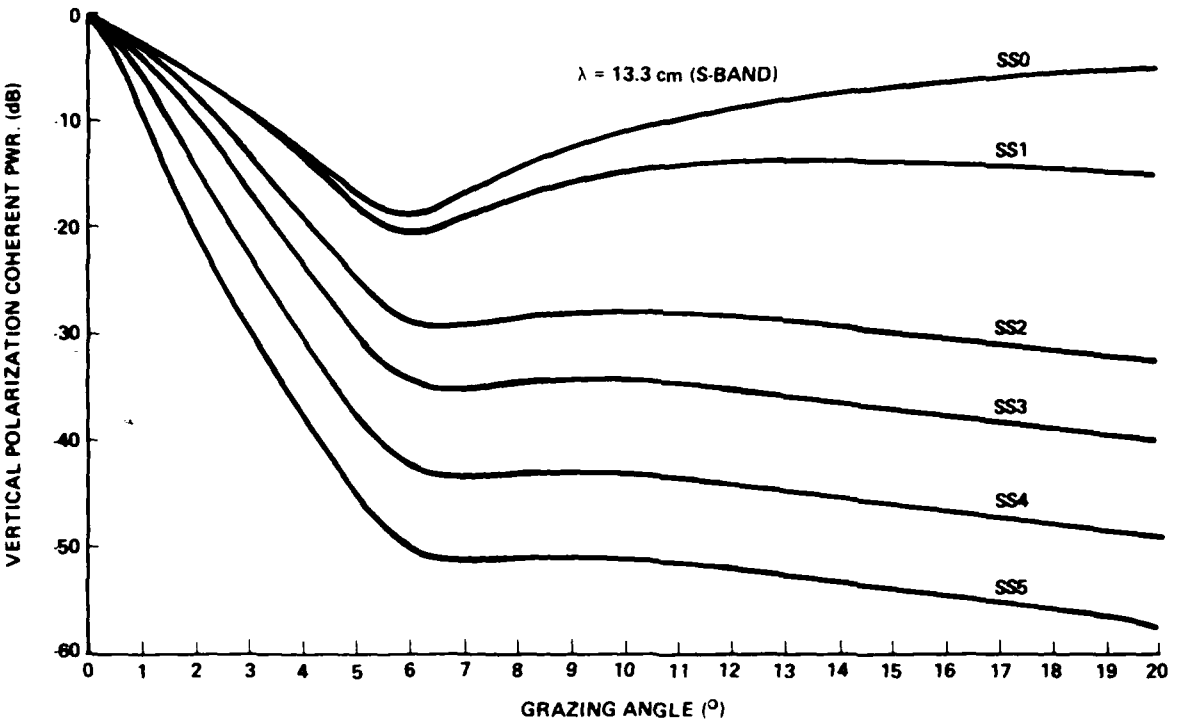

Figure 19. COHERENT POWER FACTOR AT S-BAND (2.26 GHz)

several sea states for P- and S-band representative wavelengths, respectively. Sea states 0 through 6 are characterized by waveheight standard deviation values of 0, 6.5, 21, 32, 54, 86 and 130 cm respectively, which are the upper limits of the waveheight standard deviation ranges which appear in a standard table[15]. Note that for rougher sea conditions the minimum associated with the vertical Fresnel coefficient is only a local minimum, and does not shift significantly with sea state.

The roughness factor is a much stronger function of grazing angle at S-band than at P-band as is evident from comparison of figures 18 and 19.

In figures 20 and 21 the P-band roughness factor (Eq. 12) is plotted versus RV altitude for several ARIA altitudes for sea states 4 and 5, respectively. The RV altitude range corresponds to the severe multipath environment at P-band for a 60-km baseline. Note that for higher ARIA altitudes the average roughness factor is smaller and that for a given ARIA altitude the roughness factor increases as the RV descends. Both of these results are due to the variation of the grazing angle with RV or ARIA altitude.

Figures 22, 23, 24 and 25 illustrate the corresponding relationships at S-band, for sea states 2, 3, 4 and 5 respectively. In contrast to the P-band curves, the S-band roughness factor curves are nearly horizontal, since the grazing angle does not change much in the range of RV altitudes which correspond to the much smaller S-band multipath environment. Also note that the S-band roughness factors are considerably smaller than those at P-band for a given sea state.

In figures 26, 27, and 28 the range of roughness factors encountered at S-band is plotted for several sea states as a function of ARIA altitude. RV altitudes from twice the severe multipath

IA-61,925

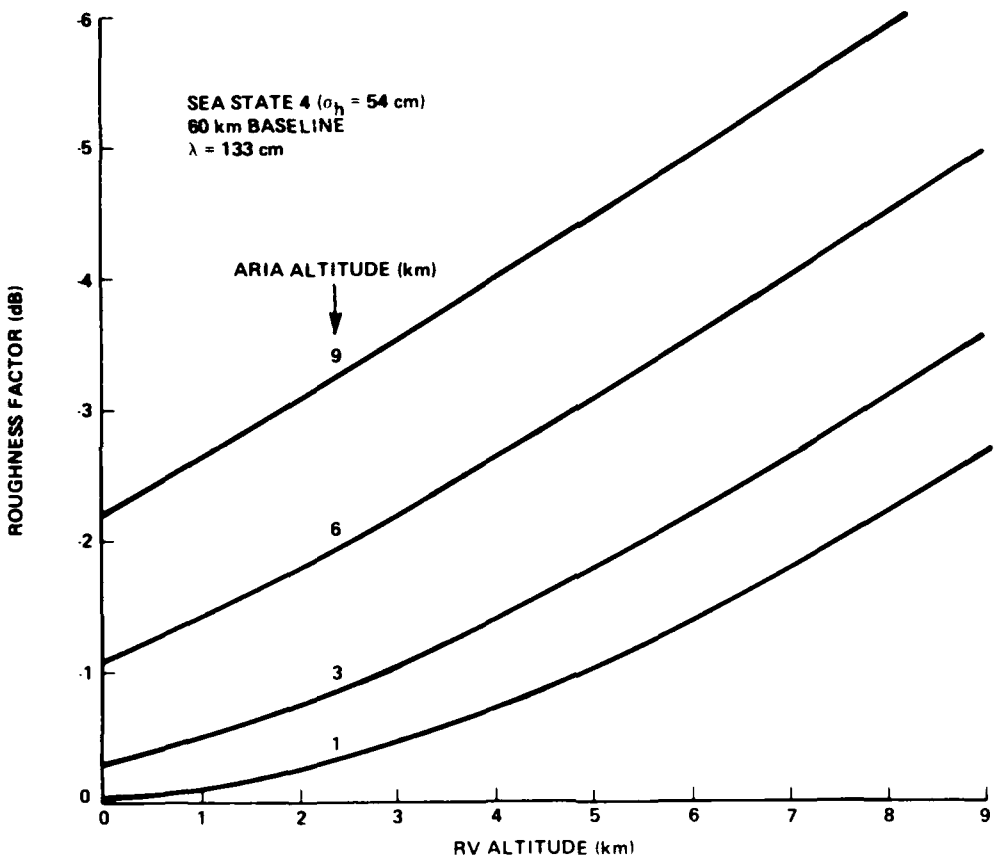

Figure 20 ROUGHNESS FACTOR VERSUS RV ALTITUDE AT P-BAND FOR SEA STATE 4

IA-61,926

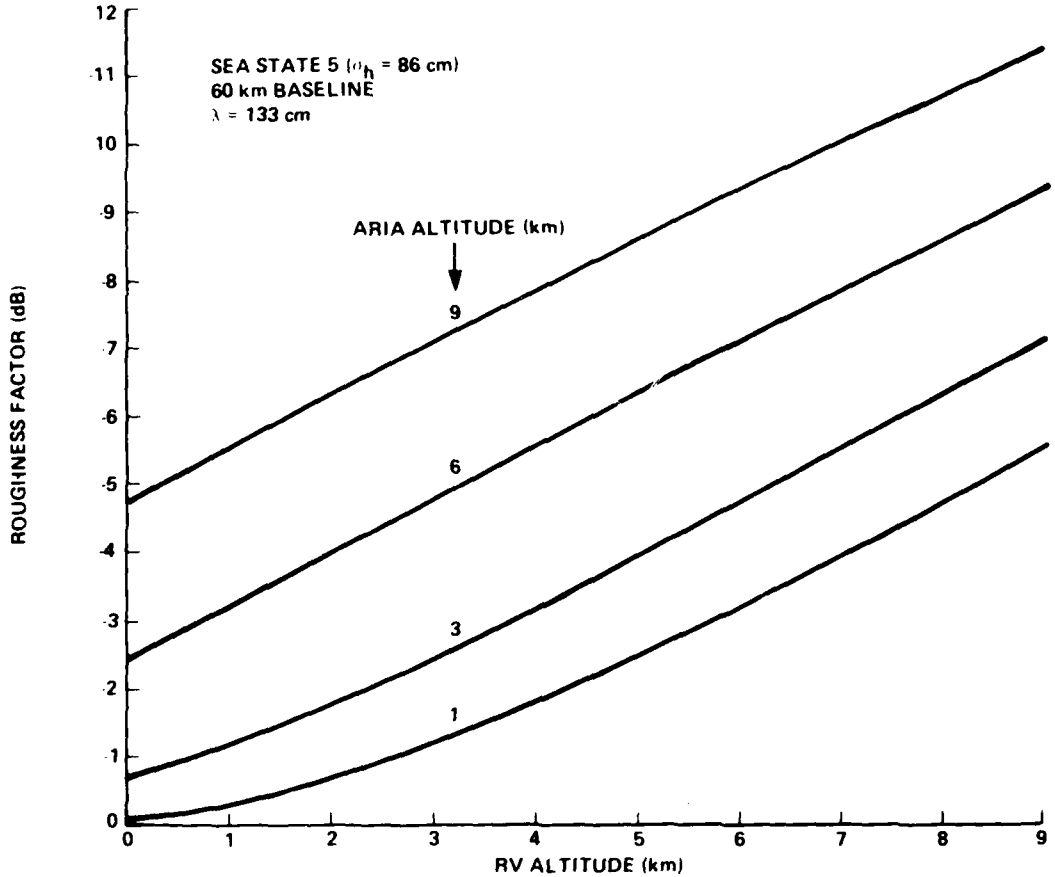

Figure 21. ROUGHNESS FACTOR VERSUS RV ALTITUDE AT P-BAND FOR SEA STATE 5

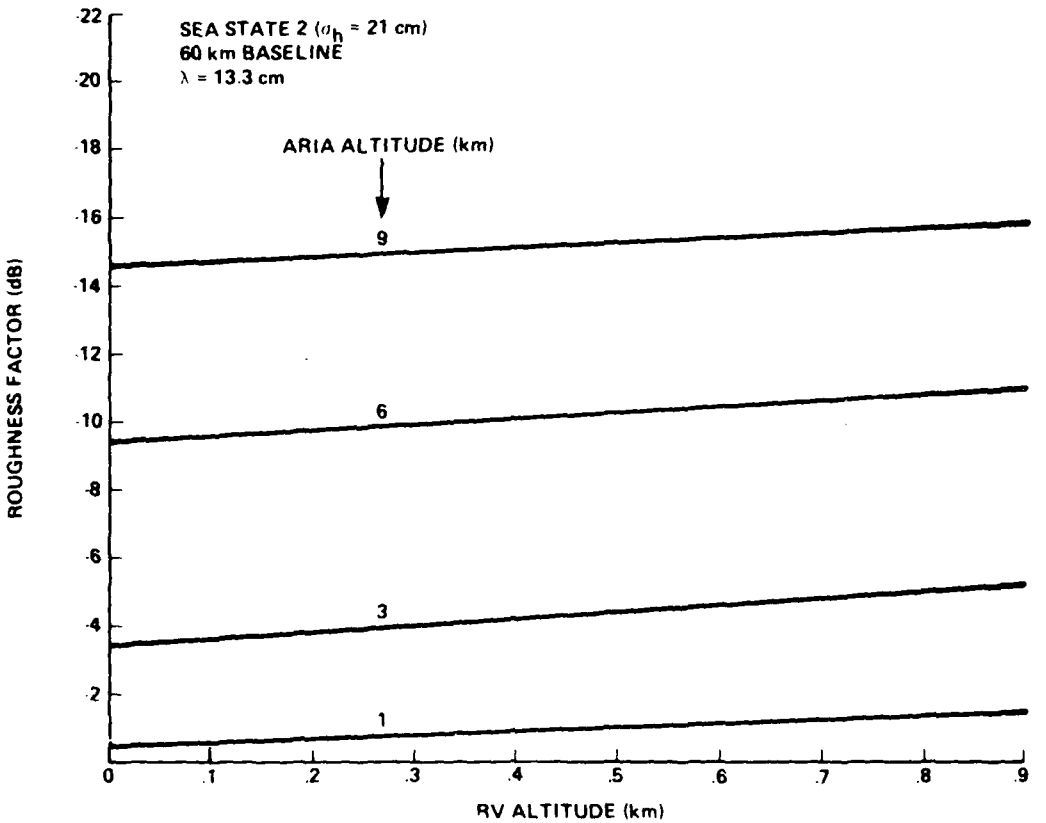

Figure 22 ROUGHNESS FACTOR VERSUS RV ALTITUDE AT S-BAND FOR SEA STATE 2

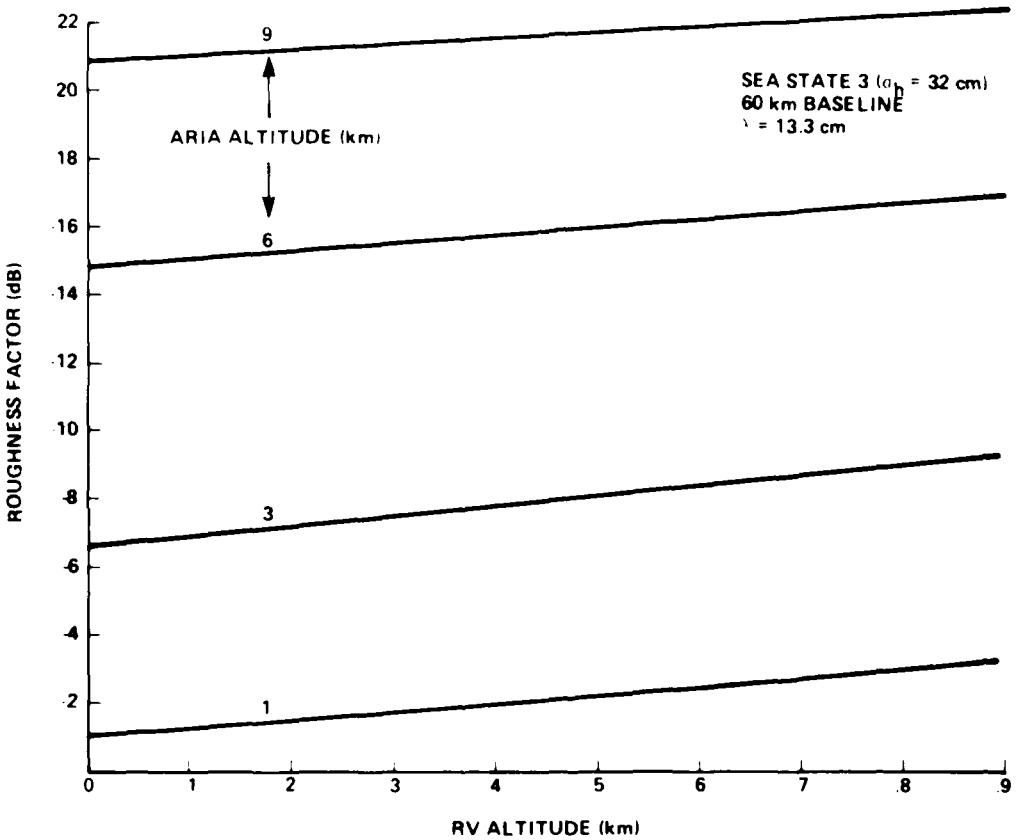

Figure 23. ROUGHNESS FACTOR VERSUS RV ALTITUDE AT S-BAND FOR SEA STATE 3

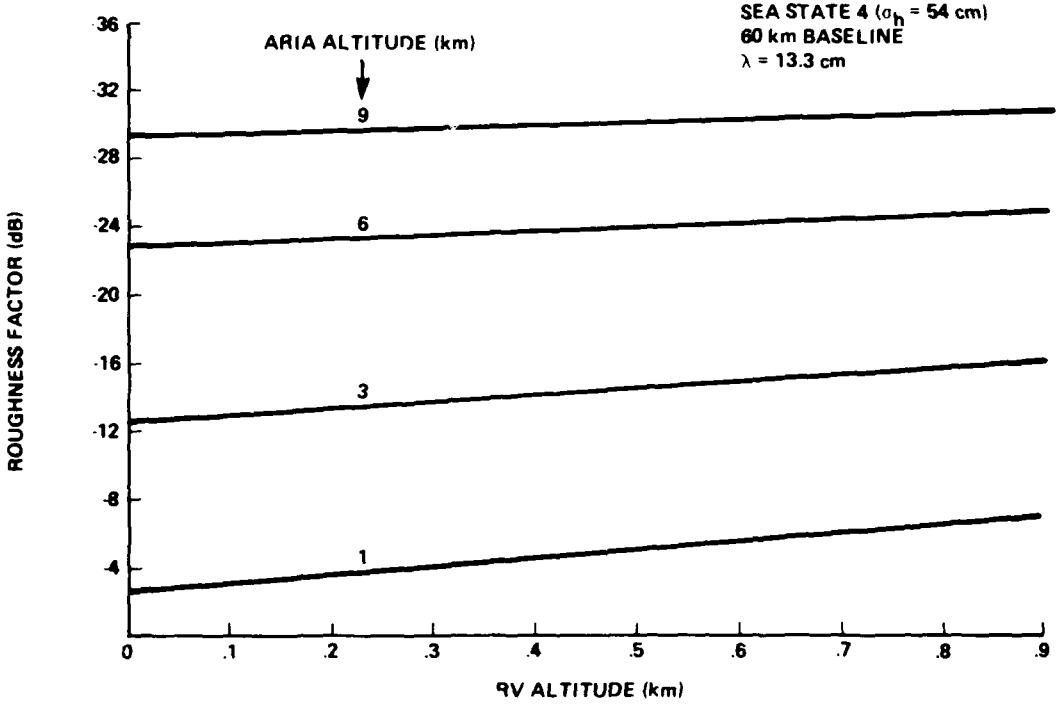

Figure 24. ROUGHNESS FACTOR VERSUS RV ALTITUDE AT S-BAND FOR SEA STATE 4

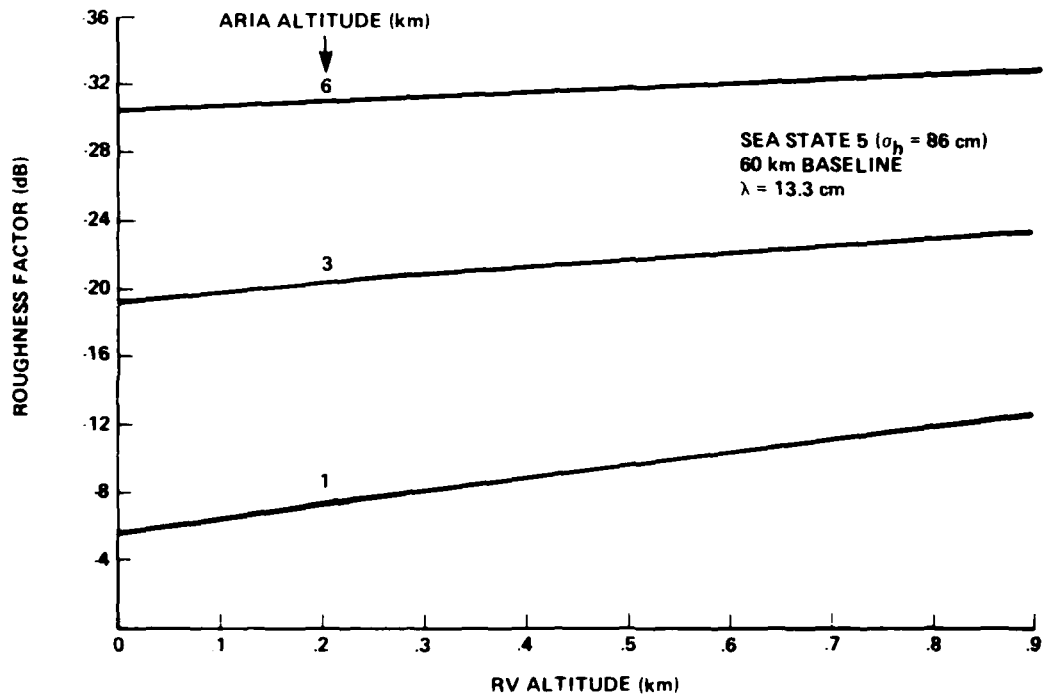

Figure 25. ROUGHNESS FACTOR VERSUS RV ALTITUDE AT S-BAND FOR SEA STATE 5

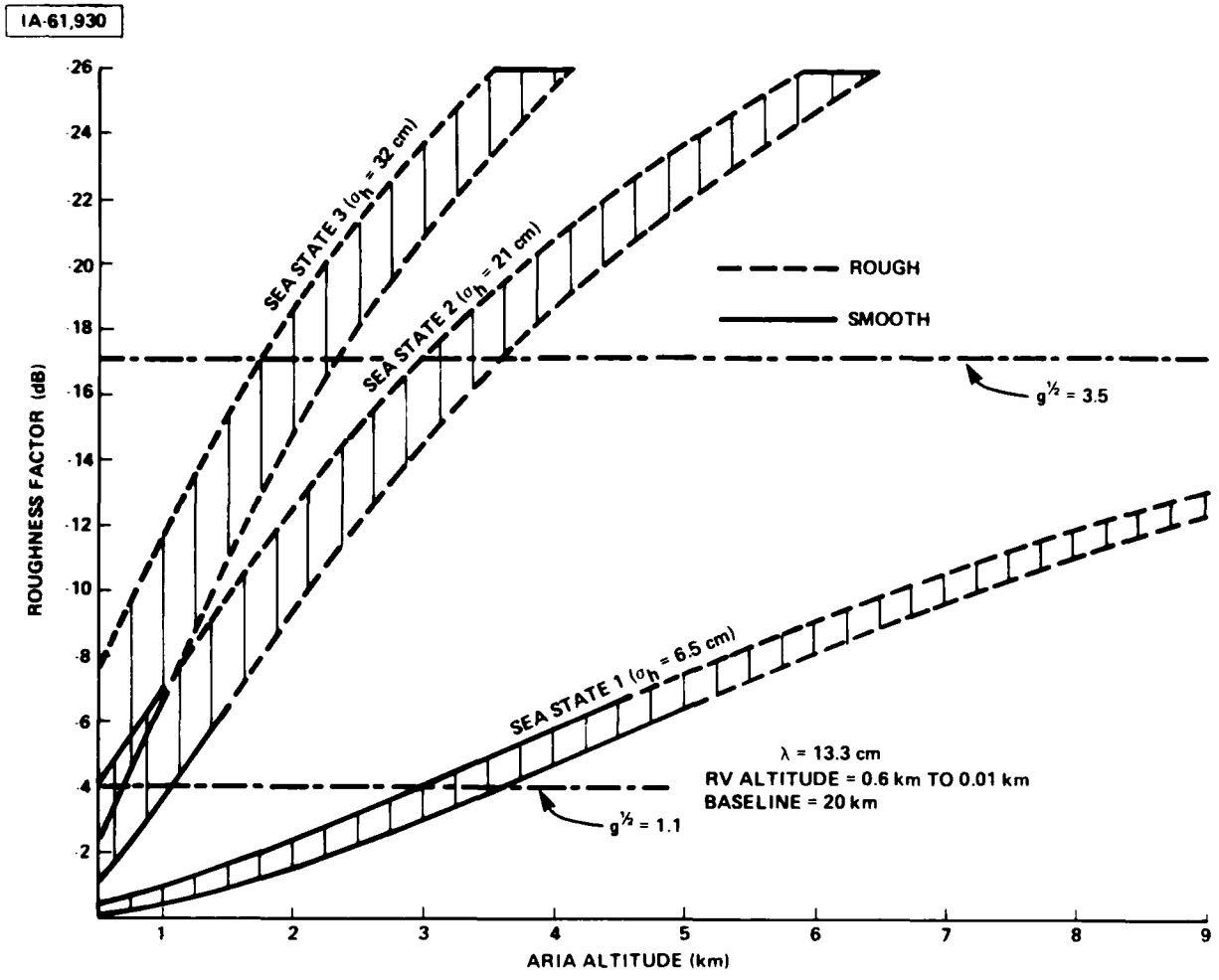

Figure 26 ROUGHNESS FACTOR RANGES VERSUS ARIA ALTITUDE FOR SEA STATES 1, 2 AND 3 AT S-BAND FOR A 20 km BASELINE

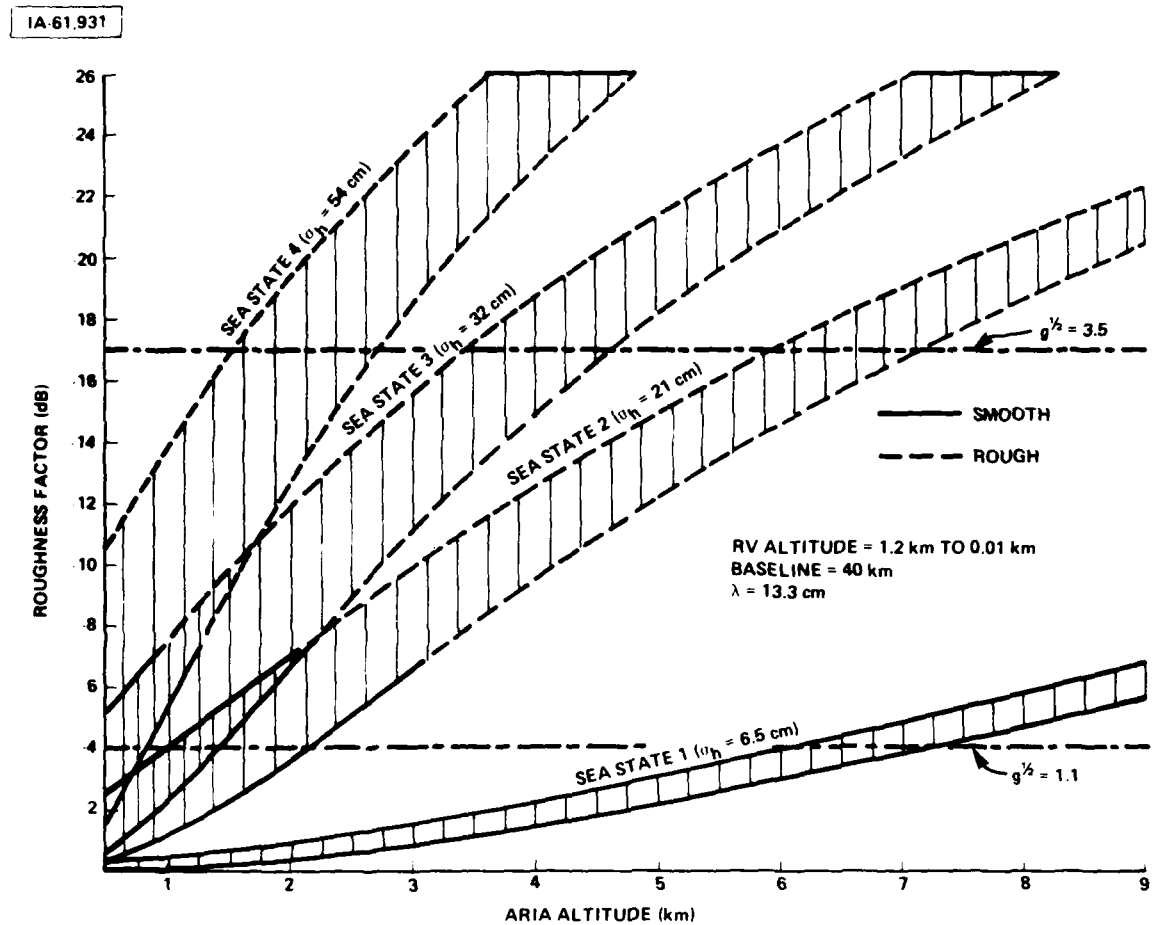

Figure 27 ROUGHNESS FACTOR RANGES VERSUS ARIA ALTITUDE FOR SEA STATES 1, 2, 3 AND 4 AT S-BAND FOR A 40 km BASELINE

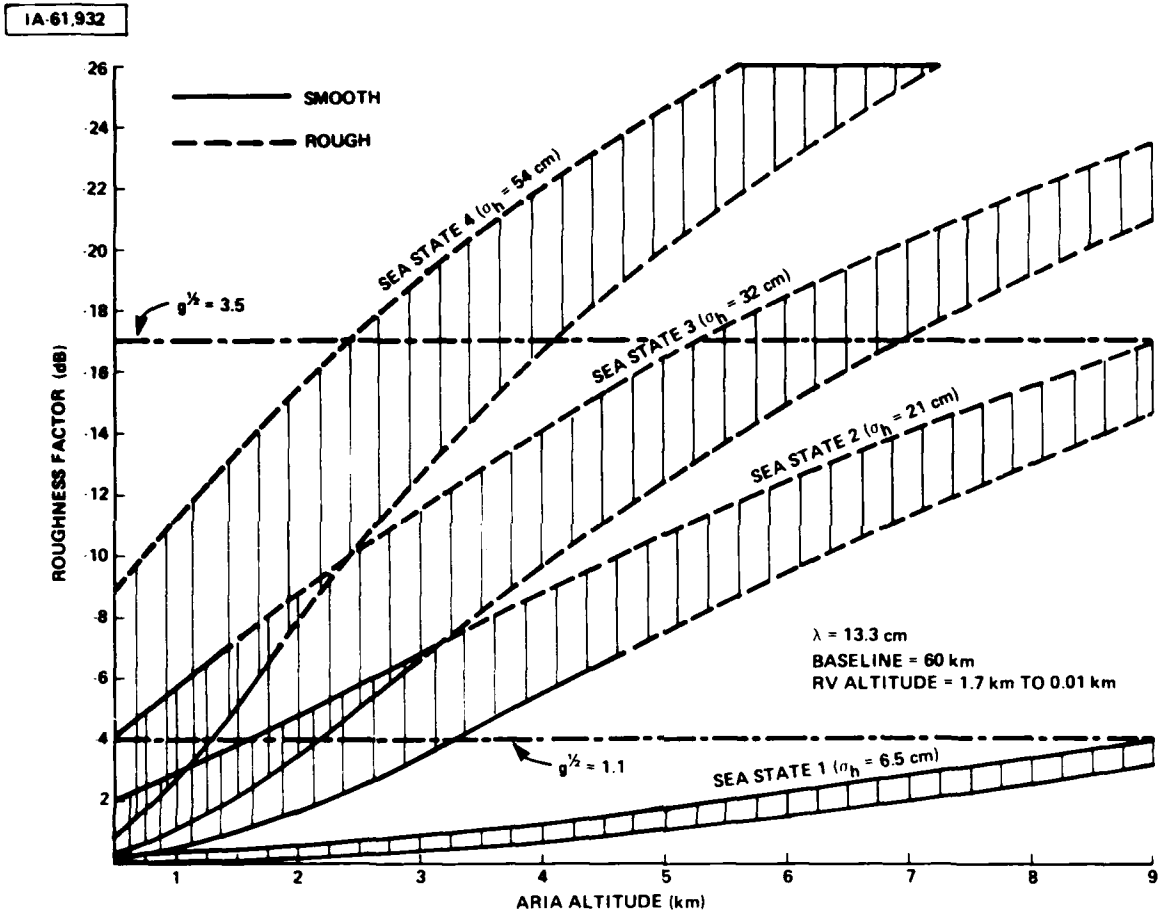

Figure 28. ROUGHNESS FACTOR RANGES VERSUS ARIA ALTITUDE FOR SEA STATES 1, 2, 3 AND 4 AT S-BAND FOR A 60 km BASELINE

threshold to splashdown for baselines of 20, 40 and 60 km are covered by the vertical ranges between the curves in this set of figures. The variation of the roughness factor is again due to the dependence of the grazing angle on RV altitude.

Figures 29, 30 and 31 illustrate the roughness factor ranges at P-band as a function of ARIA altitude for RVs which descend from twice the severe multipath threshold altitude to splashdown. Dashed lines are used when the Rayleigh criterion (Eq. 11) is not satisfied and the surface may be considered rough.

The roughness factor ranges at S-band for a high-flying ARIA are relatively narrow since the RV altitude range is considerably less than the ARIA altitude and, consequently, the grazing angle does not change much during the RV descent. On the other hand, for a very low altitude ARIA at S-band or for any feasible ARIA altitude at P-band, the CPF varies considerably over the RV altitude range, and in most cases the sea surface appears smooth just before splashdown, when the grazing angle is small.

C. The Total Reflected Power

The total, average, normalized power reflected in the specular direction can be represented as the sum of coherent and incoherent contributions,

$$\langle \rho \rho^* \rangle = \underbrace{|\langle \rho \rangle|^2}_{\text{coherent}} + \underbrace{\langle |\rho - \langle \rho \rangle|^2 \rangle}_{\text{incoherent}} \qquad (16)$$

in which averages are performed over an ensemble of sea surface profiles which are typically characterized by a surface height distribution, and surface autocorrelation function. If the random process which underlies the generation of surface profiles is

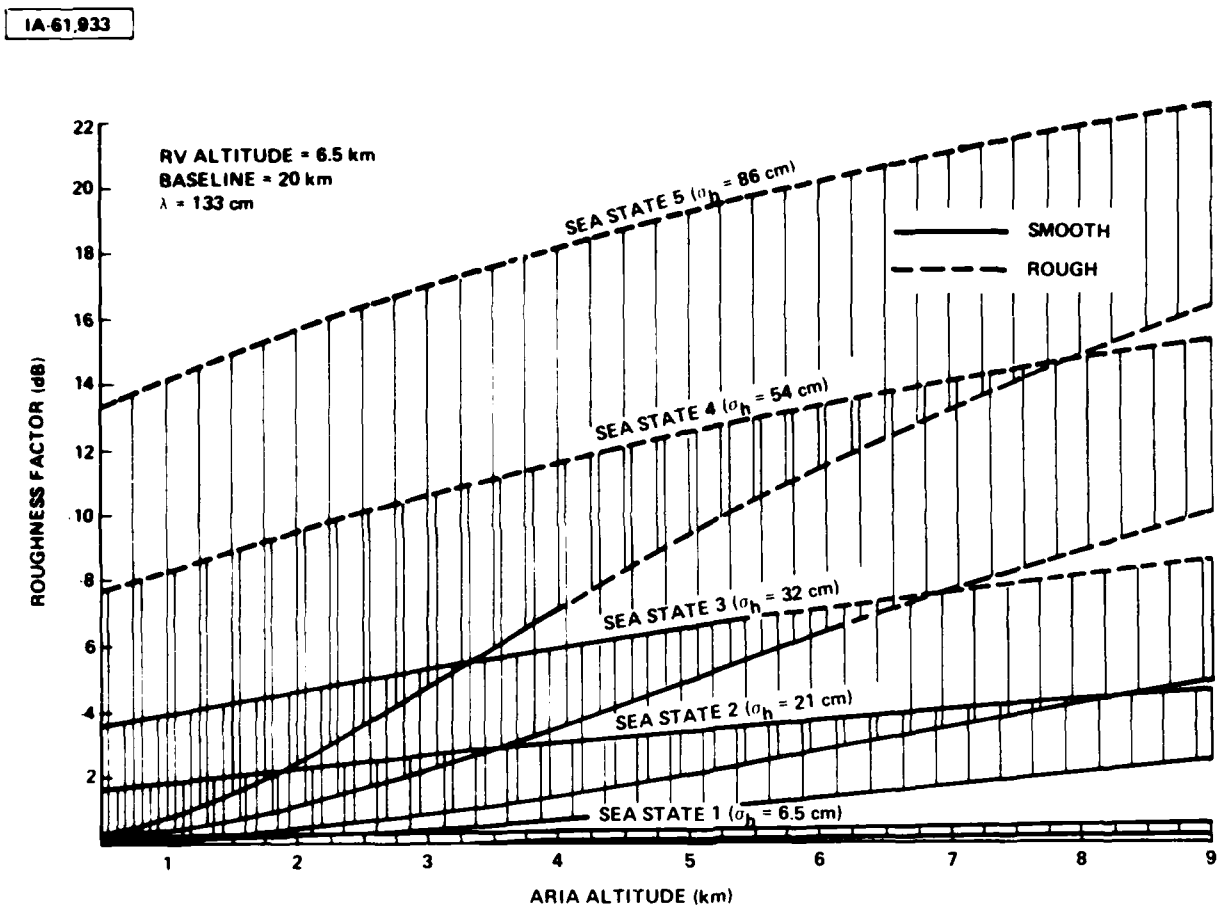

Figure 29 ROUGHNESS FACTOR RANGES VERSUS ARIA ALTITUDE FOR SEA STATES 1, 2, 3, 4 AND 5 AT P-BAND FOR A 20 km BASELINE

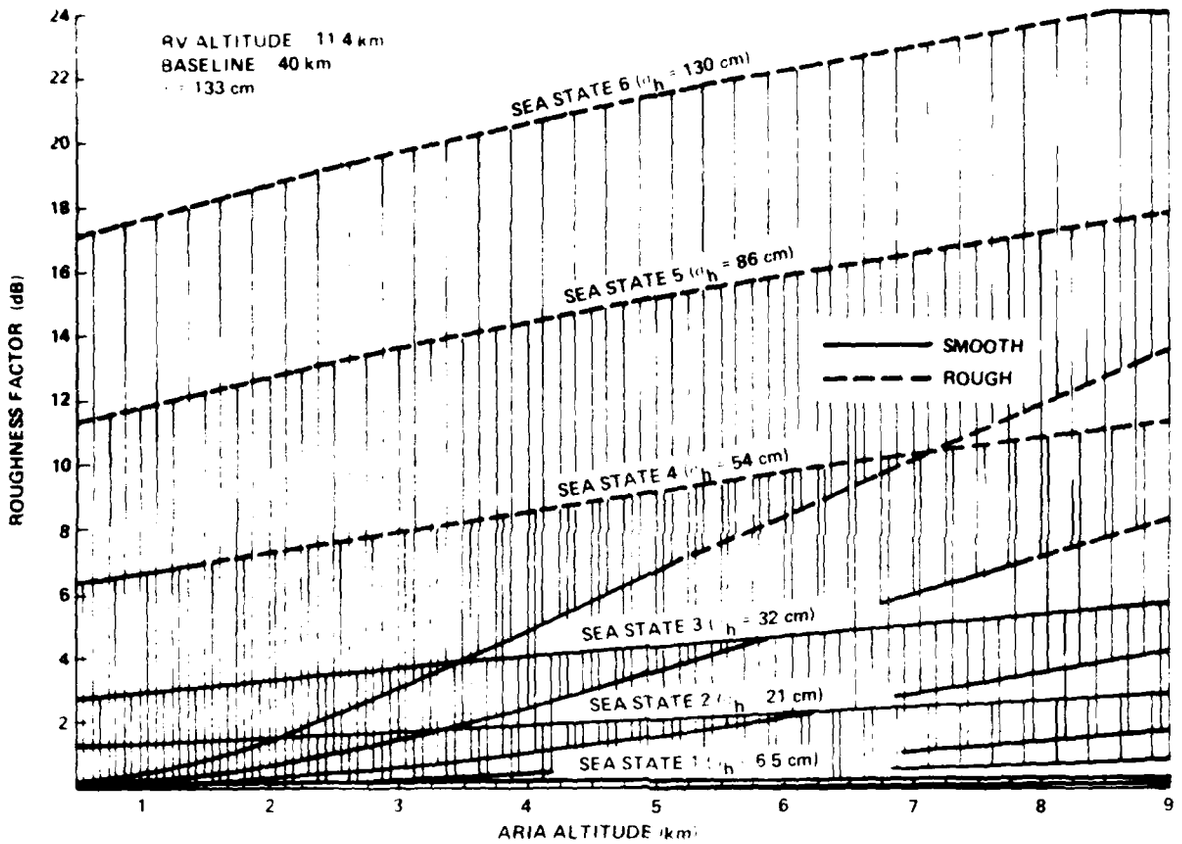

Figure 30 ROUGHNESS FACTOR RANGES VERSUS ARIA ALTITUDE FOR SEA STATES 1 2 3, 4 5 AND 6 AT P BAND FOR A 40 km BASELINE

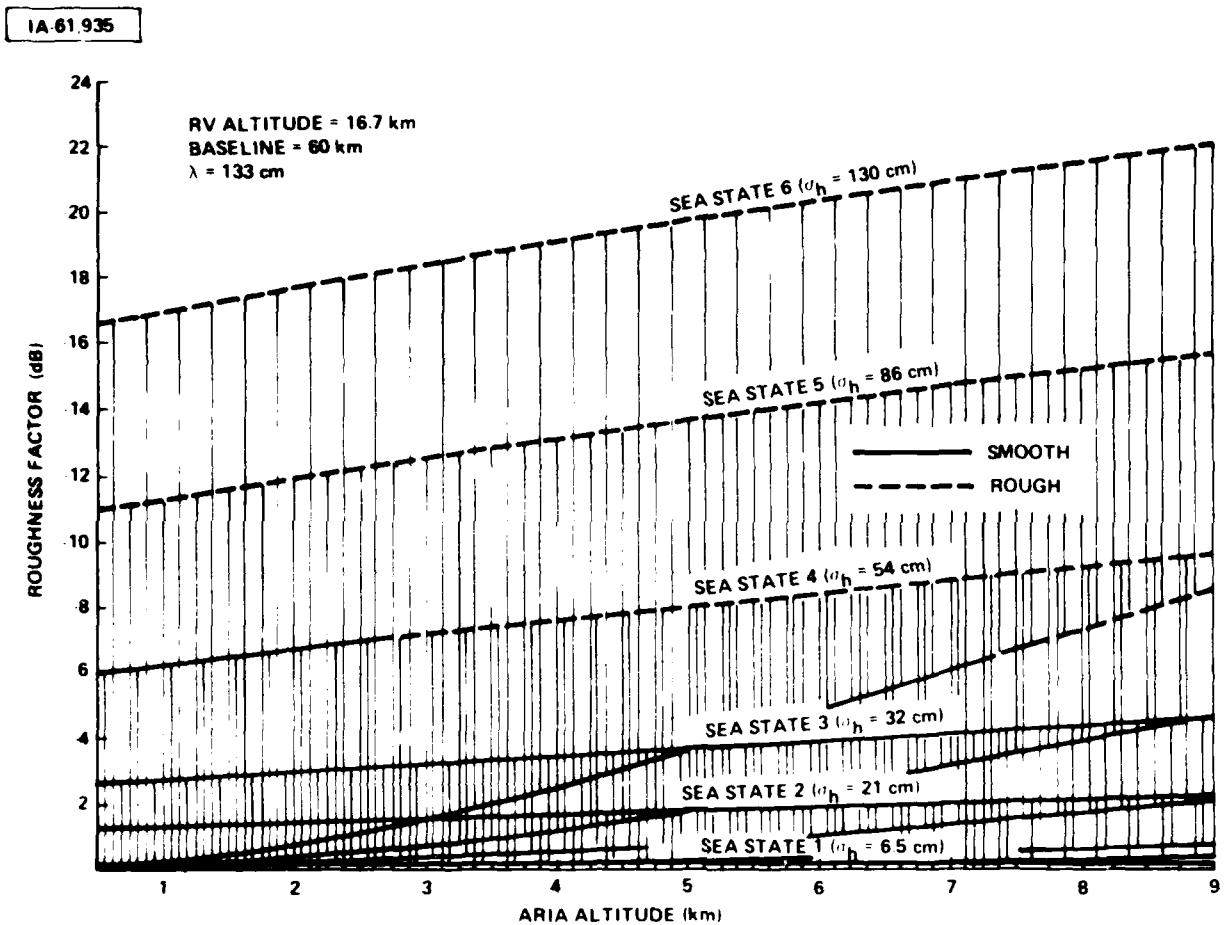

Figure 31 ROUGHNESS FACTOR RANGES VERSUS ARIA ALTITUDE FOR SEA STATES 1, 2, 3, 4, 5 AND 6 AT P BAND FOR A 60 km BASELINE

stationary, the Ergodic Hypothesis may be invoked and the averages of equation (16) can be interpreted as time averages over a given patch of surface.

Bearing in mind that the Fresnel coefficients have been normalized out of ρ (Eq. 8), theoretical evaluation of the coherent term requires only a specification of the surface height distribution, whereas, theoretical evaluation of the incoherent term is difficult and requires, in addition, a specification of the surface profile autocorrelation function. In lieu of a priori theoretical calculations, which are tedious and not necessarily reliable, a phenomenological vector model combined with experimental data[16] will be used to describe the reflected power.

The vector model of terrain and sea scattering is based on a dual classification of scatterers within the illuminated terrain or sea patch. Steady scatterers contribute to the coherent or non-fluctuating field of amplitude C, while the remaining scatterers, which have relative motions exceeding the wavelength of the incident radiation, comprise a collection of random scatterers for which the resultant, I(t), is uniformly distributed in phase and Rayleigh distributed in amplitude. Thus, the total, resultant, instantaneous field, illustrated in figure 32, is represented by,

$$R(t) = \mathrm{Re}\left[C e^{i\omega t} + I(t) e^{i(\omega t + \phi(t))} \right] \tag{17}$$

in which $\theta(t)$ and I(t) have the probability densities,

$$P(\phi)d\phi = \frac{d\phi}{2\pi} \quad ; \quad 0 < \phi < 2\pi \tag{18}$$

$$P(I)dI = \frac{I \exp\left[I^2/2\sigma\right]}{\sigma} dI \quad ; \quad 0 < I < \infty \tag{19}$$

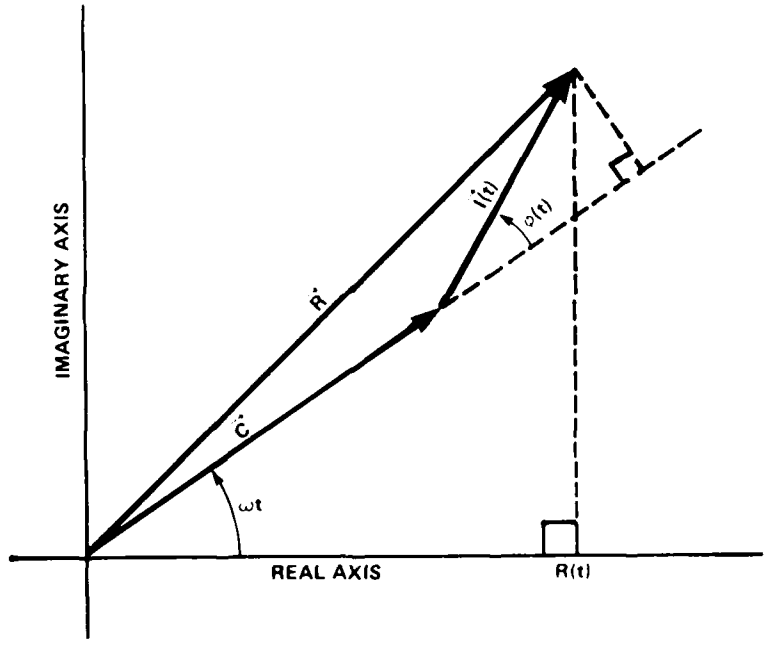

$\vec{C}$; COHERENT FIELD PHASOR

$\vec{I}$; INCOHERENT FIELD PHASOR

$\vec{R}$; TOTAL FIELD PHASOR

R(t); INSTANTANEOUS VALUE OF REFLECTED FIELD

IA-82,999

Figure 32 VECTOR MODEL FOR REFLECTED FIELD

and σ is the variance of the projection of I(t) on C. The components of I(t) along C and orthogonal to C have independent Gaussian distributions with zero means and equal variances.

The average power, in the context of this model, is proportional to,

$$\begin{aligned} < R^2(t) > &= \tfrac{1}{2} < C^2 + I^2(t) + 2CI(t)\cos\phi(t) > \\ &= \tfrac{1}{2}<C^2> + \tfrac{1}{2}<I^2(t)> + <CI(t)\cos\phi(t)> \end{aligned} \tag{20}$$

Since it is as likely for the cosine term to be negative as it is for it to be positive ($\phi(t)$ uniformly distributed) the last term vanishes, and,

$$< R^2(t) > = \frac{C^2}{2} + \frac{<I^2(t)>}{2} = \frac{C^2}{2} + \sigma \tag{21}$$

Comparision of the above with equation (16) indicates that σ is proportional to the incoherent power, as expected.

For ensembles of very rough surfaces or a patch of rough sea, random scattering dominates, and the resultant field amplitude in the specular direction is Rayleigh distributed, while for smooth surfaces the incoherent or random component is very small and the field amplitude distribution is Gaussian with a small variance. In general, the distribution of the amplitude of R(t) in equation 17, which can also be used to model narrowband noise in electrical circuits[17], is Rician[18].

Analysis of sea reflection measurements at 5.3, 3.2 and 0.86 cm transmitted wavelengths[19] indicates that the normalized root-mean-square (RMS) incoherent field amplitude increases linearly with sea roughness to a peak of 0.345 at $g^{1/2} = 1.1$, from which it decreases approximately linearly to 0.22 at $g^{1/2} = 3.5$, as shown in

figure 33[20]. The available data did not permit analysis for Rayleigh parameters greater than 3.5, however a suggested exponential extrapolation of the quoted results has been performed and appears in figure 33. The roughness factor (coherent power attenuation) values of 17.1 dB and 4.1 dB which correspond to the 3.5 and 1.1 Rayleigh parameter values, respectively, are indicated in figures 26 through 28.

Fluctuations in the amplitude of the sea-reflected field can momentarily cause its level to exceed that of the direct field. These scintillations will lead to very deep fades (destructive interference) when the direct path signal is combined with a strong coherent, specular path signal in phase opposition[21]. The probability that the reflected field amplitude will exceed the direct field amplitude is indicated in table 4 for several values of surface roughness, as characterized by the Rayleigh parameter, and sea state range at S-and P-band. The coherent or steady field amplitude is obtained from,

$$C = |\langle \rho \rangle| = \left[1 + \frac{g}{2}\right]^{-1} \tag{22}$$

which is equivalent to equation (12) and gives good agreement with experimental results[22]. The normalized RMS incoherent power values appearing in table 4 were taken from Beard[20]. For vertical polarization Fresnel coefficient magnitudes of 0.5 and 0.2 were assumed, while for horizontal polarization 1.0 was used. For the sake of simplicity, no other factors pertaining to the relative strength of the reflected and direct fields (RV antenna pattern, space loss, etc.) were taken into account.

For smooth surfaces ($g^{1/2} < \pi/2$) and horizontal polarization, the probability that the reflected field amplitude will exceed the direct field lies between 0.05 and 0.1 for surface roughnesses just below the

IA-61,936

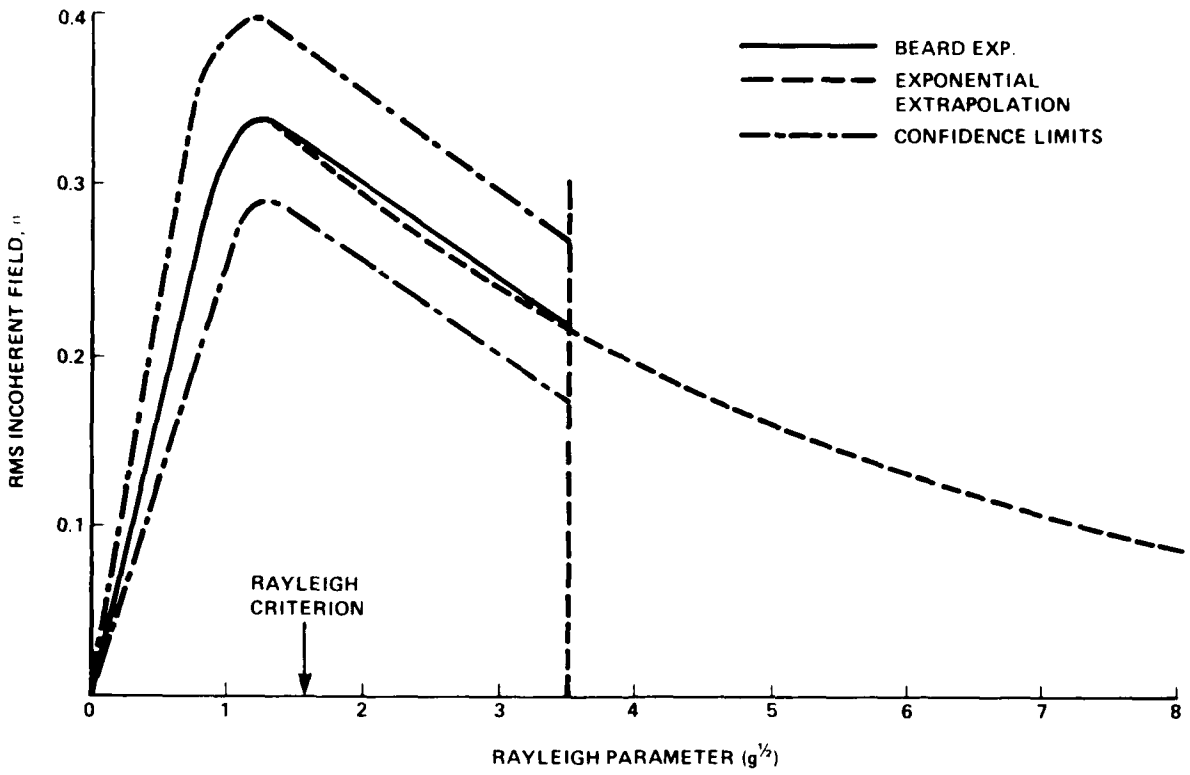

Figure 33. RMS INCOHERENT FIELD AMPLITUDE VERSUS RAYLEIGH PARAMETER

TABLE 4

REFLECTED POWER STATISTICS

$g^{1/2}$	S.S.* (S)	S.S.* (P)	AMPL.+ C	RMS‡ AMPL. I	PROBABILITY R > D		
					V-POL(F_V=.2)	V-POL(F_V=.5)	H-POL(F_H=1)
0.25	1	4	0.97	0.09	<0.0001	<0.0001	0.2-0.5
0.50	2	6	0.89	0.18	<0.0001	0.001-0.002	0.2-0.5
0.75	2	7	0.78	0.26	0.002-0.005	0.01-0.02	0.2-0.5
1.00	2	7	0.67	0.32	0.005-0.01	0.02-0.05	0.1-0.2
1.25	3	7	0.56	0.35	0.01-0.02	0.02-0.05	0.1-0.2
1.50	3	7	0.47	0.34	0.01-0.02	0.02-0.05	0.05-0.1
2.00	4	7	0.33	0.31	0.002-0.005	0.005-0.01	0.02-0.05
2.50	4	7	0.24	0.28	0.001-0.002	~0.002	0.005-0.01
3.00	5	7	0.18	0.25	~0.0005	0.0005-0.001	0.001-0.002
3.50	5	7	0.14	0.22	<0.0001	<0.0001	0.0001-0.0002
4.00	5	7	0.11	0.18	<0.0001	<0.0001	<0.0001

* 3^o Grazing Angle Assumed
\+ From Equation (12)
‡ From Ref. 25

Rayleigh criterion limit (Eq. 14), to between 0.2 and 0.5 for very smooth surfaces. Probability ranges are given since the table employed[23] to obtain these and the other results in table 4 does not permit a more precise determination. As the surface becomes rougher, less power is scattered in the specular direction and the probability that the reflected (specular) field will exceed the direct field declines, as might be anticipated and as is borne out by table 4. For vertical polarization the assumption of a 0.5 Fresnel factor reduces the coherent field component by 50%. The RMS incoherent field, however, is polarization independent, as suggested by the experimental data[19], and the known depolarization properties of rough surfaces[24].

Examination of table 4 leads to several interesting conclusions:

1) If the Fresnel reflection coefficient is close to unity, as in the case for horizontal polarization, there is a relatively high probability that the incoherent field fluctuations will produce deep fades when the direct and coherent specular fields are in phase oppostion. Even for very smooth surfaces, the small RMS amplitude incoherent field is sufficient to cause the total reflected field to exceed the direct field 20 to 50% of the time, as seen in the horizontal polarization case of Table 4.

2) If the Fresnel coefficient has an intermediate value (e.g. 0.5) deep fades are most probable when the surface roughness is in the neighborhood of the Rayleigh criterion ($0.75 < g^{1/2} < 2.00$) i.e., in the vicinity of the incoherent power peak shown in figure 33. The reduction of the coherent power caused by a Fresnel coefficient of 0.5 is sufficient to reduce the time for which the reflected power exceeds the direct power to a peak value of 2 to 5%.

3) If the Fresnel coefficient is small, as in the vicinity of the Brewster angle for vertical polarization, the coherent specular field strength is greatly reduced, and for rough surfaces the reflected field amplitude approaches the Rayleigh distribution. As in the previous case, deep fades are most likely for surface roughness which encompass the peak of the incoherent power function of figure 33. The probability values in the $F_v = .2$ column of table 4 illustrate this case.

4) The fade probability declines monotonically with increasing surface roughness for surfaces with Rayleigh parameters that exceed $\pi/2$ - the Rayleigh criterion threshold.

Once again it must be emphasized that the results which appear in table 4 apply to a simplified multipath model which neglects relative space losses and assumes isotropic transmitting and receiving antennas, since the coherent power is modified only by the Fresnel coefficient and surface roughness.

The distribution of the amplitude of the reflected field, which has been represented here as Rician, contains no information about the rate of fluctuations of the amplitude or correlation time. Experimental measurements performed at X-band[25] over the Golden Gate at San Francisco indicate that the power spectrum of the reflected field broadens with increasing roughness. For smooth surfaces the fluctuation rates are related to the fundamental water wave period and several higher harmonics so that the most rapid fluctuations are correlated over a time which is the order of one second. As the sea becomes choppy and waveheights increase, correlation times decrease to a fraction of a second - typically 0.25 - 0.5 seconds.

The roughness of the sea is characterized by the Rayleigh parameter given in equation (11). From the experimentally derived [20] curve of figure 33 it is seen that the incoherent power peaks at $g^{1/2} \sim 1.26$ and from table 4 it is evident that, for coherent fields of moderate strength, fades are most likely for roughnesses between 0.75 and 1.5. To be useful, however, the roughness ranges for which fading will be most serious must be presented in the context of the RV-ARIA geometry and sea state. In figures 34 and 35, the locus of RV and ARIA altitude pairs for which the incoherent power lies between its peak and -3 dB of peak value ($g^{1/2} \simeq 0.75$) is represented by a diagonal band whose position and width is a function of sea state, baseline and transmitted wavelength. Figure 34, which is applicable to S-band, covers sea states 1, 2 and 3, while figure 35, which is applicable to P-band, covers sea states 4, 5, and 6. For coherent fields of high strength, such as encountered for horizontally polarized fields incident upon smooth seas, the -3dB low bounds in figures 34 and 35 are not applicable since deep fades are probable over the whole range below the peak lines.

The depth and frequency of RF fading are considered in much greater detail in the section which follows.

IA-61,938

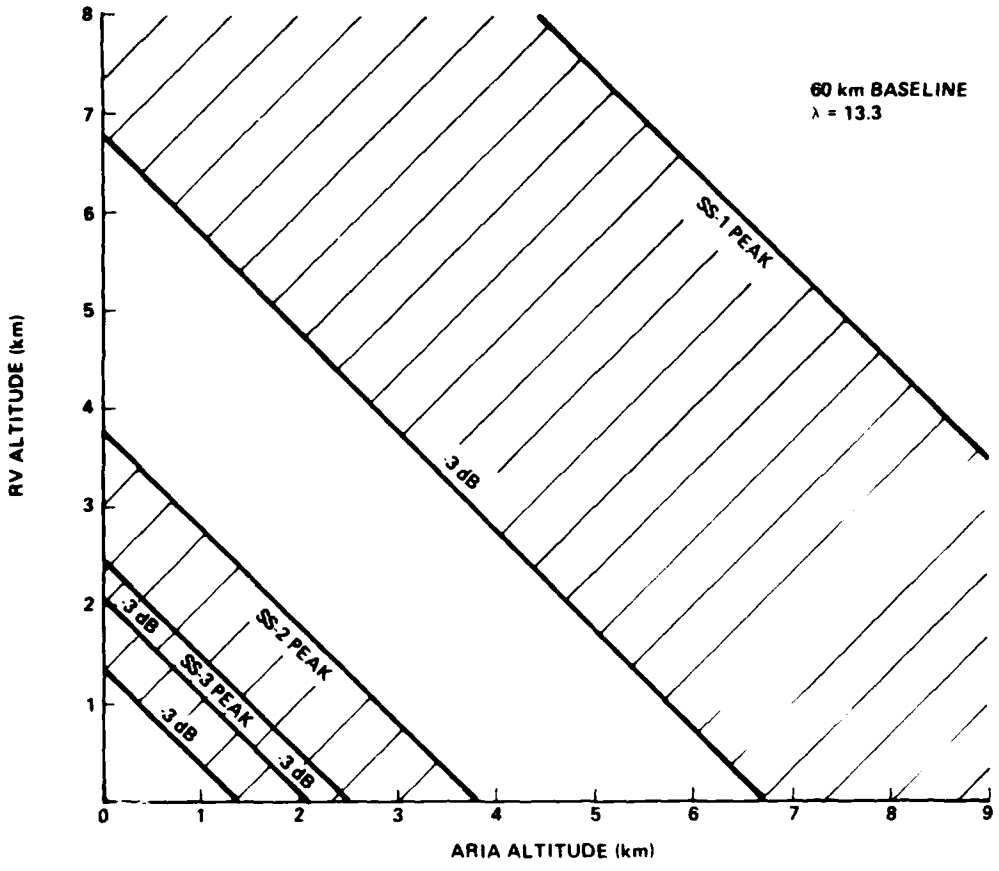

Figure 34. RV ARIA CONFIGURATIONS WHICH MAXIMIZE INCOHERENT POWER AT S-BAND FOR A 60 km BASELINE

IA 61,939

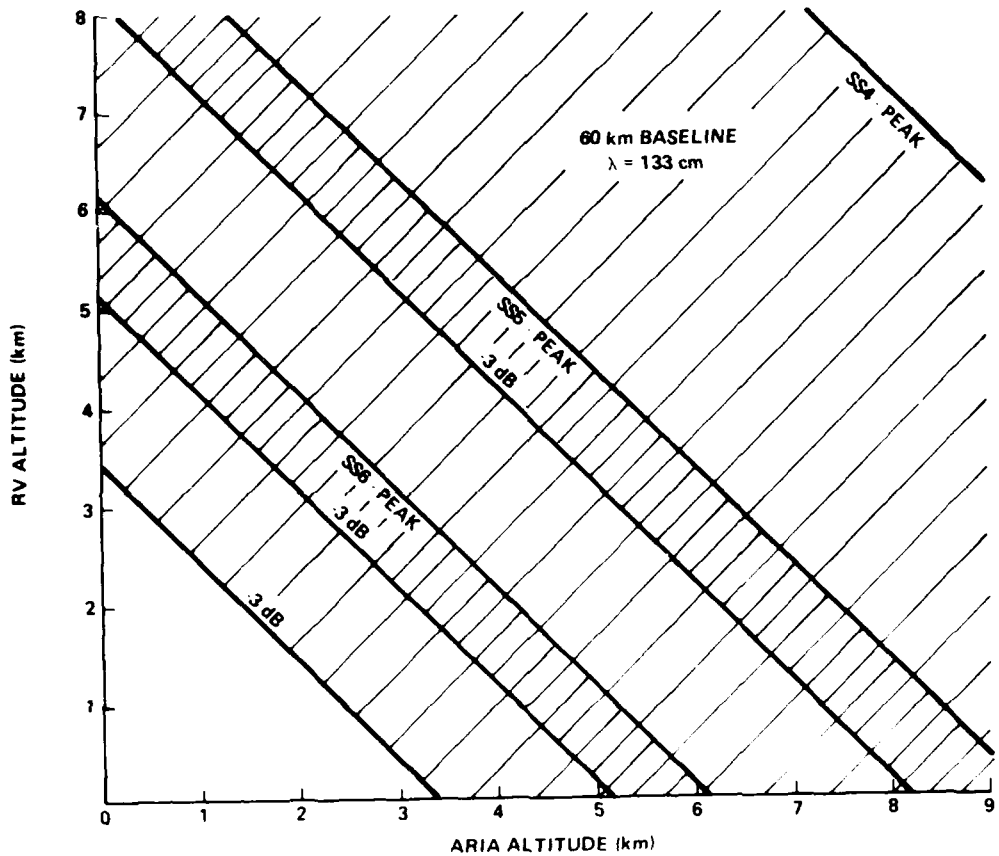

Figure 35 RV ARIA CONFIGURATIONS WHICH MAXIMIZE INCOHERENT POWER AT P-BAND FOR A 60 km BASELINE

SECTION III

FADING OF THE RF POWER

The strength of the reflected multipath signal is important in the context of intersymbol interference of the bit stream as discussed in section II-1-A, however, even if the percentage of intersymbol overlap is tolerable, e.g., 10% or less, a strong reflected wave can interfere destructively with the direct field wave to momentarily reduce the RF power. When the depth of an RF fade exceeds the link margin (surplus power) a drop-out occurs and data may be lost.

The degradation caused by RF fading also depends upon the frequency with which fades occur. The fade frequency, in the context of the two path multipath model, is the beat or difference frequency between the direct and reflected waves. These waves arrive at the ARIA with different frequencies for basically two reasons:

1) The direct and reflected waves experience different Doppler shifts associated with the relative RV-ARIA motion, and

2) The frequency modulation of the transmitted waves leads to a frequency difference when the reflected wave is delayed with respect to the direct wave.

If the beat frequency of the resultant RF field is large relative to the bit rate, the link performance may actually be improved by the reflected field contribution if envelope detection is used[26] and intersymbol overlap is negligible; however, if the beat frequency is comparable to or less than the bit rate, potentially serious data loss can occur if the link margin is not sufficient to compensate for the fades.

1. The Depth of Fade

A deterministic, theoretical, two-path multipath model of RF fading for the RV-ARIA telemetry link has been developed recently[3] in connection with multipath risk evaluation for APATS. Briefly, the model takes into account relative RV antenna and receiving array gain, RV rotation, and coherent specular sea reflection. Since scintillations arising from the incoherent reflected power are not taken into account, the fade depth calculation is deterministic.

In lieu of a measured RV antenna pattern, a model dipole-like antenna pattern with an assumed azimuthal variation intended to imitate nulls in the true pattern was employed. The model RV antenna fields are specified, in the context of figure 7, as follows:

$$E_\theta = \sin\theta\left[0.05 + 0.95\left|\cos\phi\right|^{\frac{1}{2}}\right] \tag{23}$$

$$E_\phi = 0 \tag{24}$$

The azimuthal variation of the power at $\theta = 90^\circ$ has been illustrated elsewhere[27]. The model antenna pattern has sharp nulls (-22.4 dBi at $\theta = 90^\circ$) at $\phi = 90^\circ$, 270°, and mild peaks (3.6 dBi at $\theta = 90^\circ$) at $\phi = 0^\circ$, 180°.

For fade depth calculations the local coordinate system illustrated in figure 10 is used for simplicity. The RV is assumed to roll about its longitudinal axis at a rate of two revolutions per second, and the RV velocity is assumed to be constant and along the RV longitudinal axis within the RV altitude range for which calculations are performed. The ARIA, which for this simulation is stationary, is oriented such that the array boresight (perpendicular) is horizontal

in the plane of incidence corresponding to the initial (for calculations) RV position. A smooth sea (sea state 1, σ_h = 6.5 cm) is assumed for all fade depth calculations reported here.

Maximum fade depths are displayed in figures 36 through 39. Figures 36 and 37 pertain to model scenarios in which the RV has a nearly vertical trajectory (high γ) and the ARIA is positioned at low and high altitude, respectively. The baseline of 20 km was chosen to provide a wider range of variation in the model geometry, however, baselines for most TSPs will be significantly longer. Figures 38 and 39 pertain to low γ trajectories. Three major features of these maximum RF fade plots are immediately evident:

1) On the average the fades become gradually deeper as the RV descends (the vertical polarization fades of figures 36 and 38 are exceptions which are discussed later);

2) The plots are modulated by spikes which occur at regular intervals equal to the vertical distance through which the RV moves in the time required for it to execute one half of a revolution;

3) There are many periods, as in indicated by the discrete points, during which the specular field strength exceeds the direct field strength.

The first result is a consequence of the relative ARIA antenna gain in the direct and specular directions as discussed in section II-1 and illustrated in figure 1. Since the array, in these simulations, has a vertical dimension of 1.5 m, the elevation half power beamwidth on boresight is approximately 4.5^{o} at S-band and 45^{o} at P-band. The threshold altitudes for severe multipath fading are, by equation (2), 0.47 km and 4.7 km for S-band and P-band,

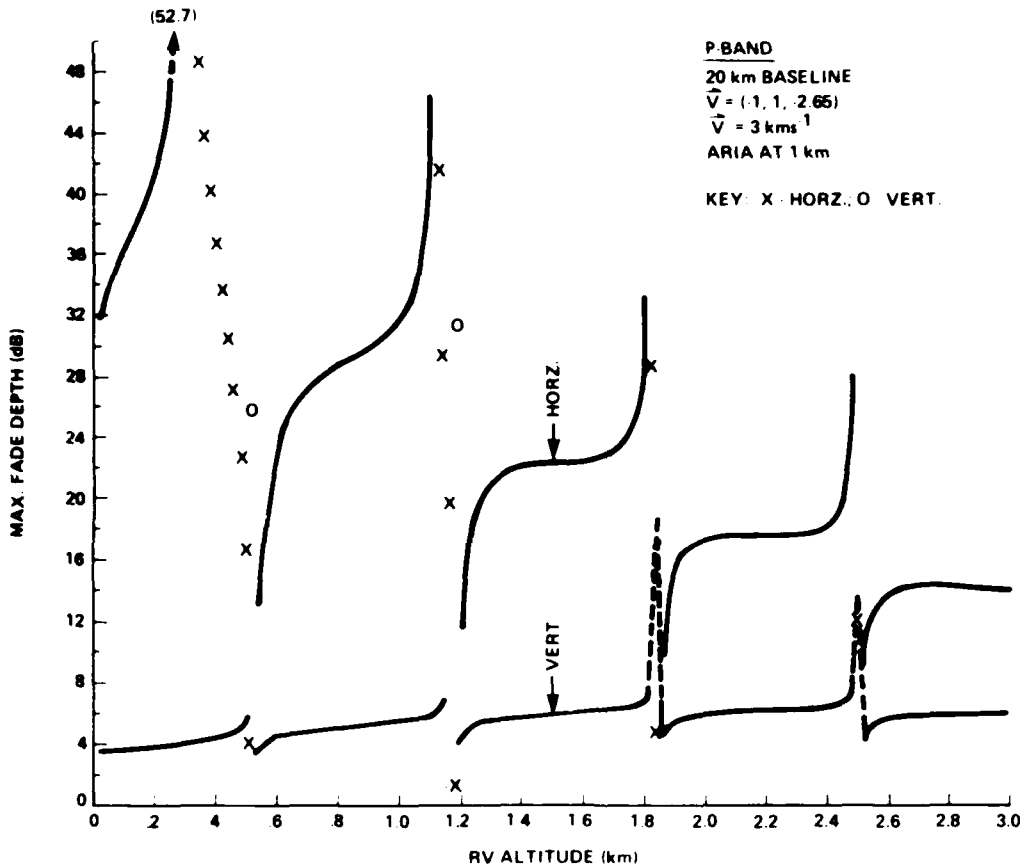

Figure 36 MAXIMUM P BAND RF POWER FADES VERSUS RV ALTITUDE FOR A HIGH $\vec{V}$ RV TRAJECTORY AND ARIA AT 1 km ALTITUDE

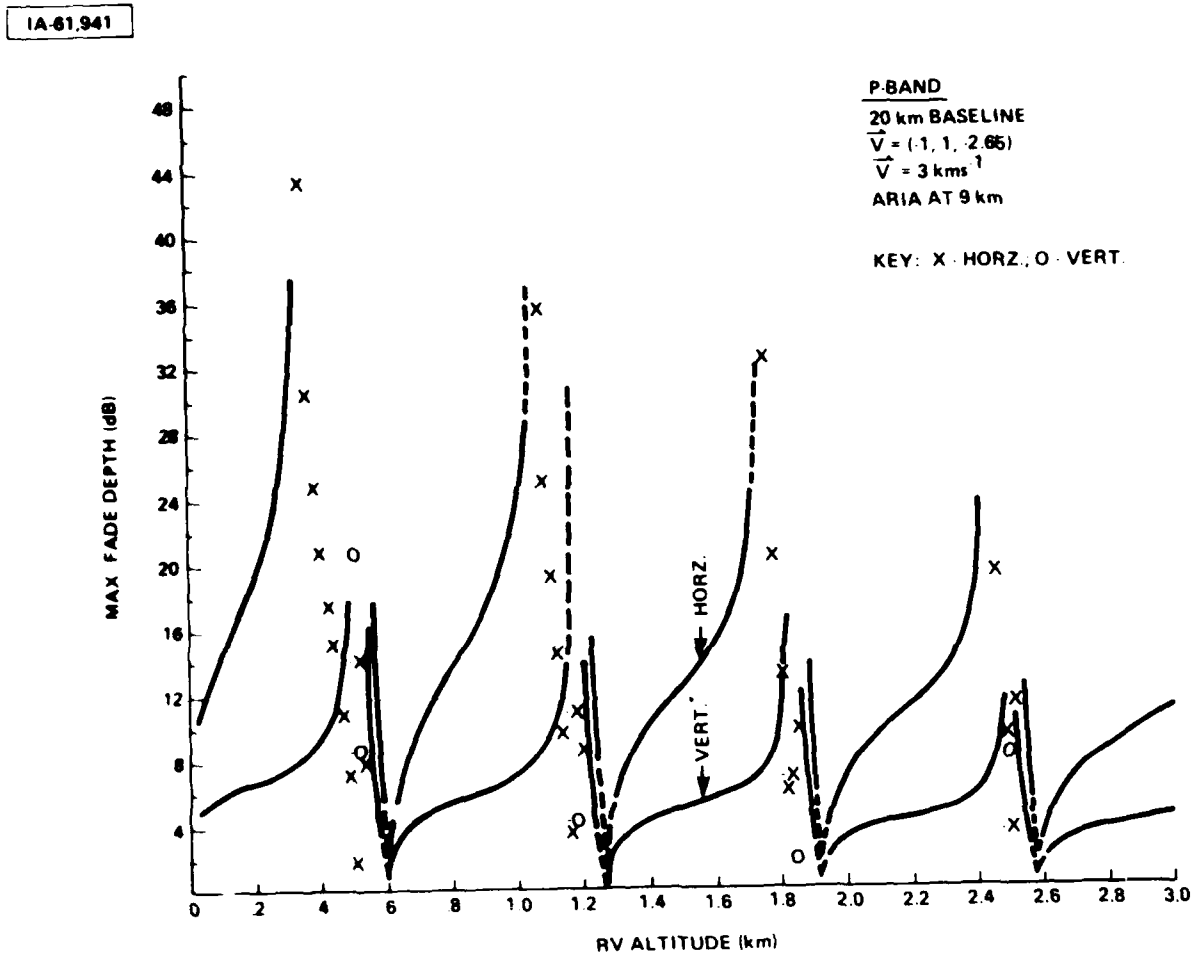

Figure 37 MAXIMUM P BAND RF POWER FADES VERSUS RV ALTITUDE FOR A HIGH $\dot{\gamma}$ RV TRAJECTORY AND ARIA AT 9 km ALTITUDE

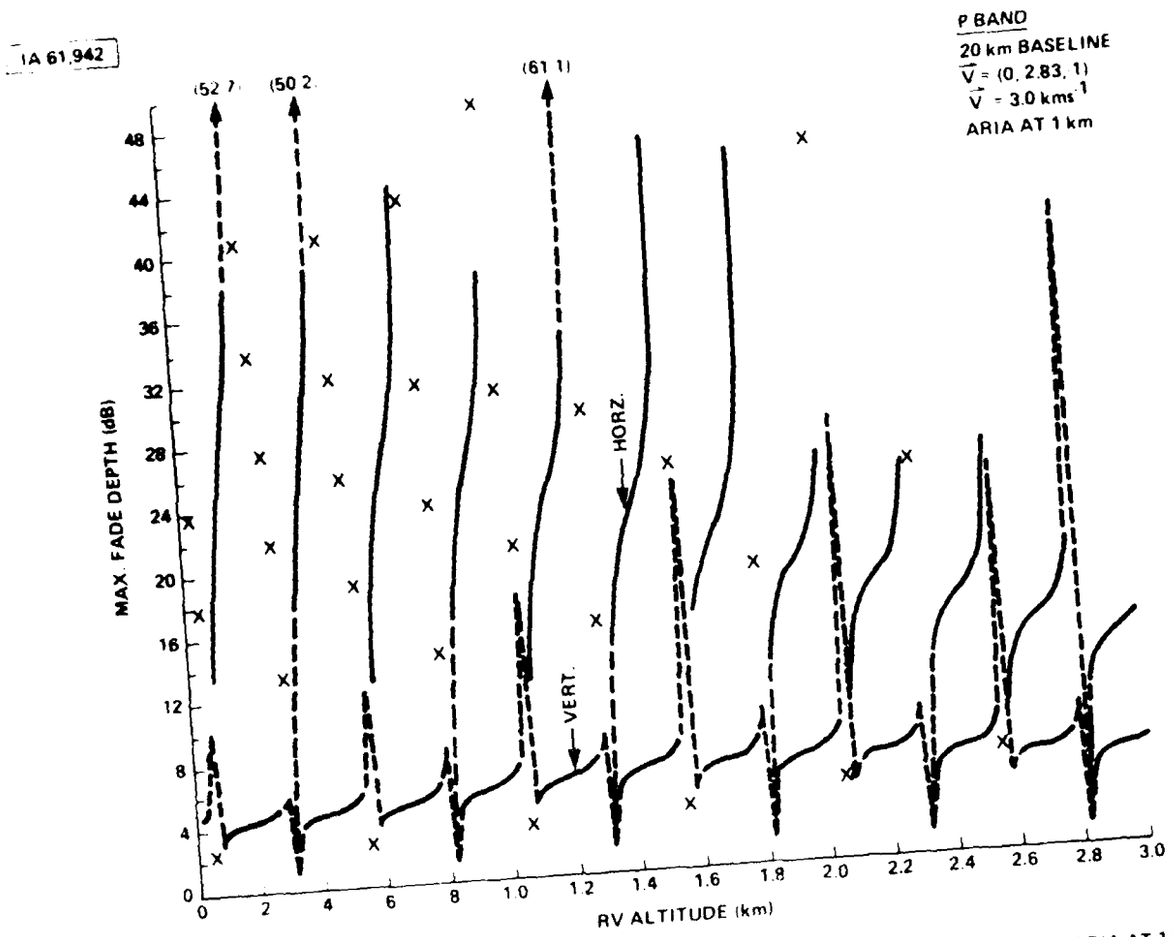

Figure 38 MAXIMUM P BAND RF POWER FADES VERSUS RV ALTITUDE FOR A LOW $\vec{V}$ RV TRAJECTORY AND ARIA AT 1 km ALTITUDE

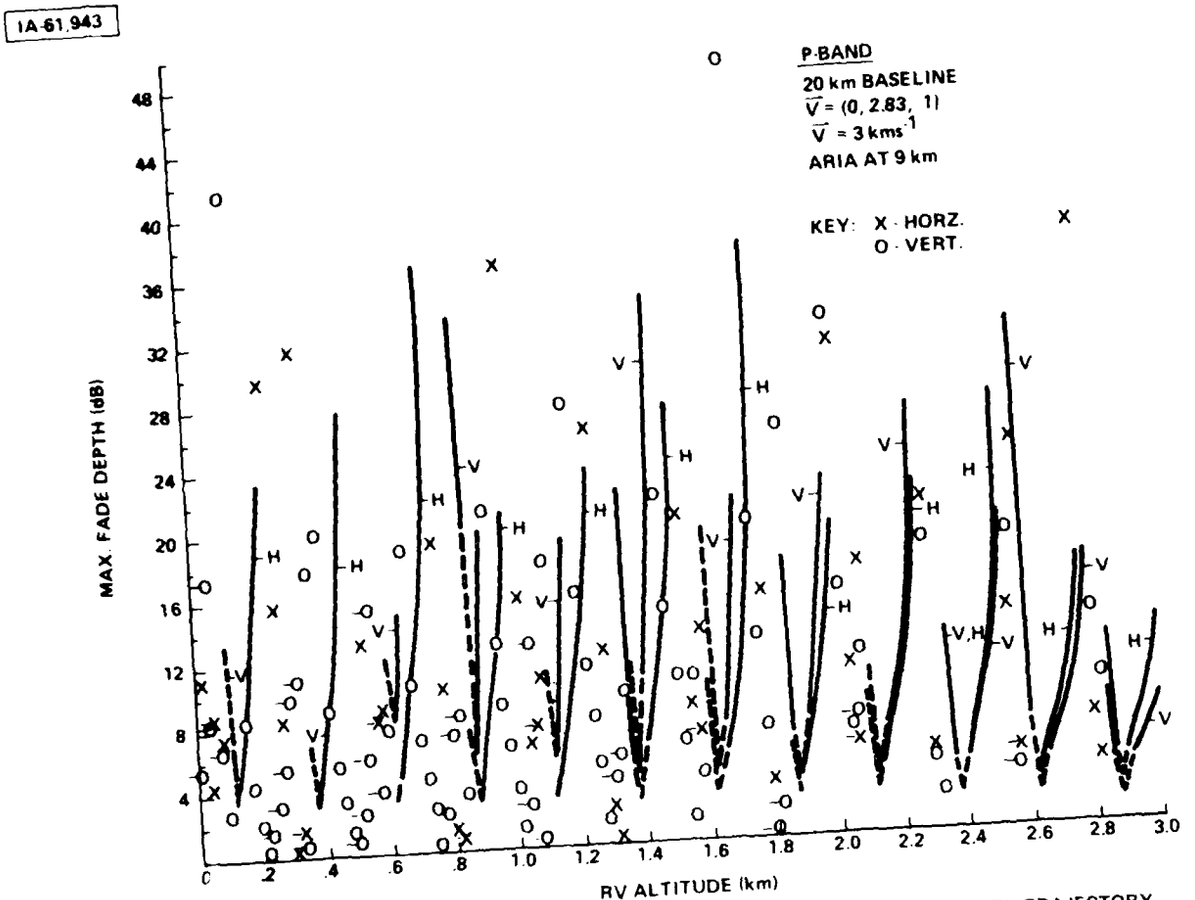

Figure 39 MAXIMUM P BAND RF POWER FADES VERSUS RV ALTITUDE FOR A LOW γ RV TRAJECTORY AND ARIA AT 9 km ALTITUDE

respectively. Therefore, the RV altitude ranges of figures 36 through 39 are well within the P-band severe fading environment.

The remaining two characteristics of the fade depth plots are a result of the inter-relationship between the RV antenna pattern, RV rotation, and the specular reflection geometry. More specifically, the direct path and specular path rays originate from different directions in the RVCCS, as discussed in section II-2-A (figure 9) and when a null in the model antenna pattern rotates through the plane of incidence, the relative strength of the direct and specular power alternates. In the simulations of figures 36 through 41, the RV rotational sense is that of a right hand screw, which information, when considered together with the RV trajectories (velocity vectors), leads to the conclusion that the specular ray falls onto a null before the direct path ray. Thus the fades are initially alleviated, but become much worse when the direct ray direction is aligned with the null several degrees or so of RV rotation later, depending upon the azimuthal separation of the direct and specular rays. These predictions are consistant with figures 36, 37 and 38, in which it is evident that the negative peak of a spike precedes the positive peak as the RV descends.

Figures 38 and 39 pertain to an RV with a nearly horizontal trajectory (low γ) for a low and high TSP ARIA respectively. Many more spikes are seen in these plots since the RV undergoes many more rotations while traveling the same vertical distance because of the low γ trajectory.

Several general results are illustrated by figures 36 through 39:

1) For horizontal polarization, fades are less severe on the average for higher ARIA or RV altitudes. This observation follows from the larger reduction of the coherent power for higher grazing angles.

2) For horizontal polarization, the fades are generally more severe than for vertical polarization. This result is a consequence of the relative magnitude of the Fresnel reflection coefficients for vertically and horizontally polarized fields as displayed in figure 17, for example.

3) When periods of severe fade occur (positive spikes), their duration is longer for higher altitude TSPs, since for higher ARIA altitudes the separation of the direct and specular rays in the RVCCS is greater, as illustrated in figures 11 through 15. For the cases of figures 36 and 37 the azimuthal separation angles are 21.5^{o} and 2.4^{o} respectively.

4) For a low ARIA TSP altitude (figures 36 and 38), the vertical polarization fades become less severe as the RV descends. This unusual result is caused by the decrease of the Fresnel reflection coefficient (see figure 17) as the grazing angle decreases from 11.3^{o} to 3^{o} for the example of figure 36, and from 11.3 to 2.7^{o} for the example of figure 38. For the vertical polarization fades of figures 37 and 39, this effect is not as pronounced since the grazing angles vary from 31^{o} to 25.5^{o} and from 31^{o} to 22.6^{o}, respectively.

5) The worst multipath interference occurs for the case represented by figure 39, for which the specular field exceeds the direct field for a substantial portion of the RV descent. This condition is attributable, primarily, to the large azimuthal

separation of the direct and specular rays for this trajectory, which is very similar to that of case "C", figure 11. More specifically, the azimuthal separation for this case is ~45° as compared to, for example, 5.3° for the case of figure 38. As was noted in section II-2-B, the low γ trajectories are generally associated with relatively large azimuthal separations of the direct and specular path rays as referenced to the RVCCS.

Figures 40 and 41 represent maximum fade depth calculations for S-band telemetry (λ = 13.3 cm) for RV-ARIA geometries and RV trajectories identical to those of figures 36 and 37, respectively. The severe multipath environment at S-band for the 1.5-m high array antenna begins at an RV altitude of 0.47 km according to equations (1) and (2). From Figure 41 it is particularly clear that deep fades (spikes) associated with nulls in the RV antenna pattern can occur well outside of the RV altitude limit of the severe multipath environment. The envelopes of the maximum fade values of Figures 40 and 41 qualitatively show the $(\sin^2 x)/x^2$ dependence of the receiving antenna gain. For figure 40 the specular ray enters a receiving antenna null for RV altitudes of 0.85, 1.75 and 2.75 km, while in Figure 41 the specular beam is nulled out at RV altitudes of 1.25 and 2.3 km.

At S-band the maximum fades over most of the RV altitude range are far milder than those predicted at P-band as anticipated on the basis of the considerations of the previous sections. Once again, however, it must be emphasized that the model upon which the calculations of Figures 36 through 41 are based is deterministic, i.e., it does not include the incoherent power, whose random fluctuations can cause deep fades under circumstances where tolerable fades would be expected. Indeed, the influence of the incoherent field is greatest at times when the direct and coherent reflected fields are in or near phase

IA-61,944

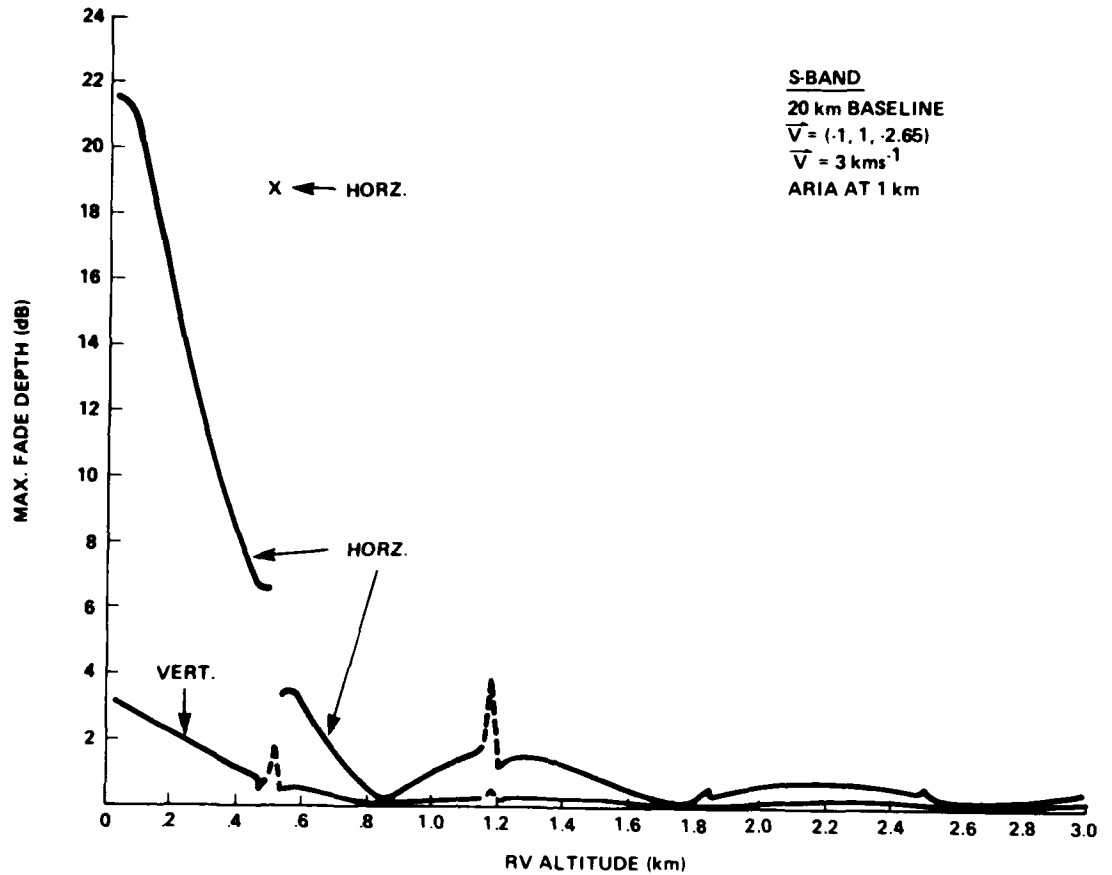

Figure 40. MAXIMUM S-BAND RF POWER FADES VERSUS RV ALTITUDE FOR A HIGH γ RV TRAJECTORY AND ARIA AT 1 km ALTITUDE

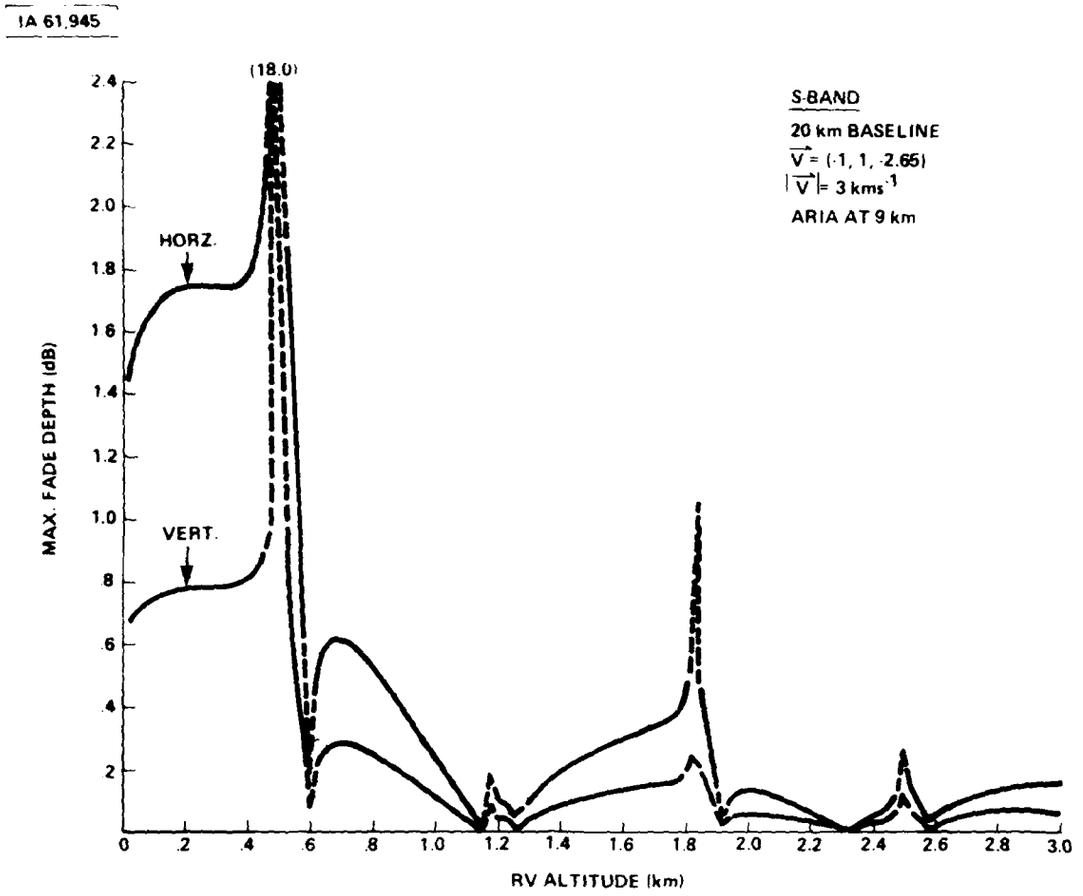

Figure 41. MAXIMUM S-BAND RF POWER FADES VERSUS RV ALTITUDE FOR A HIGH γ RV TRAJECTORY AND ARIA AT 9 km ALTITUDE

opposition and their resultant is comparable to the RMS incoherent field amplitude. Thus the depths of deeper fades, when strong coherent multipath is present, are less predictable than those for relatively mild fades.

If the depth of the RF fading is greater than the link margin, it is necessary to consider the fade frequency of interference to determine whether or not the BER will be degraded. If the fade frequency is large relative to the bit rate, the fades and reinforcements will be averaged out during a bit period (assuming envelope detection) and the data quality may actually improve if intersymbol interference is negligible[26]. If the fade frequency is comparable to or less than the bit rate, bits may be lost during periods of destructive interference, i.e., fades.

2. The Rate of Fade

A. Differential Doppler Shift

The most common telemetry modulation format used for RV-ARIA links is PCM/FM. If the RV and ARIA were both stationary and the relative channel delay were small compared to the shortest frequency modulation period, the direct and reflected waves at the receiver would have nearly the same frequency and the beat period would be very long. If, for simplicity, only RV motion is considered, the channel frequency difference or beat frequency obtained when the direct and specular fields are combined at the ARIA is given by[30],

$$f_B = \left| \frac{f_o}{c} \left[\vec{V} \cdot \hat{D} - \vec{V} \cdot \hat{S} \right] \right| \tag{25}$$

in which c is the velocity of light, f_o is the transmitter frequency, $\vec{V}$ is the RV velocity and $\hat{D}$ and $\hat{S}$ are unit vectors in the direct and

specular directions respectively, as shown in figure 9. This expression represents the difference of the Doppler shifted transmission frequencies in the direct and reflection path directions. For example, if the RV were approaching the ARIA head-on, the Doppler shift for the direct path would obviously exceed that for the specular path.

The differential Doppler factor,

$$F_D = \left| \frac{[\hat{V} \cdot \hat{D} - \hat{V} \cdot \hat{S}]}{c} \right| \tag{26}$$

is a convenient measure of the geometrical dependence of the frequency separation, f_B, of the direct and specular channels, which is obtained from,

$$f_B = F_D f_o \left| \vec{V} \right| \tag{27}$$

The Doppler factor is plotted in figures 42 and 43 (sec/km) as a function of ARIA altitude for an RV at 1 km altitude. In figure 42 the baseline used is 60 km, while for figure 43 a 20-km baseline is employed. Each curve is labeled in accordance with the unit velocity vector key which appears in figure 11, and is qualitatively characterized by the corresponding magnitude of the RV penetration angle, γ, and the designations "trans" "para" and "nom", defined in section II-2-B.

RV speeds typically lie within a range of 2 - 6 kms^{-1} in the multipath environment.

Several general conclusions which are illustrated by figures 42 and 43 are:

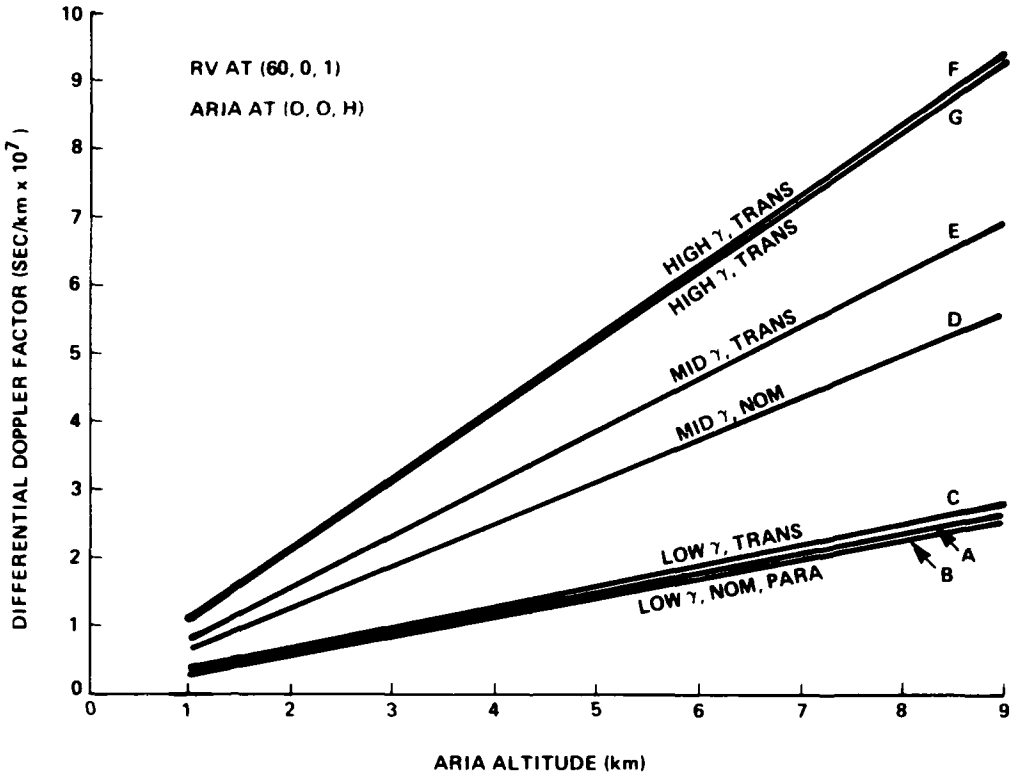

Figure 42. DIFFERENTIAL DOPPLER FACTOR VERSUS ARIA ALTITUDE FOR SEVERAL RV TRAJECTORIES, A 60 km BASELINE AND 1 km RV ALTITUDE

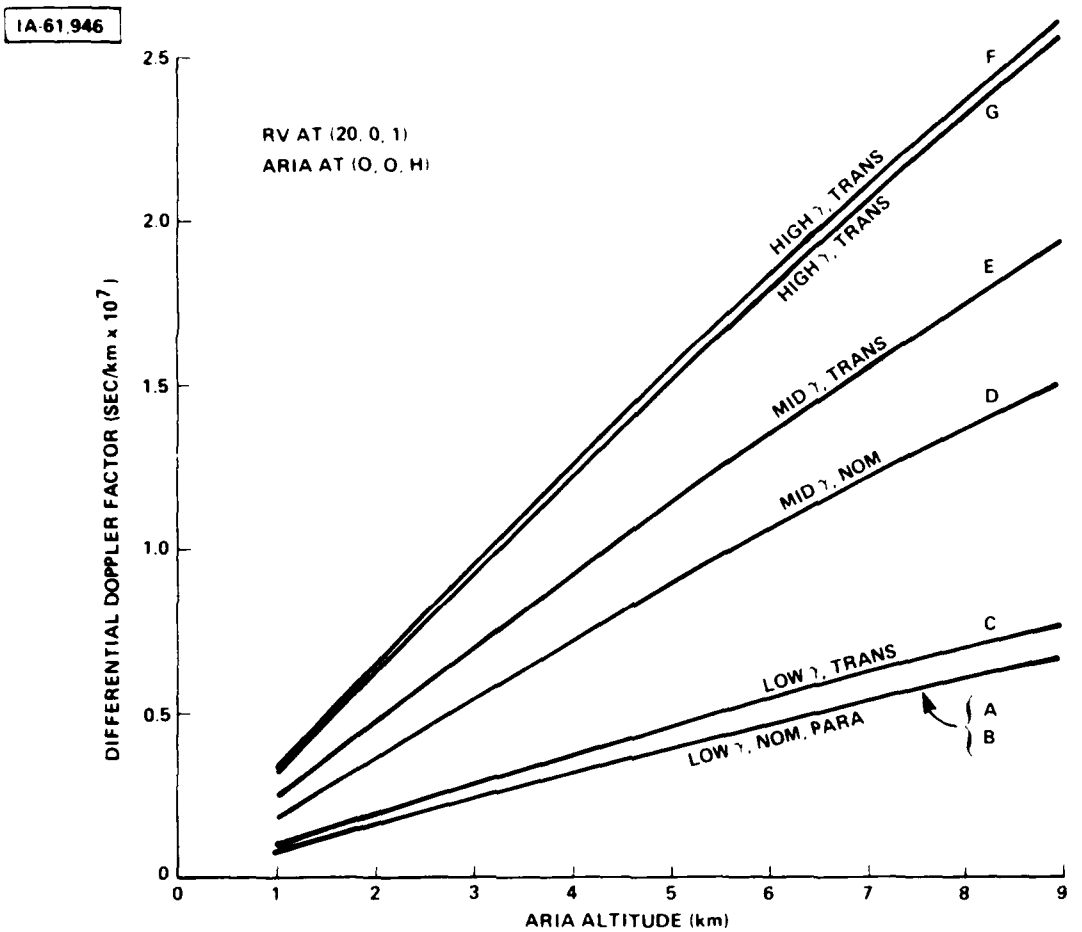

Figure 43 DIFFERENTIAL DOPPLER FACTOR VERSUS ARIA ALTITUDE FOR SEVERAL RV TRAJECTORIES. A 20 km BASELINE AND 1 km RV ALTITUDE

1) Differential Doppler factors increase linearly with ARIA altitude for a given RV position and velocity,

2) For a given RV-ARIA configuration, differential Doppler factors are larger for higher penetration angles, and

3) For fixed RV and ARIA altitudes, the difference frequency is nearly inversely proportional to baseline separation.

At P-band (226 MHz) the difference frequency can be as high as 1.8 kHz if an RV speed of 3 kms^{-1} and 20-km baseline are assumed, while at S-band (2.26 GHz) beat frequencies of 18 kHz are possible for high γ trajectories under the same conditions.

The differential Doppler factor is plotted as a function of ARIA altitude for several RV trajectories in figure 44, for which the RV altitude and baseline are 9 km and 20 km respectively. By comparison with figure 42 it seems that, in general, for higher RV altitudes the Doppler factors are larger, however for certain cases, such as A and B, the variation is negligible or contrary to the trend.

For the low γ trajectories of the specific cases corresponding to figures 38 and 39, the beat frequencies are small, since the projections of the RV velocity vectors on the propagation path directions are nearly the same. For the low ARIA TSP (1 km, figure 38) the beat frequency ranges from 7^ to 69 Hz, while for the high ARIA TSP (9 km, figure 39), the range is 600 - 580 Hz for RV altitudes from 3 km to splashdown. On the other hand, for the high γ trajectories of the cases represented in figures 36 and 37, the beat frequencies range from 180 to 210 Hz and from 1,520 Hz to 1,709 Hz respectively, for RV altitudes from 3 km to splashdown.

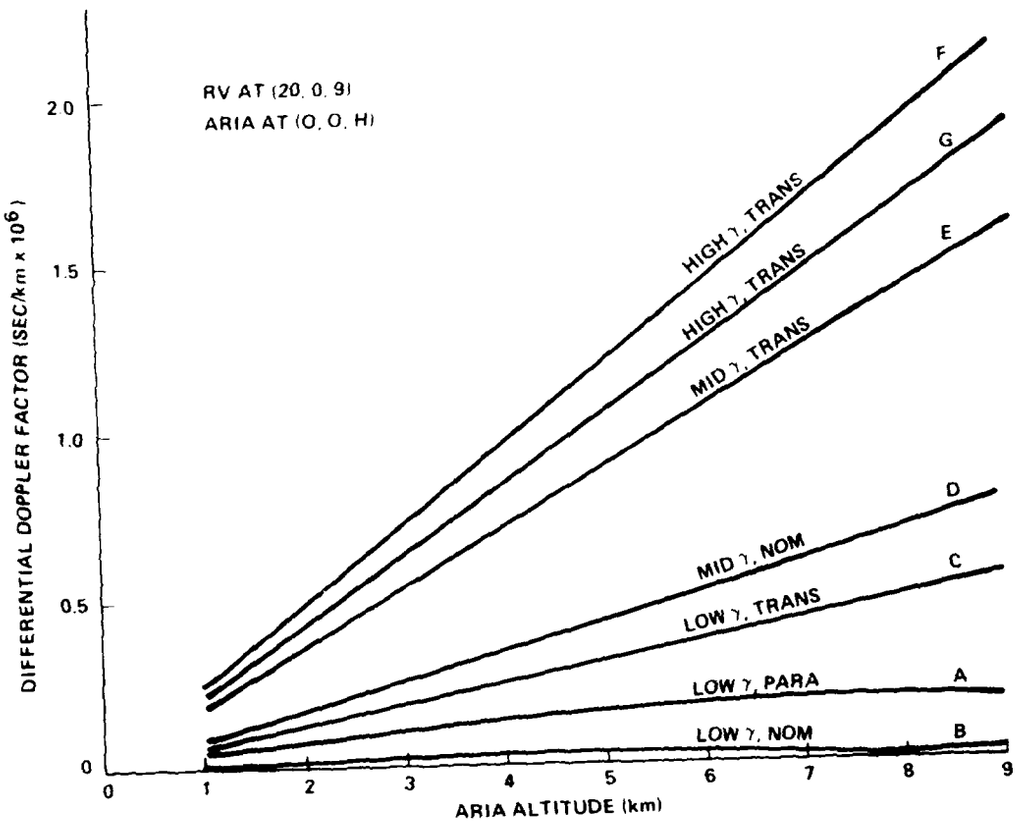

Figure 44. DIFFERENTIAL DOPPLER FACTOR VERSUS ARIA ALTITUDE FOR SEVERAL RV TRAJECTORIES, A 20 km BASELINE AND 9 km RV ALTITUDE

For S-band telemetry (2.26 GHz) the fade frequencies are about ten times greater than for P-band if link geometries are identical, since Doppler shifts are proportional to transmitter frequency, f_o. Thus for the cases corresponding to figure 40, the fade frequency ranges from 1.8 to 2.1 kHz, while for the case of figure 41 a range of 15 kHz to 17 kHz is predicted.

It is instructive to note that the geometry which would produce the greatest differential Doppler requires an ARIA TSP directly over an RV with a vertical trajectory. The beat frequency is then, from equation (25),

$$f_B = \frac{2 f_o |\vec{V}|}{c} \tag{28}$$

which gives 45 kHz for an RV speed of 3 kms^{-1} and RF of 2.26 GHz.

Since serial bit rates from 10 kbs^{-1} to 500 kbs^{-1} are ordinarily used for coding of RV telemetry data, the fade frequency is not significantly greater than the bit rate, and if the fades are sufficiently deep, link performance will suffer.

A maximum fade occurs when the direct and reflected field voltages, V_D and V_R respectively, at the receiving antenna output are in phase opposition. However, the maximum fade only represents the minimum of the envelope of the resultant RF field. The envelope function can be expressed,

$$A(t) = \left[V_R^2 + V_D^2 + 2 V_R V_D \cos\left[(\omega_R - \omega_D)t\right] \right]^{\frac{1}{2}} \tag{29}$$

in which the fade rate appears in the argument of the cosine. It can be readily shown that the reflected wave reinforces the direct wave ($A(t) > V_D$) during a fraction of the beat period given by,

$$1 - \frac{\sin^{-1}[V_R/2V_D]}{90} \tag{30}$$

which for the deepest fade ($V_R = V_D$) is 2/3. The power distribution of a fade cycle is shown in figure 45 for a 30-dB maximum fade which results when $V_R = 0.968V_D$. From this plot it can be determined, for example, that the RF power is below -25 dB (referenced to direct field power alone) only 1.5% of the time and is below -29 dB for only 0.5% of the time.

If for a 30 dB fade the fade rate is 1 kHz, the bit rate is 200 kbs^{-1} and the link margin is 25 dB, data will be lost or degraded for periods of 15 μs ($0.015/10^3$) which corresponds to 3 bit periods. If, however, the bit rate in the above example were 10 kbs^{-1}, the drop-out would affect only 15% of bit period and may not cause any degradation of the data.

B. Modulation Distortion

In the previous sub-section the rate of fade was considered for the case of telemetry for which the frequency does vary significantly in the time interval of the relative propagation channel delay. Thus the frequency separation of the direct and specular RF signals at the ARIA is primarily due to differential Doppler shift. In addition to the amplitude modulation or fades caused by the interference of the direct and multipath component, phase modulation of the stronger signal by the weaker one causes the instantaneous frequency of the resultant signal to undergo a periodic deviation which can introduce spurious baseband signal components at the output of the receiver's FM detector. This type of noise, referred to as modulation distortion, has been studied in detail[29] for an RV-ARIA telemetry link employing

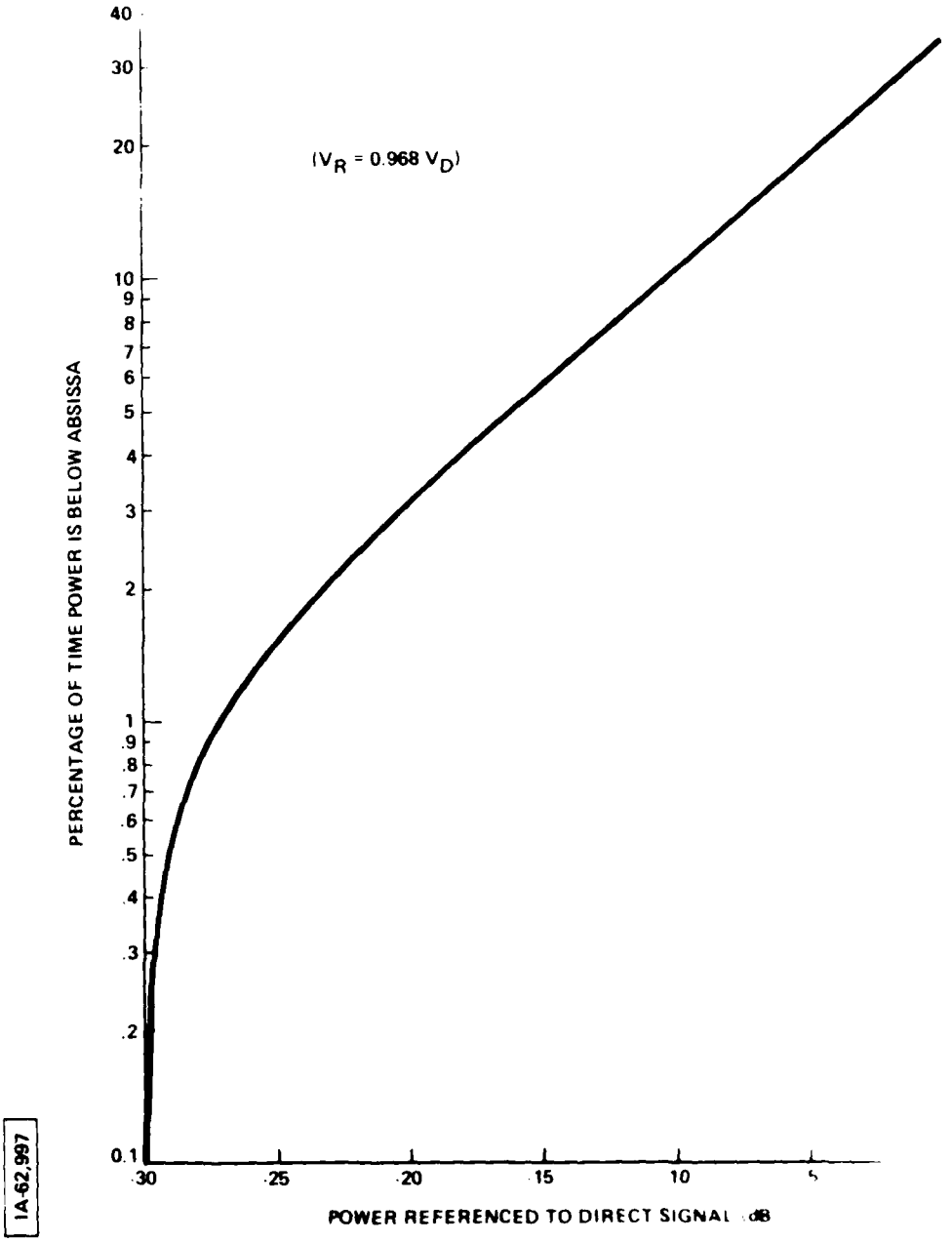

Figure 45 POWER DISTRIBUTION FOR 30 dB FADE

AD-A114 057 MITRE CORP BEDFORD MA F/G 9/6
MULTIPATH ANALYSIS OF TELEMETRY SUPPORT POSITIONS FOR APATS.(U)
APR 82 G A ROBERTSHAW F19628-82-C-0001
UNCLASSIFIED MTR-8277 ESD-TR-81-395 NL

2 OF 2
AD A
114057

END
DATE FILMED
05-82
DTIC

various modulation formats. In particular, it has been suggested[30] that the telemetry data might be improved by limiting the aircraft altitude in order to reduce the relative channel delay to 1) only a small portion of the bit period for a pure pulse code modulation (PCM) link or 2) a small fraction of the highest subcarrier period if continuous FM/FM is used. These suggestions are consistant with the recommendations of the study referred to previously[6] and also reinforce the preliminary flight constraints presented in section II-1-B.

Derivation of the frequency or modulation distortion components for the simple cases of differential Doppler shifted carrier (unmodulated) wave interference and monotone FM wave interference with Doppler shift and relative channel delay has been performed and appears elsewhere[31]. The distortion terms occur at frequencies which are the sum and difference frequencies of all combinations of the Doppler shifted modulation frequencies, their harmonics, the differential Doppler frequency and its harmonics. The number of significant distortion terms increases sharply as the interfering waves become comparable in magnitude.

A common RV telemetry format is PCM/FM or PCM/FSK, in which FSK refers to frequency shift keying. The digital PCM stream is impressed on the RF carrier by switching between a "mark" and a "space" frequency. Figure 46 displays a superposition of the direct and reflected FSK bit streams. The frequency offset, $f_R - f_D$, is caused by differential Doppler, while Δf represents the FM deviation of the carrier at f_D or f_R. The Doppler shift of the deviation is negligible and Δf is used to represent the deviation for both the direct and reflected signals. Frequency deviations of 100 to 200 kHz are typically used, which is far in excess of the differential Doppler shift, as shown. The example in figure 46 displays 20%

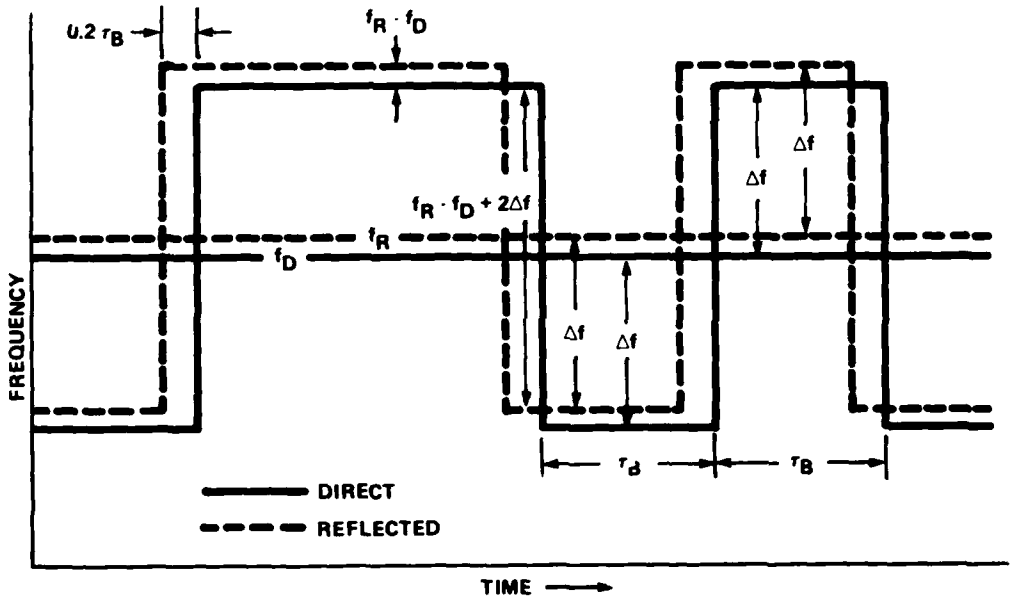

Figure 46: INTERSYMBOL INTERFERENCE FOR PCM/FSK

intersymbol interference. The bit error rate is a function of the bit overlap, the relative level of the two streams, and the type of demodulation employed. A suitable noise model must also be applied. A simple detection scheme would use mark and space filters followed by a comparator to select the stronger signal. Clearly, when marks overlap and have comparable strength, the mark filter will pass a signal which will have deep fades which occur at the rate $f_R - f_D$. When a deep fade occurs the output of the mark filter will be difficult to distinquish from the noise in the space filter and BER is increased. When a mark falls on a space the filters have comparable outputs and the BER is increased.

The literature contains analyses of BER for FSK[32] and PSK[33] (phase shift keying) in multipath environments, however these are not directly applicable to the APATS multipath environment. Further study will be required to provide a detailed analysis of BER in the context of the APATS mission.

SECTION IV

ARIA TELEMETRY SUPPORT POSITION RECOMMENDATIONS

At this point it is feasible to apply the insights obtained from the preceding analysis to suggest passive multipath alleviation strategies. Passive techniques do not require the addition of any hardware or software to the APATS or RV, but rather exploit the intrinsic physical properties of the propagation paths by tailoring the receiver location to the specific mission parameters. For example, if no more than 10% intersymbol interference is tolerable when the RV is in the severe multipath environment, the ARIA may support missions at altitudes up to but not exceeding those given in tables 1 (P-band) and 2 (S-band). Implicit in these recommendatons, however, is the assumption that higher percentage intersymbol interference is acceptable outside the severe multipath environment because the level of the reflected signals is low due to the discrimination of the receiving antenna. Furthermore it should be recalled that the altitude constraints of tables 1 and 2 are derived for a receiving antenna dish of 2.1-m diameter or array antenna of 2.1 m vertical dimension, and the tables must be revised if a receiving antenna having a significantly different aperture is employed.

The objectives of passive multipath suppression are:

1) Minimize the power of the reflected signal,

2) Hold intersymbol interference to less than 10% and,

3) Minimize the azimuthal separation of the direct and specular rays in the RVCCS.

The last objective requires elaboration since it may be argued that a large angular separation between the contributing channels would permit the specular channel to provide diversity reception when the direct channel coincides with an RV antenna null. On the other hand data may be lost during the severe RF fades which occur during the transition from one signal to the other, and the relative delay between the channels may be sufficient to cause loss of bit stream synchronization. Therefore, to be conservative, it will be assumed that during times when the specular signal level exceeds the direct signal level the data are of poor quality. Since RV antenna nulls are typically 6^{o} wide within 3 dB of the minimum, and 4 nulls are usually encountered during one RV revolution, about 7% of the RV telemetry is subject to serious degradation, even well outside of the severe multipath environment defined in section II-1-A. The typical azimuthal separation of a null and local peak in the RVCCS is approximately 10^{o} - 20^{o}, so that a more specific implementation of objective 3 might require, for example, that the azimuthal separation of the direct and specular path rays not exceed 5^{o}.

Often some of the objectives above will have to be compromised to achieve the best overall link performance. The following general results should be taken into account during pre-mission planning in order to select the most favorable TSPs:

1) Relative channel delay increases nearly linearly with RV or ARIA altitude, and varies nearly inversely with RV-ARIA baseline separation;

2) The coherent specular power, for non-smooth surfaces, decreases with increasing grazing angle, i.e., with increasing ARIA or RV altitude;

3) The Fresnel coefficient amplitudes for horizontal polarization are near unity over the practical range of grazing angles ($0 < \theta < 30^{o}$) while for vertical polarization the Fresnel coefficient amplitude goes through a minimum of 0.36 at 2.8^{o} for 226 MHz incident radiation (P-band), and 0.11 at 6^{o} for 2.26 GHz incident radiation (S-band) as shown in figure 17;

4) The contribution of the incoherent power will cause the reflected power to exceed the direct power for a fraction of time dependent upon sea roughness and Fresnel coefficient, as indicated in table 4;

5) For a given RV-ARIA configuration, the azimuthal separation of the direct and specular rays in the RVCCS is greater for RV trajectories which have lower penetration angles and;

6) The fade frequency is the difference (beat frequency) of the direct and specular RF fields at the receiver. If the relative channel delay is short compared to a bit period, the beat frequency is equal to the differential Doppler frequency which can range from 0 - 2 kHz for P-band and from 0 - 20 kHz for S-band depending upon the RVs trajectory, speed, and RV-ARIA configuration.

In the following subsections ARIA TSP recommendations for telemetry acquisition at both S- and P-band are discussed for a variety of mission scenarios. It is assumed that the receiving antenna aperture vertical dimension is about 2.1 m. Each of the cases

discussed below considers only a single RV in the APATS field of view, however, generalization to multiple RVs will involve compromises based upon the single RV recommendations.

1. P-Band

a) Case 1P: 160 kbs^{-1} or Less; High γ; Any Sea State

For high γ trajectories the azimuthal separation of the direct and specular path rays in the RVCCS is less than 5^{o} for baselines of 60 kM or greater (figure 11) if the ARIA altitude is 9 km or less. For these baselines the TSP altitude is constrained by the recommendation to limit intersymbol interference to 10% or less of a bit period in the severe multipath environment. The maximum TSP altitudes which appear in table 1 are therefore applicable. On the other hand, for shorter RV-ARIA baselines it is recommended that the TSP altitude be constained to limit the difference in RV antenna gain for the direct and specular path. For example, for trajectory F in figure 13, the ARIA must fly below 6 km (20,000 ft.) to keep the azimuthal separation of the direct and specular paths in the RVCCS to about 5^{o} or less.

Somewhat lower altitude TSPs may be desirable if the minimum in the vertical polarization coherent power can be exploited (figure 18). Additional adjustment of the ARIA TSP may be desirable depending upon sea state, to avoid configurations which are characterized by a large incoherent power component (figure 35) when the RV nears splashdown.

b) Case 2P: Bit Rate Greater Than 160 kbs^{-1}; High γ ; Any Sea State

For higher bit rates at P-band, it would be necessary to operate the ARIA at impractical or unsafe altitudes to reduce intersymbol interference to 10% or less in the severe multipath environment (table 1). The only remaining strategy is to minimize the level of the interfering field. Therefore, an RV-ARIA configuration which produces a grazing angle of incidence near RV splashdown which minimizes the vertical polarization coherent power should be arranged. Table 3 contains TSP altitude recommendations for this case.

c) Case 3P: Bit Rate 160 kbs^{-1} or Less; Low to Moderate γ; Any Sea State

For an RV trajectory having a low γ, it is recommended that the ARIA TSP altitudes be restricted to 1.4 km (4,600 ft.) and 2.0 km (6,600 ft.) or less for baselines of 40 km and 60 km respectively, if the azimuthal separation of the direct and specular channels in the RVCCS is to be held to 5^{o} or less. For a trajectory with a moderate penetration angle the corresponding maximum TSP altitudes are 2.2 km (7,300 ft.) and 3.4 km (11,000 ft.) respectively, as can be determined from figures 11 and 13. For the higher bit rates intersymbol interference alleviation may require even lower TSP altitudes, as per table 1. Although it is true that the coherent power can be greatly reduced by adoption of a 9-km TSP altitude for the higher sea states (figures 20, 21, 29, 30, 31), a strong incoherent power contribution and large RVCCS azimuthal separation angle at this altitude weigh heavily against this alternative strategy.

d) Case 4P: Bit Rate Greater Than 160 kbs^{-1}; Low to Moderate γ; Any Sea State

This case is similar to case 2P, however, since the RV penetration angle is low to moderate, the primary altitude constraints of case 3P should be observed. In addition, a configuration which provides the largest attenuation of the vertical polarization coherent reflected power (figure 18, table 3) and avoids the peak incoherent power region for the particular sea state (figure 35) when the RV is in the severe multipath environment should be employed.

B. S-Band

a) Case 1S: Bit Rate 1.5 Mbs^{-1} or Less; High γ; Sea State 1 or 2

For high γ trajectories the azimuthal separation of the direct and specular path directions, referenced to the RVCCS, is less than 5^{o} for baselines of 60 km or greater and ARIA altitudes of 9 km (29,700 ft.) or less. For shorter baselines the maximum TSP altitude must be reduced to prevent the azimuthal separation of the paths from exceeding 5^{o} in the RVCCS,. For example, for trajectory F in figure 13 (40-km baseline) the ARIA altitude during telemetry support should not exceed 6 km (20,000 ft.) In addition to these constraints, the requirement to limit bit overlap to 10% or less in the severe multipath environment may indicate that lower TSP altitudes are desirable as per table 2. Within these limitations it may be possible to adjust the ARIA altitude to take advantage of the local minimum in the vertical polarization reflected power (figure 19) as indicated in Table 3. On the other hand, RV-ARIA configurations which fall within the peak incoherent power region for the given sea state (figure 34) should be avoided.

Consider, for example, a mission for which the baseline is about 40 km, the bit rate is 160 kbs^{-1}, the trajectory has a high γ, and the sea state is 1. RV gain considerations place a 6-km (20,000 ft.) ceiling on the TSP altitude, while table 2 recommends an additional constraint of 6.5 km (21,400 ft.) based on the 160-kbs^{-1} rate. Table 3 indicates that the vertical polarization coherent power is minimized, within the above constraints, for an altitude of 4.2 km (13,900 ft.). Furthermore, reduction of the incoherent power also argues for the selection of a 4.2-km TSP altitude (figure 34).

b) Case 2S: Any Bit Rate; High γ; Sea State 3 or Greater

The high γ trajectory places the same restrictions on the maximum ARIA TSP altitude as were discussed for case 1S, e.g., 9 km or less and 6 km or less for baselines of 60 km and 40 km respectively. However, the rough (at S-band) sea states which distinguish this case should provide sufficient coherent and incoherent power reduction to permit the ARIA to use the maximum TSP altitude consistent with the above constraint. For example, if a 60-km baseline and sea state 3 exist, the coherent reflected power is down by over 20 dB and can be neglected (see figures 23 and 26) if the ARIA is at 9 km altitude. The Rayleigh parameter is about 4 or greater, the normalized incoherent power is approximately 0.18 and the probability that the specular power exceeds the direct power is less than 10^{-4} (see Table 4).

c) Case 3S: Bit Rate Greater Than 1.5 Mbs^{-1}; High γ; Sea State 1 or 2

For these relatively high bit rates it would be necessary to operate the ARIA at impractical or unsafe altitudes during telemetry support to hold intersymbol interference to 10% or less while the RV

is in the severe multipath environment defined in section II-1-A (see table 2). The only remaining strategy is to reduce the level of the interfering signal. The primary RV antenna gain derived constraints of cases 1S and 2S should be observed, and an RV-ARIA configuration which produces a grazing angle for the specular path which minimizes the vertical polarization coherent power, as per table 3, should be arranged if feasible. ARIA altitudes which incur a large incoherent power component should be avoided (see figure 34) if possible in the context of the other above recommendations.

d) Case 4S: Bit Rate 1.5 Mbs^{-1} or Less: Moderate γ; Sea States 1, 2, or 3

For an RV trajectory with a moderate (MID) γ, it is recommended that the TSP altitude be constrained to less than 2.2 km (7,300 ft.) and 3.4 km (11,000 ft.) for baselines of 40 km and 60 km respectively, if the azimuthal separation of the direct and specular rays in the RVCCS is to be held to less than 5^{o} (see figures 11 and 13). Linear interpolation and extrapolation can be used to determine the appropriate TSP altitude constaints for other baselines. Alleviation of intersymbol interference my require even lower TSPs as per table 2.

e) Case 5S: Any Bit Rate; Moderate γ; Sea State 4 or Greater

This case is similar to case 4S, however, the sea is sufficiently rough to permit the adoption of TSP altitudes up to the limits imposed by the RV antenna pattern derived constaints of case 4S. Coherent and incoherent power attenuation is sufficient, at the maximum recommended altitudes, to remove the multipath threat, as was shown for case 2S also. Thus TSP altitudes of 2.2 km (7,300 ft.) and 3.4 km (11,000 ft.) are recommended for baselines of 40 km and 60 km respectively

(see figures 11 and 13). Appropriate altitudes for other baselines may be found by linear interpolation and extrapolation from these values.

f) Case 6S: Bit Rate Greater Than 1.5 Mbs^{-1}; Low γ; Sea States 1, 2 or 3

The recommendations for this case are identical to those for case 3S, save for the RV antenna gain derived constraints, which are the same as those of cases 4S and 5S, the other two moderate penetration angle cases.

g) Case 7S: Bit Rate 1.5 Mbs^{-1} or Less; Low γ; Any Sea State

For a low γ RV trajectory it is recommended that ARIA TSP altitudes be limited to 1.4 km (4,600 ft.) or less and 2.0 km (6,600 ft.) or less for baselines of 40 km and 60 km respectively, if the azimuthal separation of the direct and specular rays in the RVCCS is to be 5^{o} or less (see figures 11 and 13). Linear interpolation and extrapolation from these values can be used to determine the proper TSP altitudes for other baselines. For the highest bit rates intersymbol interference alleviation dictates even lower TSP altitudes, as per table 2.

h) Case 8S: Bit Rate 1.5 Mbs^{-1} or Greater; Low γ; Any Sea State

Recommendations for this case are identical to those of case 3S, however, the maximum altitude constraints of case 7S apply because of the low γ trajectory.

The deep nulls in the RV antenna pattern, in the context of the two-path multipath model, are responsible for the trajectory

dependence of the altitude constraints. The above recommendations should alleviate the impact of these nulls in the multipath environment. However, if some data loss or degradation due to these nulls is acceptable, data quality during non-null periods may be improved by adopting the highest practical TSP altitude if the sea state is 2 or greater at S-Band. This conclusion rests upon the observation that at high TSP altitudes there is considerable attenuation of both the coherent and incoherent power reflected towards the ARIA when the ARIA is in the severe multipath environment, as can be gleaned from figures 22 through 28, and table 4. Thus if drop-outs associated with RV antenna nulls are acceptable, high altitude (30,000 ft.) TSPs are recommended for missions conducted at S-band over non-smooth seas.

LIST OR REFERENCES

1) S. L. Bernstein, T. A. Croft, A. J. Mallinckrodt, and B. O'Brien, "Report of the Committee on the ARIA Multipath Problem", March 1970.

2) W. R. Hedeman and M. H. Nichols, "Multipath Constraints on Telemetry Data Transmission", Aerospace Corp., Report No. TOR-0200(S4816-88)-2, June 16, 1969.

3) G. A. Robertshaw, "Analysis of Multipath Interference for APATS", The MITRE Corporation, July 10, 1981, ESD-TR-81-255, ADA108797.

4) M. I. Skolnik, Introduction to Radar Systems, (McGraw-Hill, 1980), P. 232.

5) "ARIA Operations Capability Report", Appendix C, P. C-3.

6) Op. Cit. 2, P. 22.

7) OP. Cit. 3, P. 29.

8) Op. Cit. 2, P. 10.

9) D. E. Kerr, Ed., Propagation of Short Radio Waves, (McGraw-Hill, 1951), P. 396 - 403.

10) P. Beckmann and A. Spizzichino, The Scattering of Electromagnetic Waves From Rough Surfaces, (MacMillan Co., 1963), P. 146 - 151.

11) Op. Cit. 10, P. 246.

12) M. M. Weiner and G. A. Robertshaw, "Coherent Scatter of Microwaves From Moderately Rough Surfaces," The MITRE Corporation, 1981, ESD-TR-81-147, ADA106133.

13) Op. Cit. 12, P. 15.

14) Op. Cit. 10, P. 10.

15) D. K. Barton and H. R. Ward, Handbook of Radar Measurement, (Prentice-Hall, 1969), P. 148.

16) C. I. Beard, I. Katz, and L. M. Spetner, "Phenomenological Vector Model of Microwave Reflection From the Ocean", IRE Trans., AP-4, AP-4, April 1956, P. 162 - 167.

17) M. Schwartz, W. R. Bennett and Seymour Stein, Communications Systems and Techniques, (McGraw Hill, 1966), P. 121 - 123.

18) K. A. Norton, L. E. Vogler, W. V. Mansfield and P. J. Short, "The Probability Distribution of the Amplitude of a Constant Vector Plus a Rayleigh Distributed Vector", Proc. IRE, Vol. 43, Oct. 1955, P. 1354 - 1361.

19) C. I. Beard, "Coherent and Incoherent Scattering of Microwaves From the Ocean", IRE Trans., AP-9, No. 5, Sept. 1961, P. 470 - 483.

20) Op. Cit. 19, P. 476, Fig. 4.

21) Op. Cit. 10, P. 349, 356, 357.

22) Op. Cit. 12, P. 17.

23) Op. Cit. 18, P. 1360.

24) Op. Cit. 10, P. 152 - 167.

25) C. I. Beard and I. Katz, "The Dependence of Microwave Radio Signal Spectra on Ocean Roughness and Wave Spectra", IRE Trans., AP-5, April 1957, P. 183 - 190.

26) G. P. Richards, W. T. Bisignani and S. H. Roth, "Multipath Fading in FSK Communication Links - An Experimental Investigation", IEEE Trans., Vol. AES-5, May 1969, P. 548 - 557.

27) Op. Cit. 3, P. 43.

28) Op. Cit. 3, P. 37.

29) C. H. Chen, "Effects of Multipath on Telemetry Data Transmission", 1970 International Telemetering Conf., Los Angeles, 13 - 15 Oct. 1970, P. 143 - 154.

30) Op. Cit. 29, P. 152.

31) Op. Cit. 3, P. 9 - 19.

32) H. D. Chadwick, "The Error Probability of a Wide-Band FSK Receiver in the Presence of Multipath Fading", IEE Trans., Vol. COM-19, Oct. 1971, P. 699 - 707.

33) H. Salwen, "Differential Phase-Shift Keying Performance Under Time-Selection Multipath Fading", IEEE Trans., Vol. COM-23, March 1975, P. 383 - 385.


FILMED
5-8